AD NUMBER

AD867904

NEW LIMITATION CHANGE

TO

Approved for public release, distribution unlimited

FROM

Distribution authorized to U.S. Gov't. agencies and their contractors; Critical Technology; MAR 1970. Other requests shall be referred to Air Force Weapons Lab., Attn: WLEE, Kirtland AFB, NM, 87117.

AUTHORITY

AFWL ltr dtd 16 Mar 1972

AFWL-TR-
69-106

A NONSIMILAR SOLUTION FOR MULTICOMPONENT REACTING LAMINAR AND TURBULENT BOUNDARY LAYER FLOWS INCLUDING TRANSVERSE CURVATURE

Larry W. Anderson

Robert M. Kendall

TECHNICAL REPORT NO. AFWL-TR-69-106

March 1970

AIR FORCE WEAPONS LABORATORY
Air Force Systems Command
Kirtland Air Force Base
New Mexico

AFWL-TR-69-106

AIR FORCE WEAPONS LABORATORY
Air Force Systems Command
Kirtland Air Force Base
New Mexico

A NONSIMILAR SOLUTION FOR MULTICOMPONENT REACTING LAMINAR AND TURBULENT BOUNDARY LAYER FLOWS INCLUDING TRANSVERSE CURVATURE

Larry W. Anderson

Robert M. Kendall

TECHNICAL REPORT NO. AFWL-TR-69-106

FOREWORD

This report was prepared by the Aerotherm Corporation, Mountain View, California, under Contract F29601-68-C-0062. The research was performed under Program Element 62601F, Project 5791, Task 27.

Inclusive dates of research were March 1968 through October 1969. The report was submitted 3 February 1970 by the Air Force Weapons Laboratory Project Officer, Captain Ronald H. Aungier (WLEE).

Information in this report is embargoed under the US Export Control Act of 1949, administered by the Department of Commerce. This report may be released by departments or agencies of the US Government to departments or agencies of foreign governments with which the United States has defense treaty commitments, subject to approval of AFWL (WLEE), Kirtland AFB, NM, 87117.

This technical report has been reviewed and is approved.

Ronald H. Aungier
RONALD H. AUNGIER
Captain, USAF
Project Officer

Walter M. Hart, Jr.
WALTER M. HART, JR.
Major, USAF
Chief, Fuzing Environment Branch

Carl F. Davis
CARL F. DAVIS
Colonel, USAF
Chief, Electronics Division

ABSTRACT

A mathematical model of a multicomponent reacting nonsimilar laminar or turbulent boundary layer flow including transverse curvature effects is presented, and a method of solution is given. The formulation is an extension of an earlier work in which thermal and molecular diffusion were treated in terms of a bifurcation approximation for binary diffusion coefficients. In the present analysis, a turbulent model is added which employs a mixing length model for eddy viscosity in the wall region with consideration of injection or suction effects. The wake region eddy viscosity is taken to be proportional to the free stream velocity and local velocity defect thickness. Transverse curvature effects are also incorporated into the present analysis. A modification of the Levy-Lees transformation is used to transform the equations of motion to the (ξ,η) coordinate plane, where the conservation equations are integrated across boundary layer strips. Derivatives in the normal direction are related to one another by Taylor series truncated to reflect a quadratic or cubic approximation, and streamwise derivatives are expressed in finite difference form. The resultant set of equations is solved by general Newton-Raphson iteration.

CONTENTS

ILLUSTRATIONS

ILLUSTRATIONS (concluded)

SYMBOLS

A	parameter used in the solution of the mixing length equation (defined by Equation (131))
B	parameter used in the solution of the mixing length equation (defined by Equation (132))
c	constant introduced in the α_H constraint (Equation (58))
c_t	constant introduced in the approximation for multicomponent thermal diffusion coefficients embodied in Equation (25). Tentatively established by correlation of data to be -0.5
C	product of density and viscosity normalized by their reference values (defined by Equation (66))
$\bar{C}_p$	frozen specific heat of the gas mixture (defined by Equation (17))
$\tilde{C}_p$	property of the gas mixture which reduces to $\bar{C}_p$ when diffusion coefficients are assumed equal for all species (defined by Equation (26))
C_{p_i}	specific heat of species i
d_o, d_1, d_2	coefficients defined in finite-difference representation of streamwise derivatives (defined in Equations (112) and (113) for two- and three-point difference relations, respectively)
$\bar{D}$	a reference binary diffusion coefficient introduced by the approximation for binary diffusion coefficients embodied in Equation (19)
D_i^T	multicomponent thermal diffusion coefficient for species i
D_{ij}	multicomponent diffusion coefficient for species i and j
$\mathcal{D}$	diffusion coefficient for all species when all $\mathcal{D}_{ij}$ are equal
$\mathcal{D}_{ij}$	binary diffusion coefficient for species i and j
ERROR	errors for the various equations during Newton-Raphson iteration (driven toward zero in the iteration)
f	stream function (defined by Equation (59))
F_i	diffusion factor for species i introduced by the approximation for binary diffusion coefficients embodied in Equation (19)

SYMBOLS
(continued)

h	static enthalpy of the gas (defined by Equation (15))
h_w	static enthalpy of the gas at the wall
$\tilde{h}$	property of the gas mixture which reduces to the static enthalpy h when diffusion coefficients are assumed equal for all species (defined by Equation (27))
h_c	enthalpy of surface material (e.g., char) removed by combustion, sublimation, or vaporization
h_g	enthalpy of gas which enters boundary layer without phase change at the surface (e.g., pyrolysis gases)
h_i	enthalpy of species i (defined by Equation (16))
h_i^o	heat of formation
h_ℓ	enthalpy of ℓ^{th} component surface material (e.g., silica) removed in the condensed phase (e.g., by melting with subsequent liquid runoff or by spallation)
H_T	total enthalpy (defined by Equation (14))
j_i	diffusional mass flux of species i per unit area away from the surface
j_k	diffusional mass flux of element k per unit area away from the surface
K	total number of elements; also mixing length constant
K_i	mass fraction of molecular species i
$\tilde{K}_{c_k}$	total mass fraction of element (or base gas) k contained in surface material (e.g., char) removed by combustion, sublimation, or vaporization
$\tilde{K}_{g_k}$	total mass fraction of element (or base gas) k contained in gas which enters boundary layer without phase change at the surface (e.g., pyrolysis gases)
$\tilde{K}_k$	total mass fraction of element (or base gas) k irrespective of molecular configuration (defined by Equation (10))

SYMBOLS
(continued)

ℓ	mixing length (defined by Equation (55))
$\tilde{\ell}$	dimensionless mixing length (defined by Equation (71))
L	parameter used in mixing length formulation (defined by Equation (128))
$\dot{m}$	mass flow rate per unit area
$\dot{m}_c$	mass removal rate per unit area of surface material (e.g., char) by combustion, sublimation, or vaporization
$\dot{m}_g$	mass flow rate per unit area of gas which enters boundary layer without phase change at the surface (e.g., pyrolysis gases)
$\dot{m}_{r_\ell}$	mass removal rate per unit area of ℓ^{th} component surface material (e.g., silica) in the condensed phase (e.g., by melting with subsequent liquid runoff or by spallation)
$\mathcal{M}$	molecular weight of the gas mixture
$\mathcal{M}_i$	molecular weight of species i
N	number of nodal points across the boundary layer selected for the purpose of the numerical solution procedure
p	dummy variable representing f', H_T, or $\tilde{K}_k$
P	pressure; also a parameter used in the mixing length formulation (defined by Equation (125))
P_i	partial pressure of species i
Pr	frozen Prandtl number of the gas mixture (defined by Equation (86))
Pr_t	turbulent Prandtl number (defined by Equation (69))
q_a	diffusional heat flux per unit area away from the surface
q_{cond}	heat conduction per unit area into the surface material
q_r	one-dimensional radiant heat flux (toward the surface), that is, the net rate per unit area at which radiant energy is transferred across a plane in the boundary layer parallel to the surface

SYMBOLS
(continued)

r	local radius in the boundary layer in a meridan plane for an axisymmetric shape
r_o	local radius of body in a meridian plane for an axisymmetric shape
R	universal gas constant
Re	Reynolds number; subscripted with the length scale if other than s
R_{eff}	effective nose radius for Newtonian flow
s	distance along body from stagnation point or leading edge
$\overline{Sc}$	reference system Schmidt number (defined by Equation (88))
Sc_t	turbulent Schmidt number (defined by Equation (68))
t	parameter defined to simplify problems with transverse curvature; see Equation (55)
T	static temperature
u	velocity component parallel to body surface
u_τ	shear velocity, defined in Equation (49)
v	velocity component normal to body surface
x_i	mole fraction of species i
$XP_1, XP_2, \ldots$	truncated series obtained in Taylor series expansion of $\int_{i-1}^{i} f'p\, d\eta$ (defined by Equation (117))
y	distance from surface into the boundary layer, measured normal to the surface
y^+	dimensionless y-coordinate defined by Equation (49))
y_a^+	constant in the mixing length differential equation (see Equation (45))

SYMBOLS
(continued)

Z_i	a quantity for species i which is introduced as a result of the approximation for binary diffusion coefficients and reduces to K_i when all diffusion coefficients are assumed equal (defined by Equation (20))
$\tilde{Z}_k$	a quantity for element (or base species) k which is introduced as a result of the approximation for binary diffusion coefficients and reduces to K_k when all diffusion coefficients are assumed equal (defined by Equation (28))
$ZP_1, ZP_2, \ldots$	truncated series obtained in Taylor series expansion of integrals involving nonsimilar terms (defined by Equation (124))
α^*	flux normalizing parameter (defined by Equation (82))
α_H	normalizing parameter used in definition of $\bar{\eta}$ (see Equation (59)) defined implicitly by use of a constraint such as Equation (60)
α_{ki}	mass fraction of element (or base species) k in species i
β	streamwise pressure-gradient parameter (defined by Equation (67))
δ	y-dimension normalizing parameter (defined by Equation (70))
$\ell^{\Delta}\ell\text{-}1$	logarithmic distance between two streamwise positions denoted by the subscripts ℓ and ℓ-1 (defined by Equation (114))
$\Delta f_i, \Delta f_i', \ldots$	corrections for f_i, f_i',..., during Newton-Raphson iteration
δ^*	displacement thickness (defined by Equation (52))
δ_i^*	incompressible or velocity displacement thickness (defined by Equation (53))
$\delta\eta$	distance between two boundary layer nodal points (defined by Equation (105))
$\eta, \hat{\eta}$	transformed coordinate in a direction normal to the surface (defined by Equation (61)). Note: the hat is dropped from $\hat{\eta}$ throughout most of the report
θ	angle between a surface normal and a normal to the body centerline; also time in discussions of a charring ablation program
λ	thermal conductivity

SYMBOLS
(continued)

μ	shear viscosity
$\mu_1, \mu_2, \mu_3, \mu_4$	properties of the gas mixture (defined by Equations (21) and (24)) which reduce to unity, to m, to $1/m$, and to $\ell n\ m$, respectively, for assumed equal diffusion coefficients
ν	kinematic viscosity
$\xi, \hat{\xi}$	transformed streamwise coordinate (defined by Equation (61)). Note: the hat is dropped from $\hat{\xi}$ throughout most of the report
ρ	density
$\rho_w v_w$	total mass flux per unit area into the boundary layer
$\rho\varepsilon_{D_i}$	individual species turbulent eddy diffusivity (defined by Equation (2))
$\rho\varepsilon_D$	average turbulent eddy diffusivity, where it is assumed that all $\rho\varepsilon_{D_i} = \rho\varepsilon_D$
$\rho\varepsilon_H$	turbulent eddy conductivity (defined by Equation (18))
$\rho\varepsilon_M$	turbulent eddy viscosity (defined by Equation (12))
$\rho\tilde{\varepsilon}_M$	dimensionless eddy viscosity (defined by Equation (73))
σ	Stefan-Boltzmann constant
τ	local shear stress
ϕ_k	"elemental" source term (defined by Equation (29))
ψ_i	rate of mass generation of species i per unit volume due to chemical reaction

Subscripts

edge	pertains to boundary-layer edge
equil	pertains to surface equilibrium requirement

SYMBOLS
(concluded)

i	pertains to the i^{th} species or to the i^{th} nodal point in the boundary layer, starting with i = 1 at the surface
j	pertains to j^{th} species
k	pertains to k^{th} element (or base species)
ℓ	pertains to ℓ^{th} streamwise position
m	pertains to m^{th} iteration during the Newton-Raphson iteration process
n	pertains to the n^{th} nodal points, corresponding to the outer edge of the boundary layer solution
sp	pertains to the stagnation point
s.s.	pertains to the steady state energy balance requirement
w	pertains to wall
1	reference condition, usually taken as zero streamline from inviscid solution (synonymous with boundary-layer edge in the absence of an entropy layer)

Superscripts

κ	equal to unity for axisymmetric bodies and zero for two-dimensional bodies
*	signifies that quantity is normalized by α^* (e.g., $j_k^* = j_k/\alpha^*$)
'	represents partial differentiation with respect to η or $\hat{\eta}$ (usually η unless otherwise noted). Represents turbulent fluctuation in Section II.

SECTION I

INTRODUCTION

A computational procedure is described which is suitable for obtaining accurate numerical solutions of the nonsimilar multicomponent laminar and/or turbulent boundary layer with arbitrary equilibrium or nonequilibrium chemical systems, unequal diffusion and thermal diffusion coefficients for all species, radiation absorption and emission, second order transverse curvature effects, and a variety of surface boundary conditions including intimate coupling with transient charring-ablation energy and mass balances. A Fortran IV computer program has been developed in accordance with this analysis with the exceptions that 1) the chemical system is presently limited to equilibrium in the boundary layer, with or without selected rate-controlled surface reactions or surface catalyzed reactions, and 2) radiation absorption and emission within the boundary layer is not permitted in the version of the program reported here. This computer program, designated BLIMP, for Boundary Layer Integral Matrix Procedure, is described in reference 1. The analysis and computer program described herein are extensions of the previously developed BLIMP program for laminar boundary layer flows described in reference 2. The turbulent model which has been incorporated was reported earlier with a restriction to incompressible flows in reference 3.

The computational procedure was developed while attempting to take advantage of the most attractive features of other boundary-layer procedures. In light of the application of the procedure to be adopted, certain specific requirements were appropriate. In particular, minimization of the number of "nodal points" required to obtain a solution was judged to be of prime importance as a consequence of the relatively large times associated with state calculations for a general chemical environment and, in the streamwise direction, because of the desire to couple the boundary layer procedure to a transient internal conduction or ablation solution.

For a given accuracy, the number of necessary "nodal points" in the surface normal direction is controlled primarily by the nature of the functions which relate the dependent variables (and their derivatives) to the independent variable. Thus the continuous functions typically used in integral relations approaches require fewer "nodal points" than the functions with discontinuous first derivatives implied by most finite difference approximations. In order to permit relatively flexible profiles, sets of connected quadratics and cubics were selected to represent enthalpy, velocity, and elemental concentrations. The first derivatives

(and second derivatives with cubics) of these functions were made continuous at the connecting points. The advantages of such a "spline fit" are considered, for example, in reference 4.

If the general integral relations approach is followed, weighting functions must be selected. In the present study, as in reference 2, step weighting functions similar to those used by Pallone (reference 5) were used. That is, the conservation equations are integrated between nodal points (over strips) with a unity weighting function.

In the past when relatively large spacing in the streamwise direction has been desired, iterative procedures have generally been used to assure accuracy and stability. Some of these procedures have treated the solution in a manner resembling that used for a similar solution but with the addition of finite difference representations for the nonsimilar terms, a procedure which eliminates the necessity of special starting techniques. Using this basic approach, the specific treatment adopted in the current study follows most closely the matrix procedure used by Leigh (reference 6) wherein the iteration is a consequence of the solution of a set of linear and nonlinear algebraic relations. The general Newton-Raphson technique was used in the present procedure to solve these simultaneous equations. This technique results in linearized coupling between all relations required to characterize the boundary layer, and thus assures a more general, rapid and stable iterative convergence.

This document is the second report to describe completely the analysis and solution procedure associated with the BLIMP program, reference 2 being the first. The addition of a turbulent boundary layer capability and transverse curvature effects to the program provided the impetus for this report, therefore these two topics will receive perhaps a disproportionate share of discussion. Much of the rest of the analysis and solution procedure is the same as was reported in reference 2; the reader is referred to that document for more complete discussions.

This report concentrates on the fluid mechanical aspects of the problem and describes the basic numerical solution procedure. The procedures employed for calculating the equilibrium state of the gas and suggested for including rate-controlled reactions are described elsewhere (reference 7) since they are conveniently treated as subroutines to the basic boundary layer computational procedure. However, the terms which are directly involved in the boundary layer equations such as the "elemental source term" which arises from kinetic considerations are included in the present development. Similarly, radiation absorption and emission enters directly into the conservation equations only as a net radiation flux term in the energy equation. The calculation of this term can be conveniently accomplished by a subroutine. Multicomponent transport properties are based on the approximation reported in reference 8. Modification of the

conservation equations as a consequence of this approximation is described briefly here, and more completely in reference 2. The procedures employed for coupling to a transient charring ablation program are also described here.

Section II includes the entire mathematical modeling of the boundary layer flow including discussions of the general conservation equations, turbulent flow considerations, transverse curvature effects, coordinate transformations, and boundary conditions. Section III outlines the integral matrix method for solving the simultaneous differential equations including the integral strip relations, the mixing length solution procedure, and the Newton-Raphson iteration technique. Section IV presents some of the results obtained with the program. Section V describes the CABLE (Charring Ablation and Boundary Layer Environment) program wherein the boundary layer analysis is coupled to a one-dimensional charring ablation analysis at each body station and presents the results of a sample run. Section VI contains the summary, conclusions, and recommendations for further study.

SECTION II

MATHEMATICAL MODEL OF THE BOUNDARY LAYER

1. GENERAL CONSERVATION EQUATIONS

In the present analysis, the usual turbulent flow technique of breaking the species, velocity, and enthalpy fields into mean and fluctuating components, time averaging, and making appropriate order of magnitude approximations is used. Taking the results of these manipulations as a point of departure, the species mass balance equation becomes

$$\frac{\partial}{\partial s}\left(\rho u K_i r^{\kappa}\right) + \frac{\partial}{\partial y}\left(\rho v K_i r^{\kappa}\right) = \left[\left(\rho \varepsilon_{D_i} \frac{\partial K_i}{\partial y} - j_i\right) r^{\kappa}\right] + \psi_i r^{\kappa} \tag{1}$$

where s and y are the streamwise and normal coordinates, respectively, u and v are the velocity components in the s and y directions, respectively, K_i is the mass fraction of species i, r is the radius from the body centerline to the point of interest in a meridian plane for an axisymmetric shape, κ is zero for a flat plate and unity for a body of revolution, ρ is the density, and ψ_i represents the rate of mass generation of species i per unit volume due to chemical reaction. The individual species turbulent eddy diffusivity $\rho\varepsilon_{D_i}$ is defined in terms of the correlation of the fluctuating components of concentration and normal velocity, that is,

$$\rho \varepsilon_{D_i} = - \frac{\overline{(\rho v)' K_i'}}{\partial K_i / \partial y} \tag{2}$$

and j_i is the mass-diffusion rate of species i due to molecular processes. Since transverse curvature is to be included in the present analysis, r must be treated as a function of y whereas in the typical boundary layer analysis, r is set equal to r_o, the surface radius. The relationship between r, r_o, and y is

$$r(s,y) = r_o(s) + y \cos \theta \tag{3}$$

Figure 1 helps orient the reader to the nomenclature being used.

In equation (1) and in other conservation equations to follow, turbulent transport terms are expressed in Boussinesq form, that is, eddy viscosity, eddy

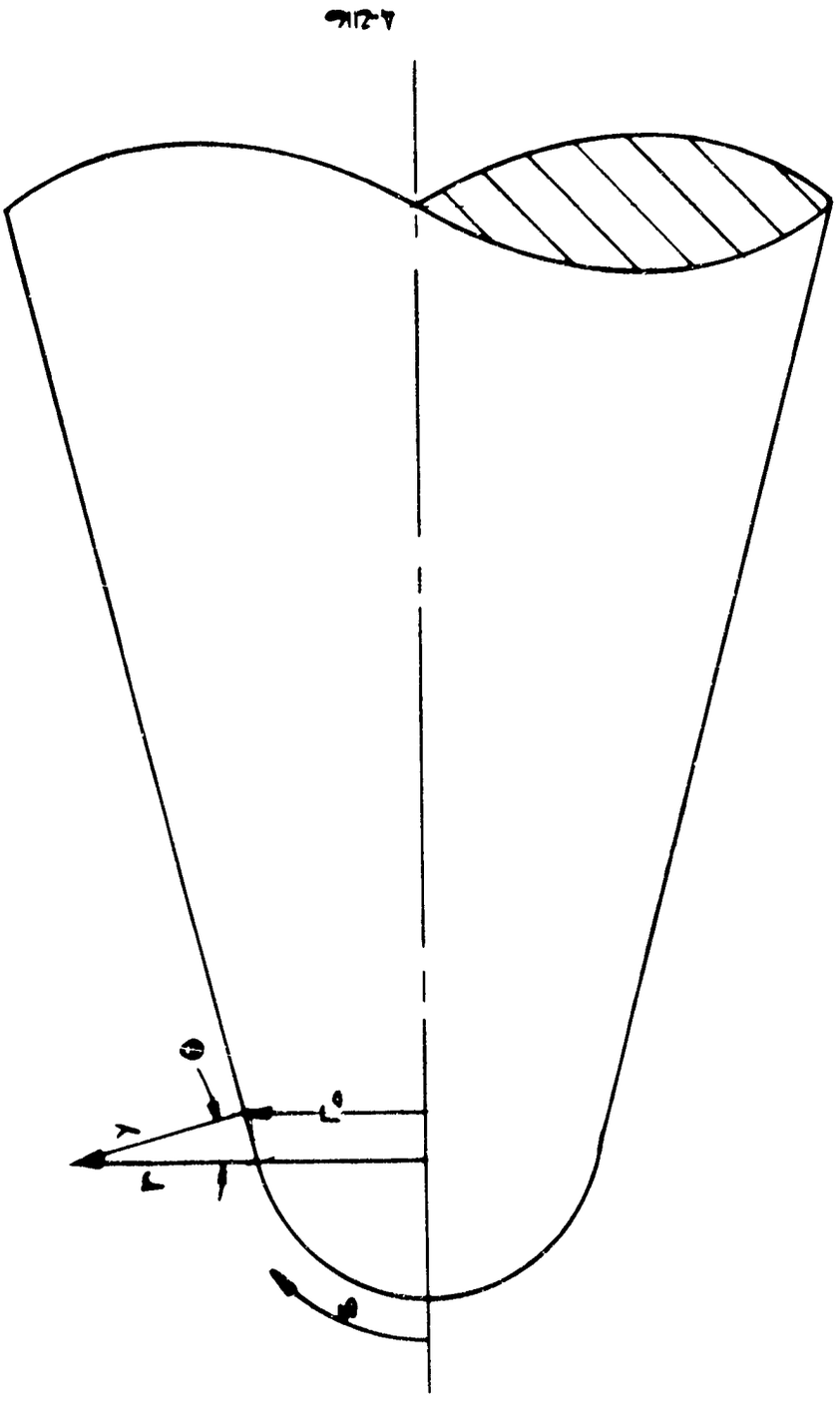

Figure 1. Definition of the Coordinate Nomenclature

diffusivity, and eddy conductivity. Hence all terms are time-averaged quantities and no need exists for using a superscript bar. In the order-of-magnitude arguments, terms of the following types have been eliminated: 1) triple correlations, 2) derivatives of turbulent correlations parallel to the wall, and 3) correlations involving turbulent components of molecular transport mechanisms.

When equation (1) is summed over all species, the global continuity equation results:

$$\frac{\partial \rho u r^K}{\partial s} + \frac{\partial \rho v r^K}{\partial y} = 0 \tag{4}$$

Combining equations (1) and (4), one obtains the species conservation equation

$$\rho u \frac{\partial K_i}{\partial s} + \rho v \frac{\partial K_i}{\partial y} = \frac{1}{r^K} \frac{\partial}{\partial y} \left[r^K \left(\rho \epsilon_{D_i} \frac{\partial K_i}{\partial y} - j_i \right) \right] + \psi_i \tag{5}$$

which can be written for each species i under consideration. The molecular diffusion rate j_i is expressed in general as

$$j_i = \frac{\rho}{\mathcal{M}^2} \sum_{j \neq i} \mathcal{M}_i \mathcal{M}_j D_{ij} \frac{\partial x_j}{\partial y} - D_i^T \frac{\partial}{\partial y} \ln T \tag{6}$$

where D_{ij} is the multicomponent diffusion coefficient of species i into j, D_i^T is the multicomponent thermal diffusion coefficient of species i, $\mathcal{M}$ is the local gas mixture molecular weight, and $\mathcal{M}_i$ is the molecular weight of species i. The Stefan-Maxwell relations may also be used

$$\frac{\partial x_i}{\partial y} = \sum_j \frac{x_i x_j}{\rho \mathcal{D}_{ij}} \left[\frac{j_j + D_j^T \frac{\partial \ln T}{\partial y}}{K_j} - \frac{j_i + D_i^T \frac{\partial \ln T}{\partial y}}{K_i} \right] \tag{7}$$

where x_i is the mole fraction of species i and $\mathcal{D}_{ij}$ is the <u>binary</u> diffusion coefficient of species i into j. Both of these expressions are complex in that the multicomponent diffusion coefficients are difficult to evaluate, and the Stefan-Maxwell relations provide only implicit expressions for the j_i. For the special case when all diffusion coefficients can be assumed equal and thermal diffusion can be ignored, Fick's law results:

$$j_i = - \rho \mathcal{D} \frac{\partial K_i}{\partial y} \tag{8}$$

This technique is not used in this analysis. A different simplification is used to work in terms of "elemental" conservation rather than species conservation however. The term"element" (in quotes) is used to refer to those atoms or groupings of atoms which according to equilibrium relations are conserved. Reference 7 discusses the merits of this approach in more detail. Defining α_{ki} as the mass fraction of "element" k in species i, multiplying the species equations by α_{ki}, and summing over all species results in the following conservation of "elements" equations:

$$\rho u \frac{\partial \tilde{K}_k}{\partial s} + \rho v \frac{\partial \tilde{K}_k}{\partial y} = \frac{1}{r^\kappa} \frac{\partial}{\partial y} [r^\kappa \quad \quad] \tag{9}$$

where $\tilde{K}_k$ is the mass fraction of "element" k [illegible] defined by

$$\tilde{K}_k = \sum_1 \alpha_{k1} K_1 \tag{10}$$

It has also been assumed that all $\varepsilon_{D_i} = \varepsilon_D$. The "elemental" approach results in significantly fewer simultaneous equations than the conservation of species approach, and the equating of all ε_{D_i} gives sufficiently accurate solutions for most types of problems.

The streamwise momentum equation can be written as

$$\rho u \frac{\partial u}{\partial s} + \rho v \frac{\partial u}{\partial y} = \frac{1}{r^\kappa} \frac{\partial}{\partial y} \left[\rho r^\kappa (\nu + \varepsilon_M) \frac{\partial u}{\partial y} \right] - \frac{\partial P}{\partial s} \tag{11}$$

where P is the local static pressure, and eddy viscosity ε_M is defined in terms of the Reynolds' stresses of turbulent flow by

$$\rho \varepsilon_M = - \frac{\overline{(\rho v)' u'}}{\frac{\partial u}{\partial y}} \tag{12}$$

The transverse direction momentum equation reduces to zero when longitudinal curvature effects are ignored.

The energy equation for this general chemistry boundary layer is

$$\rho u \frac{\partial H_T}{\partial s} + \rho v \frac{\partial H_T}{\partial y} = \frac{1}{r^K} \frac{\partial}{\partial y} \left[\rho r^K (\varepsilon_M + \nu) \frac{\partial u^2/2}{\partial y} + \right.$$

$$r^K (\lambda + \rho \varepsilon_H \bar{C}_p) \frac{\partial T}{\partial y} + r^K \sum_i \left(\rho \varepsilon_D \frac{\partial K_i}{\partial y} - j_i \right) h_i -$$

$$\left. \frac{r^K RT}{\rho} \sum_i \sum_j \frac{x_j D_i^T}{m_i \mathcal{D}_{ij}} \left(\frac{j_i}{K_i} - \frac{j_j}{K_j} \right) + r^K q_r \right] \tag{13}$$

where H_T is the total enthalpy (static plus kinetic)

$$H_T = h + \frac{u^2}{2} \tag{14}$$

h is the static enthalpy including chemical as well as sensible contributions

$$h = \sum_i K_i h_i \tag{15}$$

h_i is the static enthalpy of species i

$$h_i = \int_{T^o}^{T} C_{p_i} dT + h_i^o \tag{16}$$

T is the temperature, h_i^o is the heat of formation of spcies i at the reference temperature T^o, C_{p_i} is the specific heat of spcies i, $\bar{C}_p$ is the frozen specific heat of the gaseous mixture

$$\bar{C}_p = \sum_i K_i C_{p_i} \tag{17}$$

λ is the thermal conductivity, R is the gas constant, x_j is the mole fraction of species j, the turbulent enthalpy transport coefficient is defined by

$$\rho\varepsilon_H = - \frac{\sum_i K_i \overline{(\rho v)' h_i'}}{\sum_i K_i (\partial h_i / \partial y)} \tag{18}$$

and q_r is the net one-dimensional energy flux towards the surface due to radiation absorption and emission.

In the energy equation, as in the species conservation equations, it is necessary to evaluate molecular diffusion flux j_i. As discussed earlier, the general expressions for these terms are difficult to work with, therefore an approximate technique for multicomponent diffusion has been derived in reference 8 and is used in the present analysis. Since the present emphasis is on turbulent flow problems rather than molecular diffusion, only the results of the approximations for diffusion are presented here. Approximating $\mathcal{D}_{ij}$ by

$$\mathcal{D}_{ij} \approx \frac{\bar{D}(T,P)}{F_i F_j} \tag{19}$$

and defining

$$z_i \equiv \frac{m_i x_i}{F_i \mu_2} \tag{20}$$

$$\mu_1 \equiv \sum_j x_j F_j \tag{21}$$

$$\mu_2 \equiv \sum_j \frac{m_j x_j}{F_j} \tag{22}$$

$$\mu_3 \equiv \sum_i \frac{z_i}{m_i} \tag{23}$$

$$\mu_4 \equiv \ln(\mu_2 T^{c_t}) \tag{24}$$

$$c_t \approx -0.5 \tag{25}$$

$$\tilde{c}_p \equiv \sum_i z_i c_{p_i} \tag{26}$$

$$\tilde{h} \equiv \sum_i z_i h_i \tag{27}$$

$$\tilde{z}_k \equiv \sum_i \alpha_{ki} z_i \tag{28}$$

$$\phi_k \equiv \sum_i \alpha_{ki} \psi_i \tag{29}$$

the species and "elemental" laminar flux relations can be expressed as

$$j_i = - \frac{\rho \bar{D} \mu_2}{\mu_1 \mathcal{M}} \left[\frac{\partial z_i}{\partial y} + (z_i - K_i) \frac{\partial \mu_4}{\partial y} \right] \tag{30}$$

$$j_k = - \frac{\rho \bar{D} \mu_2}{\mu_1 \mathcal{M}} \left[\frac{\partial \tilde{z}_k}{\partial y} + (\tilde{z}_k - \tilde{K}_k) \frac{\partial \mu_4}{\partial y} \right] \tag{31}$$

Diffusive energy flux therefore becomes

$$q_a = - \left\{ \rho (\varepsilon_M + \nu) \frac{\partial \left(\frac{u^2}{2} \right)}{\partial y} + (\lambda + \rho \varepsilon_H \bar{C}_p) \frac{\partial T}{\partial y} + \rho \varepsilon_D \left(\frac{\partial h}{\partial y} - \bar{C}_p \frac{\partial T}{\partial y} \right) + \frac{\rho \bar{D} \mu_2}{\mu_1 \mathcal{M}} \left[\frac{\partial \tilde{h}}{\partial y} - \left(\tilde{C}_p + \frac{c_t{}^2 R}{\mu_1 \mu_2} \right) \frac{\partial T}{\partial y} + c_t R T \frac{\partial \mu_3}{\partial y} + (\tilde{h} - h + c_t R T \mu_3) \frac{\partial \mu_4}{\partial y} \right] \right\} \tag{32}$$

The "elemental" species conservation equation becomes

$$\rho u \frac{\partial \tilde{K}_k}{\partial s} + \rho v \frac{\partial \tilde{K}_k}{\partial y} = \frac{1}{r^\kappa} \frac{\partial}{\partial y} \left[r^\kappa \left(\rho \varepsilon_D \frac{\partial \tilde{K}_k}{\partial y} - j_k \right) \right] + \phi_k \tag{33}$$

while the energy equation can be expressed as

$$\rho u \frac{\partial H_T}{\partial s} + \rho v \frac{\partial H_T}{\partial y} = \frac{1}{r^\kappa} \frac{\partial}{\partial y} \left[r^\kappa (-q_a + q_r) \right] \tag{34}$$

If equal diffusion coefficients are assumed, $\mu_3 = 1/\mathcal{M}$, $\tilde{C}_p = \bar{C}_p$, and $\tilde{h} = h$. When thermal diffusion is to be neglected, $c_t = 0$ and $\mu_4 = \ln \mu_2$.

Equations (4), (11), (33), and (34) comprise the boundary layer conservation equations, including the approximations for unequal thermal and multicomponent diffusion coefficients of reference 8. The equations are parabolic in nature, therefore requiring specifications of the dependent variables, their derivatives,

or a linear combination thereof along the wall (y = 0), edge of the boundary layer, and at the initial body station. Typical sets of boundary conditions will be discussed later in this report. Also necessary in the mathematical formulation of the problem is the specification of the molecular transport properties, equation of state and equilibrium (or nonequilibrium) relations for the multicomponent gas, and a description of the eddy viscosity, conductivity and diffusivity. The molecular transport properties, equation of state, and equilibrium relations are discussed in references 2 and 7. The turbulent flow model is discussed in the next subsection.

2. TURBULENT FLOW CONSIDERATIONS

In the conservation equations developed above, the concepts of eddy viscosity, eddy diffusivity, and eddy conductivity were used to express the correlations of fluctuating velocity, species, and enthalpy fields in terms of mean field quantities. This is only one of several possible techniques of closing the set of equations (assuming satisfactory expressions for the eddy parameters are available), and it does not provide any information regarding the evolution of the turbulent correlations as the flow progresses downstream. Admittedly, it would be more desirable to describe the turbulent fluctuations in a more complete manner such as with an entrainment relation, turbulent kinetic energy relation, or a local turbulent constitutive equation (reference 9). However, these techniques are still in early stages of development even for incompressible single component flows, therefore a more proven approach was selected for the present analysis. The Boussinesq description of turbulent boundary layers has proved to be very useful, particularly for complex reacting flows such as are being described here, and will be used exclusively in the present analysis.

There is a wide amount of latitude possible even within the eddy viscosity framework of turbulence, particularly in applying classical incompressible models to compressible flows. The following two subsections describe how the turbulence model described in references 3 and 10 was applied to the present compressible flow problem.

a. Wall Region

Following the work of Clauser (reference 11) the boundary layer is divided into a law of the wall region and a wake region. The relatively thin wall region of the turbulent boundary layer is characterized by very steep gradients in the turbulent transport and mean field properties. Turbulent stress varies from zero at the wall to near its maximum value at the outer edge of the wall region. There is a vast amount of empirical evidence that these turbulent stresses and also the mean flow field properties can be described entirely in terms of the wall state, wall fluxes, thermodynamic and transport properties of

the fluid, and the normal coordinate y. Since the streamwise coordinate does not enter the solution for this region, the problem becomes a one-dimensional initial value problem. Eliminating s derivatives from the continuity equation and neglecting variations in r due to the thinness of the layer results in

$$\frac{d(\rho v)}{dy} = 0 \tag{35}$$

or

$$\rho v = \rho_w v_w \tag{36}$$

where the subscript w refers to the wall value. Thus the wall injection rate, $\rho_w v_w$, which may be a function of s, determines the transverse mass flux through the entire wall region. Using the same technique for the momentum equation and substituting equation (36)

$$\rho_w v_w u = \rho(\nu + \varepsilon_M) \frac{du}{dy} - \tau_w \tag{37}$$

where the wall shear, τ_w, is also typically a function of s. For flows over an impermeable wall with constant properties, this equation reduces to

$$\rho(\nu + \varepsilon_M) \frac{du}{dy} = \tau_w \tag{38}$$

or

$$\tau = \tau_w \tag{39}$$

indicating that shear can be considered constant in the wall region. For flows with injection or ablation, it is seen that shear varies with the mass injection rate and local velocity, that is,

$$\tau = \tau_w + \rho_w v_w u \tag{40}$$

This one-dimensional description of turbulence in the wall region will be useful in formulating a mixing length model for eddy viscosity as described in the following paragraphs. It should be made clear however, that only the wall region turbulent shear stress is assumed to behave in a one-dimensional fashion. In the solution procedure, the complete two-dimensional equations of motion are solved over the entire boundary layer.

A complete investigation of the validity of the mixing length postulate for flows with injection has been reported in reference 12. The analysis used in this investigation is an extension of that work; therefore, the reader should refer to reference 12 for more details.

Because of the current lack of understanding of turbulent mechanisms, "theoretical" predictions of the variation of turbulence near the wall must rely on empirical input into relations based on some phenomenological dependence. The generality of the ultimate goals of this analysis and the desire to approximate the physical situation dictated certain prerequisites for the turbulent transport relations. These were:

a) The relations must indicate a continuous variation of the turbulent transport properties from the wall to the fully turbulent region

b) The relations must be generally applicable to mass, momentum, and energy transport

c) The relations must be applicable to compressible or incompressible flows with real gas properties

d) The relations should be suitable for transpired and untranspired boundary layers without any, or a minimum, modification of form.

Two basic variations of the eddy viscosity hypothesis have been proposed in the past. The first type predicts the variation of turbulent viscosity from the wall to the fully turbulent region. Reichardt, Rannie, and Deissler, in references 13 through 15, have proposed such variations. The second type of hypothesis involves a variation of mixing length from the wall into the fully turbulent portion of the boundary layer. Rotta, von Kármán, and van Driest (references 16 to 18), have adopted this procedure. Data indicate that surface mass addition strongly affects the eddy viscosity profile, and it was found that the first type of hypothesis could not be simply modified to predict this variation. On the other hand, success of the mixing length theory in predicting profiles in the fully turbulent portion of the boundary layer with surface mass addition has been noted, for example, in references 19 and 20. It has generally been concluded that the slope of the linear relation between mixing length and distance from the wall is insensitive to surface mass addition. As a consequence of this apparent generality of the mixing length approach, it was adopted for the present studies.

The basic mixing length postulate can be expressed as

$$\overline{(\rho v)' u'} = \rho \ell^2 \left(\frac{du}{dy}\right)^2 = \rho \varepsilon_M \frac{du}{dy} \tag{41}$$

where the mixing length, ℓ, is a combination of various correlations, but retains some relationship to the scale of turbulence. Prandtl proposed that this

length will, in its simplest form, be related to the distance from a wall, at least in the region of development of turbulence. His proposition that

$$\frac{d\ell}{dy} = \text{constant, } K \tag{42}$$

has been tested under a variety of conditions and found to be quite adequate in the fully turbulent portion of the wall region.

As the wall is approached however, this simple relation is no longer appropriate, and, in fact, it can be shown theoretically that

$$\left.\begin{aligned} \lim_{y\to o} \ell &= 0 \\ \lim_{y\to o} \frac{d\ell}{dy} &= 0 \end{aligned}\right\} \tag{43}$$

This is a consequence of the Reichardt-Elrod criterion (see reference 12). Thus, two criteria are specified, namely, Prandtl's hypothesis which is appropriate in the fully turbulent portion of the wall region and the Reichardt-Elrod wall criterion as expressed by equation (43).

Several means of expressing a relation covering the full range of y and including these limiting criteria have been used by other investigators. It is advantageous in considering extensions of mixing length theory to establish some physical logic for the selected relation. Unfortunately, the understanding of transition from the laminar to the turbulent portions of the layer has not reached a state permitting any quantitative specification. Therefore, the selected model can be based only on qualitative understanding of the process, dimensional considerations, and the above limiting criteria. These criteria are satisfied for incompressible flows by a simple implicit relation of the form

$$\frac{d\ell}{dy} \propto (Ky - \ell) \tag{44}$$

which implies that the rate of increase of the mixing length is proportional to the difference between the value postulated by Prandtl (Ky) and its actual value. This rate of increase is assumed to be augmented by the local shear and retarded by the local viscosity. Using these parameters to nondimensionalize the above relation yields

$$\frac{d\ell}{dy} = (Ky - \ell)\,\frac{\sqrt{\tau/\rho}}{y_a^+ \nu} \tag{45}$$

where y_a^+ is the constant of proportionality. The coefficients K and y_a^+ were shown in reference 12 to be invariant for a wide variety of flow conditions at values of 0.44 and 11.83, respectively.

For compressible flows, the physical arguments must be changed somewhat. Rather than describing the scale of a turbulent eddy, it seems appropriate to describe the mass of the eddy, $\rho\ell$, with respect to the mass available, $\int \rho\, dy$. Thus, by analogy to equation (44), the rate of increase of the mass of an eddy will be taken to be proportional to the difference between the mass available between the wall and the point of interest (times an appropriate constant) and the mass of the eddy:

$$\frac{1}{\rho}\frac{d\rho\ell}{dy} \propto K\int_o^y \rho\, dy - \rho\ell \tag{46}$$

Nondimensionalizing as above,

$$\frac{d\rho\ell}{dy} = \left(K\int_o^y \rho\, dy - \rho\ell\right)\frac{\sqrt{\tau/\rho}}{y_a^+\nu} \tag{47}$$

The constants K and y_a^+ are left at their incompressible values of 0.44 and 11.83 for the time being. The integral-differential character of this mixing length equation indicates a difficult solution procedure in the physical coordinate plane. However, in the (η,ξ) coordinates introduced by the Levy-Lees transformation, the mixing length equation simplifies somewhat. This will be discussed further in Section II.3.

For the special case of constant properties and zero injection (constant shear), equation (47) can be integrated to yield

$$\ell = \frac{K\nu}{u_\tau}\left\{y^+ - y_a^+\left[1 - \exp\left(-\frac{y^+}{y_a^+}\right)\right]\right\} \tag{48}$$

where

$$u_\tau = \sqrt{\frac{\tau_w}{\rho}} \tag{49}$$

$$y^+ = \frac{yu_\tau}{\nu}$$

It can be seen that the Reichardt-Elrod criteria is satisfied at the wall. For large y, Rotta's (reference 16) expression

$$\ell = \frac{K\nu}{u_\tau} (y^+ - y_a^+) \tag{50}$$

is obtained. This special case result for constant property zero injection flows is not used in the general analysis technique presented here.

b. Wake Region

The wake region of a turbulent boundary layer is so named because the flow in this region tends to have a wake-like character. In particular, the outer 80 to 90 percent of the boundary layer combined with the local turbulent eddies dominates the mixing processes within the flow, and the viscous effects become second order. Gradients in the wake region are typically much smaller than those of the wall region. Since the pressure gradient and streamwise derivative terms are important in the wake region, the two-dimensional character of the turbulence must be considered in its entirety, as opposed to the approximations of the wall region.

A fortunate feature of the wake portion of the boundary layer is that eddy viscosity is nearly constant across this region, at least for equilibrium* incompressible flows. In particular, Clauser (reference 11) was able to relate the eddy viscosity to edge velocity and a length scale δ^*

$$\varepsilon_M = 0.018\, u_1 \delta^* \tag{51}$$

for a great quantity of experimental data taken in equilibrium flows.

The quantity δ^* in this relation is the displacement thickness

$$\delta^* = \int_0^\infty \left(1 - \frac{\rho u}{\rho_1 u_1}\right) dy \tag{52}$$

in which the densities cancel out for incompressible flows. For compressible flows, this length scale is inappropriate since under some conditions δ^* can be negative. Defining a velocity displacement thickness as

*Equilibrium as used here refers to a particular pressure gradient, $(\delta^*/\tau_w)(dP/dx)$, which results in self-similar velocity profiles (reference 11).

$$\delta_i^* = \int_0^\infty \left(1 - \frac{u}{u_1}\right) dy \tag{53}$$

the eddy viscosity in the wake portion of the flow will be taken as

$$\varepsilon_M = 0.018\ u_1 \delta_i^* \tag{54}$$

A satisfactory technique for choosing the correct ε_M expression at any particular body station is to use the wall region expression

$$\varepsilon_M = \ell^2 \frac{du}{dy} \tag{55}$$

until ε_M exceeds the wake value, equation (54), at which point ε_M is held constant at the wake value for the remainder of the boundary layer thickness.

c. Boundary Layer Transition

As can be seen from the form of the conservation equation, both the molecular and turbulent transport terms are considered simultaneously. This is necessary since an accurate description of the turbulent boundary layer requires that the time-averaged fluctuation terms disappear near the wall. Another reason for the inclusion of these terms is the description of laminar or transitional flows. From the form of equation (54), it can be seen that for very small δ_i^* the turbulent stresses will be small compared to the laminar ones. Without any constraints on the equations as stated above, kinematic and eddy viscosities are equal at a velocity displacement thickness Reynolds number of 56:

$$1 = \frac{\varepsilon_M}{\nu} = \frac{0.018\ u_1 \delta_i^*}{\nu}$$

$$\therefore \mathrm{Re}_{\delta_i^*} \simeq 56$$

This "natural" transition Reynolds number is too low for most situations, therefore ε_M is artificially set to zero until some other criterion is satisfied. A Reynolds number on momentum thickness, Re_θ, is currently used to trigger transition. Once the prespecified transition value for Re_θ is exceeded, turbulent transport properties are immediately brought into the solution. Being a nonsimilar solution, the influence of the upstream laminar profile is felt for some distance downstream, thus simulating a transitional region which is not too unlike the physical situation.

3. COORDINATE TRANSFORMATIONS

The equations of motion for a boundary layer flow can be solved in the physical (s,y) plane by numerous techniques, however it is generally advantageous to transform the problem to another coordinate system. The transformed coordinates offer the advantages of nondimensionalizing the solution, confining the solution to a narrower region, minimizing changes in the dependent variables, simplifying boundary conditions and occasionally result in the deletion of streamwise derivative terms. This latter possibility occurs only under very restrictive sets of boundary conditions. The coordinate transformation in the present analysis is a variation of the Levy-Lees transformation and is derived in its entirety in Appendix I. The standard Levy-Lees transformation takes the form

$$\xi = \int_o^s \rho_1 u_1 \mu_1 r_o^{2K}\, ds$$

$$\eta = \frac{r_o^K u_1}{\sqrt{2\xi}} \int_o^y \rho\, dy \tag{56}$$

The first alteration of this transformation is actually a mathematical convenience for carrying out the numerical solution. Introducing a stretching parameter α_H in the normal coordinate, a new coordinate system is defined by

$$\bar{\xi} = \xi$$

$$\bar{\eta} = \frac{\eta}{\alpha_H} \tag{57}$$

The parameter α_H is taken as a function of $\bar{\xi}$ only and is determined implicitly during the solution. Its purpose is to stretch the η coordinate such that the boundary layer remains of constant thickness in the $\bar{\eta}$ coordinates.

Since a new variable $\alpha_H(\xi)$ is introduced, an additional relation is required. This is conveniently supplied by constraining some arbitrary point near the boundary-layer edge, $\bar{\eta}_c$, to have a specified streamwise velocity, c, near (but something less than) the edge value:

$$f'\Big|_{\bar{\eta}_c} = cf'\Big|_{\bar{\eta}_{edge}} \tag{58}$$

where f is the transformed stream function defined as

$$f - f_w = \int_o^{\eta} \frac{u}{u_1} d\eta = \alpha_H \int_o^{\bar{\eta}} \frac{u}{u_1} d\bar{\eta} \tag{59}$$

and the prime denotes differentiation with respect to $\bar{\eta}$ so that

$$f' = \alpha_H \frac{u}{u_1} \tag{60}$$

Examples of the utility of the stretching parameter α_H are contained in reference 2.

The second change in the Levy-Lees transformation has to do with the transverse curvature effect. For very thin axisymmetric bodies, it is possible to have boundary layer thicknesses on the order of the body radius r_o. In this instance, it is necessary to treat r as a function of y, thereby including its variation through the boundary layer. The coordinate transformations become

$$\hat{\xi} = \int_o^s \rho_1 u_1 \mu_1 r_o^{2K} ds$$

$$\hat{\eta} = \frac{u_1}{\alpha_H \sqrt{2\hat{\xi}}} \int_o^y \rho r^K dy \tag{61}$$

Utilization of the above coordinate transformation relations results in a new set of governing equations in the $(\hat{\xi},\hat{\eta})$ coordinate plane which will be given below. The hat (^) notation will be dropped for the remainder of the text for simplicity, however ξ and η are given by equation (61). Primes will refer to derivatives with respect to η except when noted otherwise.

The global continuity equation is automatically satisfied by the definition of a transformed stream function $f(\xi,\eta)$, shown in equation (59), and redefined here in the final coordinate system:

$$f - f_w = \alpha_H \int_o^{\eta} \frac{u}{u_1} d\eta \tag{62}$$

$$f_w = -\frac{1}{\sqrt{2\xi}} \int_o^\xi \frac{\rho_w v_w}{\rho_1 u_1 \mu_1 r_o^K} d\xi \tag{63}$$

The other governing equations will be discussed separately.

Streamwise momentum equation

$$ff'' + \left[\frac{tC\left(1 + \frac{\varepsilon_M}{\nu}\right)}{\alpha_H} f''\right]' + \beta\left(\alpha_H^2 \frac{\rho_1}{\rho} - f'^2\right)$$

$$= 2\left(f' \frac{\partial f'}{\partial \ln \xi} - f'^2 \frac{\partial \ln \alpha_H}{\partial \ln \xi} - f'' \frac{\partial f}{\partial \ln \xi}\right) \tag{64}$$

In this equation, utilizing the technique of reference 21, the transverse curvature effect is included entirely in the coordinate transformation and in the definition of t:

$$t \equiv \left(\frac{r}{r_o}\right)^2 = 1 + \frac{2\alpha_H \sqrt{2\xi} \cos\theta}{u_1 r_o^2} \int_o^\eta \frac{1}{\rho} d\eta \tag{65}$$

where θ is the angle between the surface normal and a plane normal to the body centerline (see Figure 1). Other definitions of interest are:

$$C \equiv \frac{\rho\mu}{\rho_1 \mu_1} \tag{66}$$

$$\beta \equiv 2 \frac{\partial \ln u_1}{\partial \ln \xi} \tag{67}$$

For solutions without consideration of transverse curvature, t is set to 1.0 throughout the boundary layer.

Turbulent model equations

The turbulent fluctuations are related to the mean field through the eddy models described in equations (2), (12), and (18). Eddy viscosity is described by a wall law and wake law, while eddy diffusivity and conductivity are related to eddy viscosity by turbulent Schmidt and Prandtl numbers:

$$Sc_t \equiv \frac{\varepsilon_M}{\varepsilon_D} \tag{68}$$

$$Pr_t \equiv \frac{\varepsilon_M}{\varepsilon_H} \tag{69}$$

Defining

$$\delta \equiv \frac{\sqrt{2\xi}}{\rho_1 u_1 r_o^K} \tag{70}$$

$$\tilde{\ell} \equiv \frac{\rho \ell}{\rho_1 \delta} \tag{71}$$

$$Re_\delta \equiv \frac{\rho_1 u_1 \delta}{\mu_1} \tag{72}$$

$$\tilde{\varepsilon}_M \equiv \frac{\rho^2 \varepsilon_M}{\rho_1 \mu_1} \tag{73}$$

The wall region eddy viscosity relation becomes

$$\tilde{\varepsilon}_M = \frac{\rho(Re_\delta)}{\rho_1 \alpha_H^2} \tilde{\ell}^2 f'' \qquad \text{(wall region)} \tag{74}$$

$$\tilde{\varepsilon}_M = 0.018 \left(\frac{\rho}{\rho_1}\right)^2 Re_{\delta_i^*} \qquad \text{(wake region)} \tag{75}$$

where

$$\delta_i^* = \delta \alpha_H \int_0^\infty \left(1 - \frac{f'}{\alpha_H}\right) \frac{\rho_1}{\rho} \, d\eta \tag{76}$$

Transverse curvature is not considered in determining the wake region length scale δ_i^*. The governing equation for mixing length, which must be solved for the entire boundary layer although it is used only in the wall region, is

$$\frac{d\tilde{\ell}}{d\eta} = \frac{\alpha_H \rho_1 \delta \sqrt{\tau/\rho}}{y_a^+ \mu} \left(K \alpha_H \eta - \tilde{\ell}\right) \tag{77}$$

Since mixing length is used only in the wall region, it is valid to use the one-dimensional expression for shear stress, equation (40). In transformed coordinates, this becomes

$$\frac{\tau}{\rho} = \frac{u_1^2}{\alpha_H}\frac{\rho_1}{\rho}\left[\frac{C_w}{\alpha_H}\frac{f''_w}{Re_\delta} + \frac{\rho_w v_w}{\rho_1 u_1} f'\right] \tag{78}$$

Energy equation

$$fH_T' + \left[t(-q_a^* + q_r^*)\right]' = 2\left(f'\frac{\partial H_T}{\partial \ln \xi} - H_T'\frac{\partial f}{\partial \ln \xi}\right) \tag{79}$$

where q_a^* is the normalized diffusive energy flux away from the surface including turbulent fluxes and q_r^* is the normalized radiant energy flux toward the surface:

$$q_a^* = q_a/\alpha^* \tag{80}$$

$$q_r^* = q_r/\alpha^* \tag{81}$$

The flux normalizing parameter α^* is defined by

$$\alpha^* \equiv \frac{\rho_1 u_1 \mu_1 r_o^\kappa}{\sqrt{2\xi}} = \frac{\mu_1}{\delta} \tag{82}$$

Diffusive energy flux q_a in the transformed coordinates is defined later in this section.

"Elemental" species equations

$$f\tilde{K}_k' + \left[t\left(\frac{\tilde{\varepsilon}_M}{\alpha_H Sc_t}\tilde{K}_k' - j_k^*\right)\right]' + \alpha_H \phi_k = 2\left(f'\frac{\partial \tilde{K}_k}{\partial \ln \xi} - \tilde{K}_k'\frac{\partial f}{\partial \ln \xi}\right) \tag{83}$$

where j_k^* is the normalized diffusive flux of "element" k:

$$j_k = j_k^* \alpha^* \tag{84}$$

Diffusive fluxes

The normalized diffusive energy flux is given by

$$q_a^* = -\frac{C}{\alpha_H}\left[\frac{f'f''}{\alpha_H^2}u_1^2 + \frac{\bar{C}_p}{Pr}T' + \frac{1}{\overline{Sc}}\left(\tilde{h}' - \left(\tilde{C}_p + \frac{c_t^2 R}{\mu_1\mu_2}\right)T' + c_t RT\mu_3' + (\tilde{h} - h + c_t RT\mu_3)\mu_4'\right)\right]$$
$$- \frac{\tilde{\varepsilon}_M}{\alpha_H}\left[\frac{f'f''}{\alpha_H^2}u_1^2 + \frac{\bar{C}_p}{Pr_t}T' + \frac{1}{Sc_t}(h' - \bar{C}_p T')\right] \qquad (85)$$

where Pr is the Prandtl number based on the frozen specific heat

$$Pr \equiv \frac{\bar{C}_p\mu}{\lambda} \qquad (86)$$

The turbulent contribution to the diffusive energy flux is contained in the last bracketed term, which is left uncombined with the other terms for clarity. The fact that the gross simplifications of the turbulent model are included in the same equation with the rather sophisticated unequal molecular diffusion model is merely a mathematical convenience stimulated by the requirement for calculations in all types of flow situations, including both laminar and turbulent flows. Unequal molecular diffusion and thermal diffusion effects may be important in the laminar sublayer region of a turbulent boundary layer, however.

Normalized molecular diffusive flux of species i is

$$j_i^* = -\frac{C}{\alpha_H \overline{Sc}}\left[\tilde{z}_i' + (\tilde{z}_i - \tilde{K}_i)\mu_4'\right] \qquad (87)$$

where $\overline{Sc}$ is a system property defined by

$$\overline{Sc} \equiv \frac{\mu_1\mu_m}{\rho\bar{D}\mu_2} \qquad (88)$$

The $\overline{Sc}$ is a Schmidt number based on the self-diffusion coefficient for a fictitious species representative of the system as a whole. The normalized molecular diffusive flux of the k^{th} "elemental" species is

$$j_k^* = - \frac{C}{\alpha_H \overline{Sc}} \left[\tilde{z}_k' + (\tilde{z}_k - \tilde{K}_k) \mu_4' \right] \tag{89}$$

When certain groupings of parameters are constant so that the flow similarity assumption is valid, the terms on the right-hand side of the conservation equations (equations (64), (79) and (83)) vanish, in which case the conservation equations become ordinary differential equations. It should be emphasized that the equations as presented herein are equivalent to the corresponding boundary-layer equations presented in Section II.1. That is, no similarity assumptions have been made in their development.

Equations (82), (67), and (63) for α^*, β, and f_w, respectively, are indeterminant at the stagnation point of a blunt body. Special forms for these equations valid at the stagnation point are shown in reference 2 to be given by

$$\alpha_{sp}^* = \left(\rho_1 \mu_1 \frac{du_1}{ds} \Big/ \beta \right)_{sp}^{1/2} \tag{90}$$

$$f_{w_{sp}} = - \left(\rho_w v_w / \alpha^* \right)_{sp} \tag{91}$$

where for Newtonian flow

$$\beta_{sp} = 1/(\kappa + 1) \tag{92}$$

and

$$\left. \frac{du_1}{ds} \right|_{sp} = (2P/\rho)_{sp}^{1/2} \Big/ R_{eff} \tag{93}$$

with R_{eff} an effective nose radius taking into account the shock shape. Alternatively, β_{sp} and $(du_1/ds)_{sp}$ can be computed from curve fits of the inviscid pressure distribution. The transverse curvature parameter t also requires some special treatment at a stagnation point. The troublesome term is $\cos \theta / r_o$ which is evaluated at a stagnation point by

$$\left(\frac{\cos\theta}{r_o} \right)_{sp} = \left[6 \frac{d^2(1 - \frac{r_o}{s})}{ds^2} \right]^{1/2} \tag{94}$$

In addition, to improve the accuracy of numerical integration procedures in the nose region, ξ and f_w can be computed by the following relations

$$\xi = \frac{1}{2(\kappa + 1)} \int_0^{s^{2\kappa+2}} \left[\rho_1 \mu_1 \left(\frac{u_1}{s}\right) \left(\frac{r_o}{s}\right)^{2\kappa} \right] d(s^{2\kappa+2}) \tag{95}$$

$$f_w = - \frac{(2\xi)^{-1/2}}{(\kappa + 1)} \int_0^{s^{\kappa+1}} \left[\rho_w v_w \left(\frac{r_o}{s}\right)^{\kappa} \right] d(s^{\kappa+1}) \tag{96}$$

which take advantage of the fact that u_1/s and r_o/s vary more nearly linearly in the stagnation region than do u_1 and r_o. These equations are also discussed more thoroughly in reference 2.

4. BOUNDARY CONDITIONS

The usual set of boundary conditions for the boundary layer flow problem consists of the specification of initial profiles for the dependent variables f', H_T, and $\tilde{K}_k$, plus additional specifications of these quantities along the wall and at the edge of the boundary layer, and the specification of f_w along the wall. However, since the main utilization for the analytical technique presented here is to compute boundary layer properties for flows over ablating or transpired surfaces (heat shields, rocket nozzles, etc.), these boundary conditions have been greatly generalized. The numerous options resulting from this generalization are discussed below.

The boundary layer edge conditions typically are found from an isentropic expansion from known elemental gas composition and stagnation conditions. Thus, given a set of stagnation conditions and a description of local static pressure along the surface of interest, the techniques of reference 7 may be used to establish the entropy of the gaseous mixture which, when combined with the specified pressures, can be used to establish the complete equilibrium edge gas state at each body station. Edge boundary conditions then would consist of

$$\begin{aligned} f'_{edge} &= \alpha_H \\ H_{T_{edge}} &= H_{T_{edge}} \Big|_{actual} \\ \tilde{K}_{k_{edge}} &= \tilde{K}_{k_{edge}} \Big|_{actual} \end{aligned} \tag{97}$$

where the subscript "edge" refers to conditions specified at η_{edge}, chosen to be outside the boundary layer (see Section II.3). An additional constraint at the boundary layer edge which is necessary only when cubics are used is the requirement of zero slope, i.e.,

$$\begin{aligned} f''_{edge} &= 0 \\ H'_{edge} &= 0 \\ \tilde{K}'_{k_{edge}} &= 0 \end{aligned} \tag{97a}$$

It is possible to specify edge entropy as well as pressure. The techniques of reference 7 are then used to establish the complete edge gas state for a non-isentropic expansion around the body of interest.

Initial profiles of f', H_T, and $\tilde{K}_k$ are more difficult to establish for the general problem, therefore calculations are often started with reasonable assumed profiles far upstream of the region of interest so that effects of erroneous assumptions will die out. Another possibility for initially laminar problems is to assume a similar solution as a starting profile. This assumption reduces the equations to ordinary differential equations at the starting point, which may be solved simultaneously for a set of profiles unique to the assumed edge and wall state. The similar solution is exact at a body stagnation point, therefore this option is particularly valuable for blunt body problems.

The wall boundary conditions allow the widest selection of options. The simplest combination is the straightforward assignment of velocities, enthalpy, and elemental concentrations at the wall:

$f'_w = 0$	no slip	
$f_w = f_w(\xi)$	specified $\rho_w v_w$	
$H_{T_w} = h_w(\xi)$	specified enthalpy of gas at the wall	(98)
$\tilde{K}_{k_w} = \check{K}_{k_w}(\xi)$	specified wall gas elemental composition*	

Wall temperature may be used to find wall enthalpy in the above formulation. Also, wall mass diffusive fluxes of up to three individual injectants may be

*It is physically unrealistic in most cases to assign $\tilde{K}_{k_w}$ when diffusion coefficients are unequal since the contribution to $\tilde{K}_{k_w}$ by preferential diffusion of the various "elements" to the surface is not known a priori.

assigned in lieu of $\tilde{K}_{k_w}$ and $\rho_w v_w$. With the values of the dependent variables all directly assigned in this manner, the boundary layer problem is uncoupled from the surface chemistry interaction.

The inclusion of surface material/boundary layer gas interaction chemistry in the boundary layer problem forms the second major set of wall boundary condition options. Using the surface thermochemistry techniques of reference 7, it is possible to specify given mass fluxes of the (up to) three injectants at the wall and require chemical equilibrium between the injectants, the wall material, and the adjacent gas stream. In this instance, the values of H_{T_w} (i.e., T_w) and $\tilde{K}_{k_w}$ are found by simultaneous solution of the local surface chemical equilibrium equations, surface mass balances, and the no-slip velocity boundary conditions. Alternatively, selected chemical reactions at the wall can be kinetically controlled through Arrhenius-type rate law formulations and included in the surface chemistry description.

In the use of this boundary layer technique in conjunction with in-depth charring ablation analyses, the chemically active injectants might result from the pyrolysis of an internally decomposing material, surface material combustion or phase change, and mechanical removal. A variation of this type of wall boundary condition is to specify the wall temperature or enthalpy and allow the surface chemistry calculations to compute the necessary $\rho_w v_w$ and $\tilde{K}_{k_w}$. In summary, the surface equilibrium wall boundary condition is

$$
\begin{aligned}
f'_w &= 0 && \text{no slip} \\
f_w &= f_w(\xi) && \text{specified } \rho_w v_w \\
H_{T_w} &= H_{T_{w_{equil}}} && \text{from surface equilibrium requirement} \\
\tilde{K}_{k_w} &= \tilde{K}_{k_{w_{equil}}} &&
\end{aligned}
\qquad (99)
$$

The final wall boundary condition category involves the use of a steady state energy balance at the surface. A general surface energy balance can best be understood by examination of a schematic representation of the energy fluxes to an ablating or nonablating ($\dot{m}_c = 0$) surface:

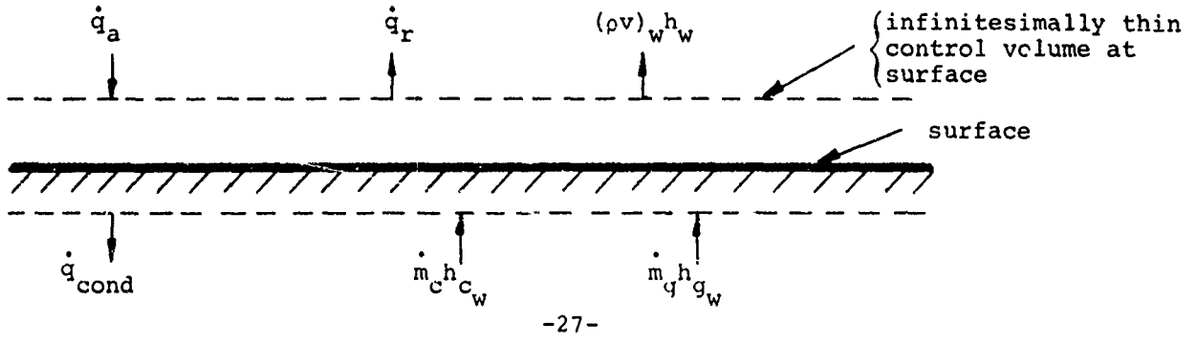

Summing terms,

$$\dot{m}_g h_{g_w} + \dot{m}_c h_{c_w} + \dot{q}_a - \dot{q}_r - (\rho v)_w h_w - \dot{q}_{cond} = 0 \tag{100}$$

which is valid in either a transient or steady-state situation. In general, an in-depth charring ablation solution would be needed to provide the conduction term $\dot{q}_{cond}$ and the pyrolysis gas rate, $\dot{m}_g$. Under steady state conditions, the internal pyrolysis "front" and the charred surface are assumed to be receding at the same rate, therefore requiring that the energy conducted into the wall material must equal the enthalpy rise of the wall material and pyrolysis gases. In equation form

$$\dot{q}_{cond} - \dot{m}_c(h_{c_w} - h_c^o) - \dot{m}_g(h_{g_w} - h_g^o) = 0 \tag{101}$$

Substituting into equation (100), the steady state energy balance becomes

$$\dot{q}_{a_w} - \dot{q}_{r_w} - (\rho v)_w h_w + \dot{m}_c h_c^o + \dot{m}_g h_g^o = 0 \tag{102}$$

In this equation, $\dot{q}_{a_w}$ is the wall value of the energy flux defined in equation (85), and is found in the course of the boundary layer solution. The surface equilibrium requirement is always used in conjunction with the steady state energy balance. Therefore, if one specifies the compositions and heats of formation of the pyrolysis gas and char materials, the simultaneous solution of the energy equation above and the surface chemistry relations mentioned earlier completely couples the boundary layer flow to the surface response. The steady state assumption is good even in transient situations for large ablation rates or small thermal diffusivity of the ablation material (reference 22). In summary, the use of the steady state energy balance results in the following:

$$\begin{aligned}
&f'_w = 0 && \text{no slip}\\
&H_{T_w} = H_{T_{w_{s.s.}}} && \text{steady state energy balance}\\
&\left.\begin{aligned} f_w &= f_{w_{equil}} \\ \tilde{K}_{k_w} &= \tilde{K}_{k_{w_{equil}}} \end{aligned}\right\} && \text{surface equilibrium requirement}
\end{aligned} \tag{103}$$

SECTION III

INTEGRAL MATRIX SOLUTION PROCEDURE

The solution of the transformed boundary layer equations presented in Section II uses an integral matrix method which has been developed specifically for the solution of chemically reacting, nonsimilar, coupled boundary layers. A complete presentation of the integral matrix procedure was included in reference 2, where solution of laminar flow problems was discussed. In the present effort, this technique has remained essentially unchanged, however new variables and equations have been added to describe the turbulent aspects of the flow and to include transverse curvature effects. The present discussion will therefore review only the highlights of the method, and the reader may refer to reference 2 for more details.

In the integral matrix procedure, the primary dependent variables and their derivatives with respect to η are related by Taylor series expansions such that these dependent variables are represented by connected quadratics or cubics (either option is available). That is, f', H_T, and $\tilde{K}_k$ are expanded in Taylor series form and the series are truncated to reflect the proper polynomial representation. A nodal network is defined through the boundary layer and the Taylor series expansions are assumed valid between each set of nodes, with an additional requirement of continuous first and second derivatives (a spline fit). Primarily for convenience, the conservation equations are integrated across each "strip" (between nodal points) using a unity weighting function. The linear Taylor series expansions together with linear boundary conditions form a very sparse matrix which has to be inverted only once for a given problem. The nonlinear boundary layer equations and nonlinear boundary conditions are then linearized, the errors being driven to zero using Newton-Raphson iteration.

In Section III.1, the Taylor series expansions are presented, the integrated form of the momentum equation is discussed, and techniques for evaluating integral terms are demonstrated. In Section III.2, the special techniques applied to the mixing length differential equation are discussed, and in Section III.3 the actual simultaneous equation solution procedure is summarized.

1. INTEGRAL STRIP EQUATIONS WITH SPLINED INTERPOLATION FUNCTIONS

Consider the boundary layer in the region of a given streamwise station s as being divided into N-1 strips connecting N nodal points. These nodal points are designated by η_i where i = 1 at the wall and N at the edge of the boundary layer. Consider a function $p(\eta)$ which with all its derivatives is continuous

in the neighborhood of the point $\eta = \eta_i$. Then, for any value of η in this neighborhood, $p(\eta)$ may be expressed in a Taylor series expansion as

$$p_{i+1} = p_i + p_i'\delta\eta + p_i'' \frac{(\delta\eta)^2}{2} + p_i''' \frac{(\delta\eta)^3}{6} + p_i'''' \frac{(\delta\eta)^4}{24} + \ldots \tag{104}$$

where

$$\delta\eta = \eta_{i+1} - \eta_i \tag{105}$$

Conventional finite difference schemes, in effect, typically truncate the Taylor series after the first term and use the resulting expression to relate p' to p, etc., that is

$$p_i' = \frac{p_{i+1} - p_i}{\delta\eta} \tag{106}$$

Round-off error is then of order $(\delta\eta)^2$ and many nodes must be chosen to bring this value down to acceptable limits. One can achieve a reduction in the number of nodes for a given accuracy by employing a quadratic or cubic relation representing the function p over the interval of interest. This can be achieved by truncating the Taylor series after the third or fourth term. The cubic approximation will be used for the remainder of this discussion. The p_i can be considered to be any of f_i, f_i', f_i'', f_i''', H_{T_i}, H_{T_i}', H_{T_i}'', $\tilde{K}_{k_i}$, $\tilde{K}_{k_i}'$, or $\tilde{K}_{k_i}''$. Since the highest derivatives of the dependent variables which appear in the boundary layer equations are f_i''', H_{T_i}'' and $\tilde{K}_{k_i}''$, it is reasonable to truncate the series at the next highest derivative and to consider that derivative as being constant between η_i and η_{i+1}, that is,

$$\begin{aligned}
{}_i f_{i+1}'''' &= \frac{f_{i+1}''' - f_i'''}{\delta\eta} \\
{}_i H_{T_{i+1}}''' &= \frac{H_{T_{i+1}}'' - H_{T_i}''}{\delta\eta} \\
{}_i \tilde{K}_{k_{i+1}}''' &= \frac{\tilde{K}_{k_{i+1}}'' - \tilde{K}_{k_i}''}{\delta\eta}
\end{aligned} \tag{107}$$

Thus, rather than using finite difference approximations similar to equation (106) which are substitued directly into the governing differential equations,

a set of linear relations between the dependent variables and their derivatives is obtained and is solved simultaneously with the governing differential equations. These linear relations are of the form

$$- f_{i+1} + f_i + f_i'\delta\eta + f_i''\frac{(\delta\eta)^2}{2} + f_i'''\frac{(\delta\eta)^3}{8} + f_{i+1}'''\frac{(\delta\eta)^3}{24} = 0 \tag{108}$$

$$- p_{i+1} + p_i + p_i'\delta\eta + p_i''\frac{(\delta\eta)^2}{3} + p_{i+1}''\frac{(\delta\eta)^2}{6} = 0 \tag{109}$$

$$- p_{i+1}' + p_i' + p_i''\frac{\delta\eta}{2} + p_{i+1}''\frac{\delta\eta}{2} = 0 \tag{110}$$

where in equations (109) and (110) the p_i represents f_i', represents H_{T_i}, and represents each of the K sets of $\tilde{K}_{k_i}$.

Notice that f' has been taken to be a cubic over each strip, rather than the stream function, f, since it was desired to represent velocity ($u = u_1 f'/\alpha_H$) with the cubic. Equations (108) through (110) above, when written for each adjacent pair of nodes, give $(3 + 2K)(N - 1)$ simultaneous algebraic equations for the $N(4 + 3K) + 1$ unknowns, f_n, f_n', f_n'', f_n''', α_H, H_{T_n}, H_{T_n}', H_{T_n}'' $\tilde{K}_{k_n}$, $\tilde{K}_{k_n}'$, $\tilde{K}_{k_n}''$ at each streamwise station, where K is the number of elemental species.* The Taylor series equations are written for only K-1 species since the overall mass balance equation supplies the remaining elemental concentration. Additional relations must come from the governing differential equations and the boundary conditions. It is important to note that the f, f', etc., are treated as individual variables related by algebraic equations. It is also important to note that the coefficients in equations (108) through (110) are functions of $\delta\eta$ only; therefore, this portion of the resulting matrix need be inverted only once for a given problem.

The conservation equations (64), (79), and (83) contain streamwise derivative or "nonsimilar" terms. In the present solution technique, two or three point finite difference formulas are considered sufficient to express these derivatives, since gradients in this direction are not severe. As in reference 2

$$2\left[\frac{d(\ )}{d(\ln \xi)}\right]_\ell = d_0(\ )_\ell + d_1(\ )_{\ell-1} + d_2(\ )_{\ell-2} \tag{111}$$

where $(\ )_{\ell-1}$ refers to the previous streamwise station,

*The mixing length is not included in this variables count since mixing length (as well as ε_M in the wake region) is treated as a state property.

$$d_o = \frac{2}{\ell^{\Delta}\ell-1} , \quad d_1 = -\frac{2}{\ell^{\Delta}\ell-1} , \quad d_2 = 0 \tag{112}$$

for two-point difference and

$$d_0 = 2\,\frac{\ell^{\Delta}\ell-1 + \ell^{\Delta}\ell-2}{\ell^{\Delta}\ell-1\ \ell^{\Delta}\ell-2} , \quad d_1 = -2\cdot\frac{\ell^{\Delta}\ell-2}{\ell^{\Delta}\ell-1\ \ell-1^{\Delta}\ell-2} ,$$

$$d_2 = 2\,\frac{\ell^{\Delta}\ell-1}{\ell^{\Delta}\ell-2\ \ell-1^{\Delta}\ell-2} \tag{113}$$

for three-point difference where typically

$$\ell^{\Delta}\ell-1 = \ln \xi_{\ell} - \ln \xi_{\ell-1} = \ln(\xi_{\ell}/\xi_{\ell-1}) \tag{114}$$

The three-point difference relation is generally used unless a similar solution is desired (in which case $d_o = d_1 = d_2 = 0$) or unless the point in question is the first point after either (1) a similar solution or (2) a discontinuity (e.g., where the body changes shape abruptly, or where mass injection is suddenly terminated).

The next step in the treatment of the conservation equations is their integration across the boundary layer "strips". The primary reason for this integration is to simplify the η-derivative terms in the energy and species conservation equations, since it is not convenient to express the complex q_a^* and j_k^* terms in derivative form. The solution can actually proceed very nicely without integrating across strips (see reference 10) without any noticeable change in speed, accuracy, or stability for simplified problems such as incompressible, nonreacting flows. The weighting function for integration between nodes in this integral method is unity. In the terminology of the general method of integral relations, where integrals are carried from 0 to ∞ in η (reference 23), a square wave weighting function is used which is unity across the strip in question and zero elsewhere. The equations are then integrated N-1 times with the square wave applied to each strip in succession. Using the momentum equation as an example, the integration from i-1 to i results in

$$\int_{i-1}^{i} ff''d\eta + \left[\frac{t(C + \tilde{\varepsilon}_M)}{\alpha_H} f''\right]_{i-1}^{i} + \beta\alpha_H^2 \int_{i-1}^{i} \frac{\rho_1}{\rho} d\eta - \beta \int_{i-1}^{i} f'^2 d\eta$$

$$= \int_{i-1}^{i} f'(d_o f' + d_1 f'_{\ell-1} + d_2 f'_{\ell-2}) d\eta - \int_{i-1}^{i} f'^2 \left[d_o \ln \alpha_H \right.$$

$$\left. + d_1 (\ln \alpha_H)_{\ell-1} + d_2 (\ln \alpha_H)_{\ell-2}\right] d\eta - \int_{i-1}^{i} f''(d_o f + d_1 f_{\ell-1}$$

$$+ d_2 f_{\ell-2}) d\eta \qquad (115)$$

The Taylor series approximations introduced earlier can also be used to express the integral terms above. As demonstrated in reference 2, the term $\int_{i-1}^{i} f'p\, d\eta$ becomes

$$\int_{i-1}^{i} f'\, p\, d\eta = f'_i\, XP_1 + f''_i\, XP_2 + f'''_i\, XP_3 + f'''_{i-1}\, XP_4 \qquad (116)$$

where

$$\begin{aligned}
XP_1 &= \delta\eta \left(p_i - p'_i \frac{\delta\eta}{2} + p''_i \frac{(\delta\eta)^2}{8} + p''_{i-1} \frac{(\delta\eta)^2}{24} \right) \\
XP_2 &= -(\delta\eta)^2 \left(\frac{p_i}{2} - p'_i \frac{\delta\eta}{3} + p''_i \frac{11(\delta\eta)^2}{120} + p''_{i-1} \frac{(\delta\eta)^2}{30} \right) \\
XP_3 &= (\delta\eta)^3 \left(\frac{p_i}{8} - p'_i \frac{11(\delta\eta)}{120} + p''_i \frac{11(\delta\eta)^2}{420} + p''_{i-1} \frac{5(\delta\eta)^2}{504} \right) \\
XP_4 &= (\delta\eta)^3 \left(\frac{p_i}{24} - p'_i \frac{\delta\eta}{30} + p''_i \frac{5(\delta\eta)^2}{504} + p''_{i-1} \frac{(\delta\eta)^2}{252} \right)
\end{aligned} \qquad (117)$$

This technique is used to rewrite each of the integral terms in equation (115) above of the form $\int_{i-1}^{i} f'p\, d\eta$. The remaining integral term in the momentum equation, $\int_{i-1}^{i} (\rho_1/\rho) d\eta$, and the "elemental" source term in the "elemental" conservation equation are evaluated by approximating these functions as cubics over the strip and integrating directly. This yields

$$\int_{i-1}^{i} \frac{\rho_1}{\rho} d\eta = \left(\frac{\rho_1}{\rho} + \frac{\rho_1}{\rho_{i-1}} \right) \frac{\delta\eta}{2} + \left(\frac{\rho_1 \rho_i}{\rho_i^2} - \frac{\rho_1 \rho'_{i-1}}{\rho_{i-1}^2} \right) \frac{\delta\eta^2}{12} \qquad (118)$$

Similarly for the integral of ϕ_k

$$\int_{i-1}^{i} \phi_k \, d\eta = \left(\phi_{k_i} + \phi_{k_{i-1}}\right) \frac{\delta\eta}{2} - \left(\phi'_{k_i} - \phi'_{k_{i-1}}\right) \frac{(\delta\eta)^2}{12} \tag{119}$$

These approximations are not quite as good as the approximations for f', H_T and $\tilde{K}_k$ since continuity of derivatives is not guaranteed at the nodal point.

Direct substitution of these approximations for integral terms into the governing equations results in the following forms.

Momentum

$$\left[\frac{t(C + \tilde{\varepsilon}_M)}{\alpha_H} f'' + f'\left((1 + d_o) f + d_1 f_{\ell-1} + d_2 f_{\ell-2}\right)\right]_{i-1}^{i}$$

$$+ \beta \alpha_H^2 \left[\left(\frac{\rho_1}{\rho_i} + \frac{\rho_1}{\rho_{i-1}}\right) \frac{\delta\eta}{2} + \left(\frac{\rho_1 \rho'_i}{\rho_i^2} - \frac{\rho_1 \rho'_{i-1}}{\rho_{i-1}^2}\right) \frac{(\delta\eta)^2}{12}\right]$$

$$- \left(1 + \beta + d_0 - \frac{d_1 \alpha_{H_{\ell-1}} + d_2 \alpha_{H_{\ell-2}}}{\alpha_H}\right)\left[f'_i \, XP_1 + f''_i \, XP_2\right.$$

$$\left. + f'''_i \, XP_3 + f'''_{i-1} XP_4\right]_{p_i = f'_i} - 2\left[f'_i ZP_1 + f''_i ZP_2 + f'''_i \, ZP_3\right.$$

$$\left. + f'''_{i-1} ZP_4\right]_{p_i = f'_i} = 0 \tag{120}$$

Energy

$$\left[t(-q_a^* + q_r^*) + H_T\left((1 + d_o)\, f + d_1 f_{\ell-1} + d_2 f_{\ell-2}\right)\right]_{i-1}^{i}$$

$$- (1 + 2d_o)\left[f'_i XP_1 + f''_i XP_2 + f'''_i \, XP_3 + f'''_{i-1} XP_4\right]_{p_i = H_{T_i}}$$

$$- \left[f'_i ZP_1 + f''_i ZP_2 + f'''_i \, ZP_3 + f'''_{i-1} ZP_4\right]_{p_i = H_{T_i}}$$

$$- \left[H_{T_i} ZP_1 + H'_{T_i} ZP_2 + H''_{T_i} ZP_3 + H''_{T_{i-1}} ZP_4\right]_{p_i = f'_i} = 0 \tag{121}$$

"Elemental" Species

$$\left[t\left(\frac{\tilde{\varepsilon}_M}{\alpha_H Sc_t}\tilde{K}'_k - j^*_k\right) + \tilde{K}_k\left((1+d_0)\ f + d_1\ f_{\ell-1} + d_2\ f_{\ell-2}\right)\right]_{i-1}^{i}$$

$$+ \alpha_H\left[\left(\phi_{k_i} + \phi_{k_{i-1}}\right)\frac{\delta\eta}{2} - \left(\phi'_{k_i} - \phi'_{k_{i-1}}\right)\frac{(\delta\eta)^2}{12}\right]$$

$$- (1+2d_0)\left[f'_i\ XP_1 + f''_i\ XP_2 + f'''_i\ XP_3 + f'''_{i-1}\ XP_4\right]_{p_i = \tilde{K}_{k_i}}$$

$$- \left[f'_i\ ZP_1 + f''_i\ ZP_2 + f'''_i\ ZP_3 + f'''_{i-1}\ ZP_4\right]_{p_i = \tilde{K}_{k_i}}$$

$$- \left[\tilde{K}_{k_i}\ ZP_1 + \tilde{K}'_{k_i}\ ZP_2 + \tilde{K}''_{k_i}\ ZP_3 + \tilde{K}''_{k_{i-1}}\ ZP_4\right]_{p_i = f'_i} = 0 \qquad (122)$$

The following definitions are necessary:

$$ZP_1 = \delta\eta\left(YP_1 - YP_2\frac{\delta\eta}{2} + YP_3\frac{(\delta\eta)^2}{8} + YP_4\frac{(\delta\eta)^2}{24}\right)$$

$$ZP_2 = -(\delta\eta)^2\left(\frac{YP_1}{2} - YP_2\frac{\delta\eta}{3} + YP_3\frac{11(\delta\eta)^2}{120} + YP_4\frac{(\delta\eta)^2}{30}\right) \qquad (123)$$

$$ZP_3 = (\delta\eta)^3\left(\frac{YP_1}{8} - YP_2\frac{11\delta\eta}{120} + YP_3\frac{11(\delta\eta)^2}{420} + YP_4\frac{5(\delta\eta)^2}{504}\right)$$

$$ZP_4 = (\delta\eta)^3\left(\frac{YP_1}{24} - YP_2\frac{\delta\eta}{30} + YP_3\frac{5(\delta\eta)^2}{504} + YP_4\frac{(\delta\eta)^2}{252}\right)$$

with

$$\begin{aligned} YP_1 &= d_1 p_{\ell-1,i} + d_2 p_{\ell-2,i} \\ YP_2 &= d_1 p'_{\ell-1,i} + d_2 p'_{\ell-2,i} \\ YP_3 &= d_1 p''_{\ell-1,i} + d_2 p''_{\ell-2,i} \\ YP_4 &= d_1 p''_{\ell-1,i-1} + d_2 p''_{\ell-2,i-1} \end{aligned} \qquad (124)$$

and p_i is defined adjacent to the brackets in each term that uses these definitions.

The conservation equations provide (K+1)(N-1) more equations for the N(3K + 4) + 1 unknowns, thereby closing the problem. However, before discussing how this set of algebraic equations is solved, Section III.2 describes in detail how the mixing length differential equation is solved.

2. SOLUTION OF THE MIXING LENGTH EQUATION

The mixing length equation is a first order linear differential equation whose solution can be written directly in general terms. The differential equation is

$$\frac{d\tilde{\ell}}{d\eta} = \frac{\alpha_H \rho_1 \delta\sqrt{\tau/\rho}}{y_a^+ \mu} \left(K\alpha_H \eta - \tilde{\ell}\right) \tag{77}$$

Defining

$$P(\eta) \equiv \frac{\alpha_H \rho_1 \delta\sqrt{\tau/\rho}}{y_a^+ \mu} \tag{125}$$

results in

$$\frac{d\tilde{\ell}}{d\eta} = \left(K\alpha_H \eta - \tilde{\ell}\right) P \tag{126}$$

The solution to this equation is

$$\tilde{\ell} = K\alpha_H \left[\eta - \frac{\int_o^\eta e^{\int_o^{\eta'} P \, d\eta'} \, d\eta'}{e^{\int_o^\eta P \, d\eta'}} \right] \tag{127}$$

The remaining problem is to evaluate the integral terms. Defining

$$L(\eta) \equiv \frac{\int_o^\eta e^{\int_o^{\eta'} P \, d\eta''} \, d\eta'}{e^{\int_o^\eta P \, d\eta'}} \tag{128}$$

yields

$$\tilde{\ell} = K\alpha_H(\eta - L) \tag{129}$$

Appendix II presents a complete description of the technique used to evaluate $L(\eta)$. In essence, $P(\eta)$ is assumed to vary linearly over the interval η_{i-1} to η_i, and the integrals are expressed in a more tractable form. The final expression is

$$L_i = BL_{i-1} + A\left\{ D_w\left(\frac{AP_i}{2}\right) - BD_w\left(\frac{AP_{i-1}}{2}\right) \right\} \tag{130}$$

where

$$A \equiv \left[\frac{2\Delta\eta_i}{P_i - P_{i-1}}\right]^{\frac{1}{2}} \tag{131}$$

$$B \equiv e^{-\Delta\eta_i\left[\frac{P_i - P_{i-1}}{2}\right]} \tag{132}$$

$$\Delta\eta_i \equiv \eta_i - \eta_{i-1} \tag{133}$$

$$D_w(\ ) = e^{-(\ )^2}\int_0^{(\ )} e^{+y^2}\, dy \tag{134}$$

The Dawson Integral, $D_w(\ )$, can be evaluated from tables (reference 24) or by a series method. A series evaluation method is used in the present analysis. Thus, combining equations (129) and (130), an explicit recursion formula for mixing length at each node is obtained. This mixing length is a function of local shear, viscosity, and density through the variation of $P(\eta)$, and is re-evaluated at each node on each iteration during the course of a solution.

3. NEWTON-RAPHSON ITERATION FOR A SOLUTION

A complete description of the Newton-Raphson iteration procedure as applied to the laminar equations of motion was given in reference 2. Since the procedure is basically unchanged with the addition of turbulent flow and transverse curvature equations, it will be reviewed only briefly here, with emphasis on the recent additions.

To illustrate the Newton-Raphson method, consider two simultaneous nonlinear algebraic equations

$$F(x,y) = 0 \qquad G(x,y) = 0 \tag{135}$$

the solution for which is given by $x = \bar{x}$, $y = \bar{y}$. Define x_m and y_m as the values of x and y for the m^{th} iteration. The desired solution $f(\bar{x},\bar{y})$ can be expressed in a Taylor series expansion

$$\begin{aligned} 0 = F(\bar{x},\bar{y}) &= F(x_m,y_m) + (\bar{x} - x_m)\,\frac{\partial F(x_m,y_m)}{\partial x} \\ &\quad + (\bar{y} - y_m)\,\frac{\partial F(x_m,y_m)}{\partial y} + \cdots \\ 0 = G(\bar{x},\bar{y}) &= G(x_m,y_m) + (\bar{x} - x_m)\,\frac{\partial G(x_m,y_m)}{\partial x} \\ &\quad + (\bar{y} - y_m)\,\frac{\partial G(x_m,y_m)}{\partial y} + \cdots \end{aligned} \tag{136}$$

The Newton-Raphson method consists of replacing $(\bar{x},\bar{y})$ by (x_{m+1},y_{m+1}) on the right-hand side of these expressions and neglecting nonlinear terms in $x_{m+1} - x_m$ and $y_{m+1} - y_m$. This yields the set of simultaneous equations

$$\begin{aligned} \Delta x_m \frac{\partial F(x_m,y_m)}{\partial x} + \Delta y_m \frac{\partial F(x_m,y_m)}{\partial y} &= -F(x_m,y_m) \\ \Delta x_m \frac{\partial G(x_m,y_m)}{\partial x} + \Delta y_m \frac{\partial G(x_m,y_m)}{\partial y} &= -G(x_m,y_m) \end{aligned} \tag{137}$$

or in matrix form

$$\begin{bmatrix} \dfrac{\partial F(x_m,y_m)}{\partial x} & \dfrac{\partial F(x_m,y_m)}{\partial y} \\ \dfrac{\partial G(x_m,y_m)}{\partial x} & \dfrac{\partial G(x_m,y_m)}{\partial y} \end{bmatrix} \begin{bmatrix} \Delta x_m \\ \Delta y_m \end{bmatrix} = \begin{bmatrix} -F(x_m,y_m) \\ -G(x_m,y_m) \end{bmatrix} \tag{138}$$

where

$$\Delta x_m \equiv x_{m+1} - x_m \qquad \Delta y_m \equiv y_{m+1} - y_m \tag{139}$$

The Δx_m and Δy_m are the corrections to be added to x_m and y_m, respectively, to yield the values of the dependent variables for the $m + 1^{th}$ iteration. Here $F(x_m,y_m)$ and $G(x_m,y_m)$ are the values of the original functions $F(x,y)$ and $G(x,y)$ evaluated for $x = x_m$ and $y = y_m$. As the corrections approach zero, the $F(x_m,y_m)$ and $G(x_m,y_m)$ approach zero. Hence, it is appropriate to look upon these as errors associated with the original equation (135). It is apparent that this procedure can be extended to an arbitrary number of functions and a corresponding number of primary variables.

For the purpose of the present analysis, it has been found most convenient to consider the primary variables as f_i, f_i', f_i'', f_i''', H_{T_i}, H_{T_i}', H_{T_i}'', $\tilde{K}_{k_i}$, $\tilde{K}_{k_i}'$, $\tilde{K}_{k_i}''$, and α_H. This amounts to $(3K + 4)N + 1$ unknowns where N is the number of nodes and K is the number of elemental species to be considered in the boundary layer. Recounting the number of equations, we have

	Eqn. Numbers	No. of Equations
Taylor series expansions	(103) - (110)	$(N - 1)[5 + 2(K - 1)]$
Boundary layer equations	(120) - (122)	$(N - 1)(K + 1)$
Boundary conditions	(97), (97a), (98) or equivalent	$3K + 4$
α_H definition	(58)	1
Total		$N(3K + 4) + 1$

Other secondary variables such as ε, ρ, T, etc. are expressed in terms of those listed above. The corrections in these secondary variables are therefore found in terms of the corrections to the primary variables.

The use of the Newton-Raphson technique for the current set of equations requires the evaluation of the partial derivatives of each equation with respect to each variable. The partial derivatives of the Taylor series equations and linear boundary conditions are exactly the same as in reference 2. The derivatives of the conservation equations are:

Momentum

$$\left[\frac{t(C + \tilde{\varepsilon}_M)f''}{\alpha_H}\left(\frac{\Delta f''}{f''} + \frac{\Delta C}{C} + \frac{\Delta\tilde{\varepsilon}_M}{\tilde{\varepsilon}_M} - \frac{\Delta\alpha_H}{\alpha_H} + \frac{\Delta t}{t}\right) + \left[(1 + d_o)f + d_1 f_{\ell-1} + d_2 f_{\ell-2}\right]\Delta f'\right.$$

$$\left. + f'(1 + d_o)\Delta f\right]_{i-1}^{i} - \beta\alpha_H^2\frac{\rho_1}{\rho_i^2}\frac{\delta\eta}{2}\left\{\left(1 + \frac{\delta\eta}{3}\frac{\rho_i'}{\rho_i}\right)\Delta\rho_i - \frac{\delta\eta}{6}\Delta\rho_i'\right.$$

$$+\left(\frac{\rho_1}{\rho_{i-1}}\right)^2\left[\left(1-\frac{\delta\eta}{3}\frac{\rho'_{i-1}}{\rho_{i-1}}\right)\Delta\rho_{i-1}+\frac{\delta\eta}{6}\Delta\rho'_{i-1}\right]\Bigg\}+\beta\alpha_H\delta\eta\,\frac{\rho_1}{\rho_i}\left[1+\frac{\rho_i}{\rho_{i-1}}\right.$$

$$\left.+\frac{\delta\eta}{6}\left(\frac{\rho'_i}{\rho_i}-\frac{\rho_i}{\rho_{i-1}}\frac{\rho'_{i-1}}{\rho_{i-1}}\right)\right]\Delta\alpha_H-\left[1+\beta+d_o-\left(\frac{d_1\alpha_{H_{\ell-1}}+d_2\alpha_{H_{\ell-2}}}{\alpha_H}\right)\right]$$

$$\times\left[f'_i\,\Delta XP_1+f''_i\,\Delta XP_2+f'''_i\,\Delta XP_3+f'''_{i-1}\,\Delta XP_4+XP_1\Delta f'_i+XP_2\Delta f''_i\right.$$

$$\left.+XP_3\Delta f'''_i+XP_4\Delta f'''_{i-1}\right]_{p_i=f'_i}-\left(\frac{d_1\alpha_{H_{\ell-1}}+d_2\alpha_{H_{\ell-2}}}{\alpha_H^2}\right)\left[f'_iXP_1+f''_iXP_2\right.$$

$$\left.+f'''_iXP_3+f'''_{i-1}XP_4\right]_{p_i=f'_i}\Delta\alpha_H-2\left[ZP_1\Delta f'_i+ZP_2\Delta f''_i+ZP_3\Delta f'''_i\right.$$

$$\left.+ZP_4\Delta f'''_{i-1}\right]_{p_i=f'_i}=-\text{ERROR} \qquad (140)$$

where the ERROR is given by the left-hand side of equation (120) evaluated for the m^{th} iteration.

Energy

$$\left[t(-\Delta q_a^*+\Delta q_r^*)+(-q_a^*+q_r^*)\Delta t+\left((1+d_o)\,f+d_1f_{\ell-1}+d_2f_{\ell-2}\right)\Delta H_T\right.$$

$$\left.+H_T(1+d_o)\Delta f\right]_{i-1}^{i}-(1+2d_o)\left[f'_i\,\Delta XP_1+f''_i\,\Delta XP_2+f'''_i\,\Delta XP_3\right.$$

$$\left.+f'''_{i-1}\,\Delta XP_4+XP_1\Delta f'_i+XP_2\Delta f''_i+XP_3\Delta f'''_i+XP_4\Delta f'''_{i-1}\right]_{p_i=H_{T_i}}-\left[ZP_1\Delta f'_i\right.$$

$$\left.+ZP_2\Delta f''_i+ZP_3\Delta f'''_i+ZP_4\Delta f'''_{i-1}\right]_{p_i=H_{T_i}}-\left[ZP_1\Delta H_{T_i}+ZP_2\Delta H'_{T_i}\right.$$

$$\left.+ZP_3\Delta H''_{T_i}+ZP_4\Delta H''_{T_{i-1}}\right]_{p_1=f'_i}=-\text{ERROR} \qquad (141)$$

where the ERROR is given by the left-hand side of equation (121) for the m^{th} iteration and Δq_a^* is given by

$$\Delta q_a^* = -\Bigg\{ \frac{(C + \tilde{\varepsilon}_M) f' f'' u_1^2}{\alpha_H^3} \left(\frac{\Delta C}{C} + \frac{\Delta \tilde{\varepsilon}_M}{\tilde{\varepsilon}_M} + \frac{\Delta f'}{f'} + \frac{\Delta f''}{f''} - 3 \frac{\Delta \alpha_H}{\alpha_H} \right) + \frac{C C_p T'}{\alpha_H Pr} \left(\frac{\Delta C}{C} \right.$$

$$\left. + \frac{\Delta \bar{C}_p}{\bar{C}} + \frac{\Delta T'}{T'} - \frac{\Delta \alpha_H}{\alpha_H} - \frac{\Delta Pr}{Pr} \right) + \frac{\tilde{\varepsilon}_M \bar{C}_p T'}{\alpha_H Pr_t} \left(\frac{\Delta \tilde{\varepsilon}_M}{\tilde{\varepsilon}_M} + \frac{\Delta C_p}{\bar{C}_p} + \frac{\Delta T'}{T'} - \frac{\Delta \alpha_H}{\alpha_H} \right)$$

$$+ \frac{C}{\alpha_H \overline{Sc}} \left[\tilde{h}' - \left(\tilde{C}_p + \frac{c_t^2 R}{\mu_1 \mu_2} \right) T' + c_t R T \mu_3' + (\tilde{h} - h + c_t R T \mu_3) \mu_4' \right] \left[\frac{\Delta C}{C} \right.$$

$$\left. - \frac{\Delta \alpha_H}{\alpha_H} - \frac{\Delta \overline{Sc}}{\overline{Sc}} \right] + \frac{\tilde{\varepsilon}_M}{\alpha_H Sc_t} \left(h' - \bar{C}_p T' \right) \left[\frac{\Delta \tilde{\varepsilon}_M}{\tilde{\varepsilon}_M} - \frac{\Delta \alpha_H}{\alpha_H} \right] + \frac{C}{\alpha_H \overline{Sc}} \left[\Delta \tilde{h}' \right.$$

$$\left. - \left(\tilde{C}_p + \frac{c_t^2 R}{\mu_1 \mu_2} \right) \Delta T' - T' \Delta \tilde{C}_p + \frac{c_t^2 R T'}{(\mu_1 \mu_2)^2} \Delta(\mu_1 \mu_2) + c_t R T \mu_3' \left(\frac{\Delta T}{T} \right. \right.$$

$$\left. \left. + \frac{\Delta \mu_3'}{\mu_3'} \right) + (\tilde{h} - h + c_t R T \mu_3) \Delta \mu_4' + \mu_4' \left(\Delta \tilde{h} - \Delta h + c_t R T \mu_3 \left(\frac{\Delta \mu_3}{\mu_3} \right. \right. \right.$$

$$\left. \left. \left. + \frac{\Delta T}{T} \right) \right) \right] + \frac{\tilde{\varepsilon}_M}{\alpha_H Sc_t} \left[\Delta h' - \bar{C}_p \Delta T' - T' \Delta \bar{C}_p \right] \Bigg\} \qquad (142)$$

"Elemental" Species

$$\left[-t \Delta j_k^* - j_k^* \Delta t + \frac{\tilde{\varepsilon}_M \tilde{K}_k t}{\alpha_H Sc_t} \left(\frac{\Delta \tilde{K}_k}{\tilde{K}_k'} - \frac{\Delta \alpha_H}{\alpha_H} + \frac{\Delta \tilde{\varepsilon}_M}{\tilde{\varepsilon}_M} + \frac{\Delta t}{t} \right) + \left((1 + d_o) f + d_1 f_{\ell-1} \right.\right.$$

$$\left.\left. + d_2 f_{\ell-2} \right) \Delta \tilde{K}_k + \tilde{K}_k (1 + d_o) \Delta f \right]_{i-1}^{i} + \alpha_H \frac{\delta \eta}{2} \left[\Delta \phi_{k_i} + \Delta \phi_{k_{i-1}} \right.$$

$$- \frac{\delta\eta}{6}\left(\Delta\phi'_{k_i} - \Delta\phi'_{k_{i-1}}\right)\Bigg] + \frac{\Delta\eta}{2}\left[\phi_{k_i} + \phi_{k_{i-1}} - \left(\phi'_{k_i} - \phi'_{k_{i-1}}\right)\frac{\delta\eta}{6}\right]\Delta\alpha_H$$

$$- (1 + 2d_o)\Big[f'_i\Delta XP_1 + f''_i\Delta XP_2 + f'''_i\Delta XP_3 + f'''_{i-1}\Delta XP_4 + XP_1\Delta f'_i$$

$$+ XP_2\Delta f''_i + XP_3\Delta f'''_i + XP_4\Delta f'''_{i-1}\Big]_{p_i=\tilde{K}_{k_i}} - \Big[ZP_1\Delta f'_i + ZP_2\Delta f''_i$$

$$+ ZP_3\Delta f'''_i + ZP_4\Delta f'''_{i-1}\Big]_{p_i=\tilde{K}_{k_i}} - \Big[ZP_1\Delta\tilde{K}_{k_i} + ZP_2\Delta\tilde{K}'_{k_i} + ZP_3\Delta\tilde{K}''_{k_i}$$

$$+ ZP_4\Delta\tilde{K}''_{k_{i-1}}\Big]_{p_i=f'_i} = - \text{ERROR} \tag{143}$$

where the ERROR is given by the left-hand side of equation (122) evaluated for the m^{th} iteration and Δj^*_K is given by

$$\Delta j^*_K = - \frac{C}{\alpha_H\overline{Sc}}\left[\left(\tilde{z}'_k + (\tilde{z}_k - \tilde{K}_k)\mu'_4\right)\left(\frac{\Delta C}{C} - \frac{\Delta\alpha_H}{\alpha_H} - \frac{\Delta\overline{Sc}}{\overline{Sc}}\right)\right.$$

$$\left. + \Delta\tilde{z}'_k + (\tilde{z}_k - \tilde{K}_k)\Delta\mu'_4 + \mu'_4(\Delta z_k - \Delta\tilde{K}_k)\right] \tag{144}$$

The technique of relating corrections on secondary variables such as C, ρ, T, Pr, etc., to corrections in primary variables was fully explained in reference 2. The same techniques are used for the new corrections Δt and $\Delta\tilde{\epsilon}_M$.

Once the correction coefficients (partial derivatives with respect to each primary variable) for each equation at each nodal point are found, they are arranged in matrix form for further manipulation. The order of the primary variables and the order of the equations is of some importance in the matrix formulation. It is most convenient to divide the variables into "linear" (symbol L) and "nonlinear" (symbol NL) sets, namely

$$\left[\begin{array}{c|c} AL & BL \\ \hline ANL & BNL \end{array}\right]\left[\begin{array}{c} VL \\ \hline VNL \end{array}\right] = -\left[\begin{array}{c} EL \\ \hline ENL \end{array}\right] \tag{145}$$

where the linear equations are the Taylor series equations and some of the boundary conditions. The purpose of the partitioning is to allow operations on sections of the coefficient matrix which result in significant simplification of the overall inversion. In particular, since the coefficients of the linear equations are all constant or functions of the fixed nodal spacing, this portion of the matrix (the AL portion) can be diagonalized once and for all in any given problem. In essence, the corrections on the linear variables ΔVL are always expressed in terms of the nonlinear variable corrections ΔVNL. The choice of linear and nonlinear labels for the variables is somewhat arbitrary, but care must be taken that the AL matrix not be singular. It has been found convenient to arrange the variables into the linear and nonlinear groups as follows: ΔVL_F (Δf_2, Δf_3,... Δf_n, $\Delta f_2''$, $\Delta f_3''$,... $\Delta f_n''$, $\Delta f_1'''$, $\Delta f_2'''$,... $\Delta f_n'''$); ΔVL_H (ΔH_{T_n}, $\Delta H'_{T_2}$ $\Delta H'_{T_3}$,... $\Delta H'_{T_n}$, $\Delta H''_{T_w}$, $\Delta H''_{T_2}$,... $\Delta H''_{T_n}$); and K-1 sets of ΔVL_K(ΔK_{k_n}, $\Delta \tilde{K}'_{k_2}$, $\Delta \tilde{K}'_{k_3}$,... $\Delta \tilde{K}'_{k_n}$, $\Delta \tilde{K}''_{k_w}$, $\Delta \tilde{K}''_{k_2}$,... $\Delta \tilde{K}''_{k_n}$). The nonlinear variables are then arranged in the following order: ΔVNL_F ($\Delta\alpha_H$, Δf_w, $\Delta f_w''$, $\Delta f_1'$, $\Delta f_2'$,... $\Delta f_n'$); ΔVNL_H ($\Delta H'_{T_w}$, ΔH_{T_w}, ΔH_{T_2},... $\Delta H_{T_{n-1}}$); and K-1 sets of ΔVNL_K ($\tilde{K}'_{k_w}$, $\tilde{K}_{k_w}$, $\tilde{K}_{k_2}$,... $\tilde{K}_{k_{n-1}}$). The order of the linear equations in the present matrix procedure is:

No. of Equations	Description of Equations
3N-2	Linear boundary conditions and Taylor series for f, f', f", f"'
2N	Linear boundary conditions and Taylor series for H_T, H'_T, H''_T
(K - 1)(2N)	Linear boundary conditions and Taylor series for K_k, K'_k, K''_k

The nonlinear equations are sequenced as follows:

No. of Equations	Description of Equations
4	Nonlinear boundary conditions and α_H constraint
N - 1	Momentum equation for each pair of nodes
N	Energy equation for each pair of nodes plus wall enthalpy equation
(K -1) (N)	K-1 sets of "elemental" species equations for each pair of nodes plus wall species equation

Special logic has been written for the matrix inversion, taking advantage of the regular sparseness of the matrix. Once the corrections for the linear

and nonlinear variables are found, these corrections are added to the variables to form the new guesses. The magnitude of the errors for each equation are checked and the procedure advances to the next iteration if the absolute values of the errors exceed prescribed upper limits. If the errors are acceptable, iteration is completed for the current streamwise position ξ. Typically, three to six iterations are required to reach a satisfactory solution.

SECTION IV

SOME RESULTS FOR MULTICOMPONENT BOUNDARY LAYERS

The fact that the BLIMP computer program works well for a myriad of multicomponent reacting laminar flow situations including stagnation points, transpiration cooled surfaces and rocket nozzles is well documented in references 25 through 27, among others. The purpose of this section is to present results for the recent additions of turbulent flow and transverse curvature.

1. ABLATING FLAT PLATE IN TURBULENT FLOW

This sample problem is the formulation of a typical turbulent channel or turbulent pipe flow situation such as might be found in some of the major test facilities around the country. The flow stagnation conditions were P_o = 43.4 atmospheres, H_o = 2100 Btu/lb. The flat plate model was taken to be constructed of graphite phenolic, and the wall temperature was assigned at T_w = 4760°R. Assuming that the plate ablates in a steady state mode, the chemical composition of the virgin material exactly equals the chemical composition of the char plus pyrolysis gas ablation products. The chemical composition of graphite phenolic which was used is

0.9236 lbs. C/lb.
0.0209 lbs. H/lb.
0.0554 lbs. O/lb.

These numbers were calculated from data on graphite phenolic given in reference 28. Pressure and ablation rate or mass flux were also input to the BLIMP program. The variations of these quantities in the streamwise direction are shown in Figures 2 and 3. The decision to specify both the wall temperature and ablation rate precluded the possibility of using either the surface equilibrium or steady state energy balance logic in the BLIMP program. Indeed, no surface chemistry is needed at all when T_w and $\dot{m}$ are specified. This choice was made however, since it was felt that a more representative boundary layer would be obtained by foregoing surface equilibrium than by demanding equilibrium and attempting to calculate T_w in the sensitive diffusion controlled ablation region (see Section V).

Using the above information, the calculation was started at S = 0.03125 feet. At the first station, streamwise derivative terms are automatically dropped since no upstream information is available. The solution was turbulent

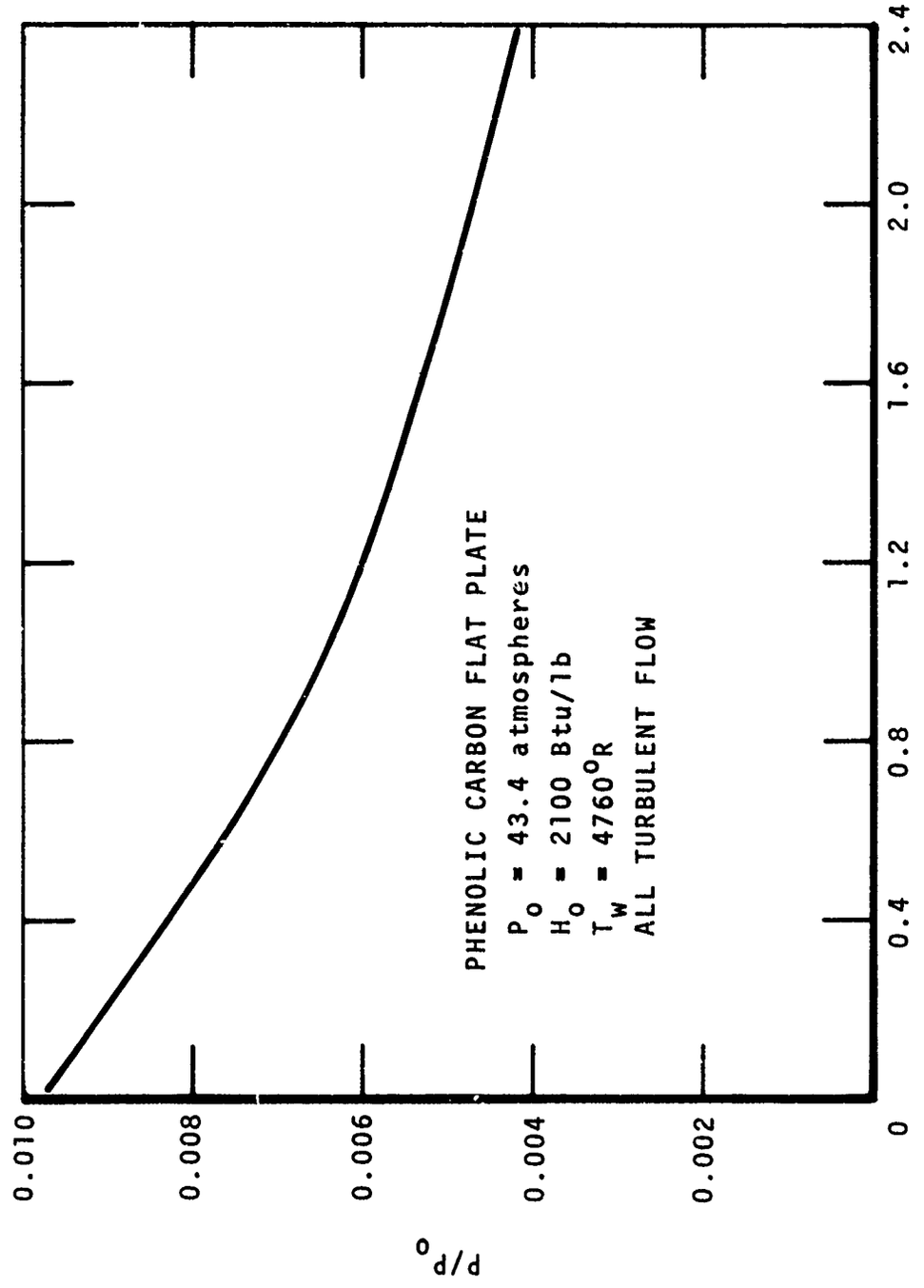

Figure 2. Streamwise Variation of Pressure

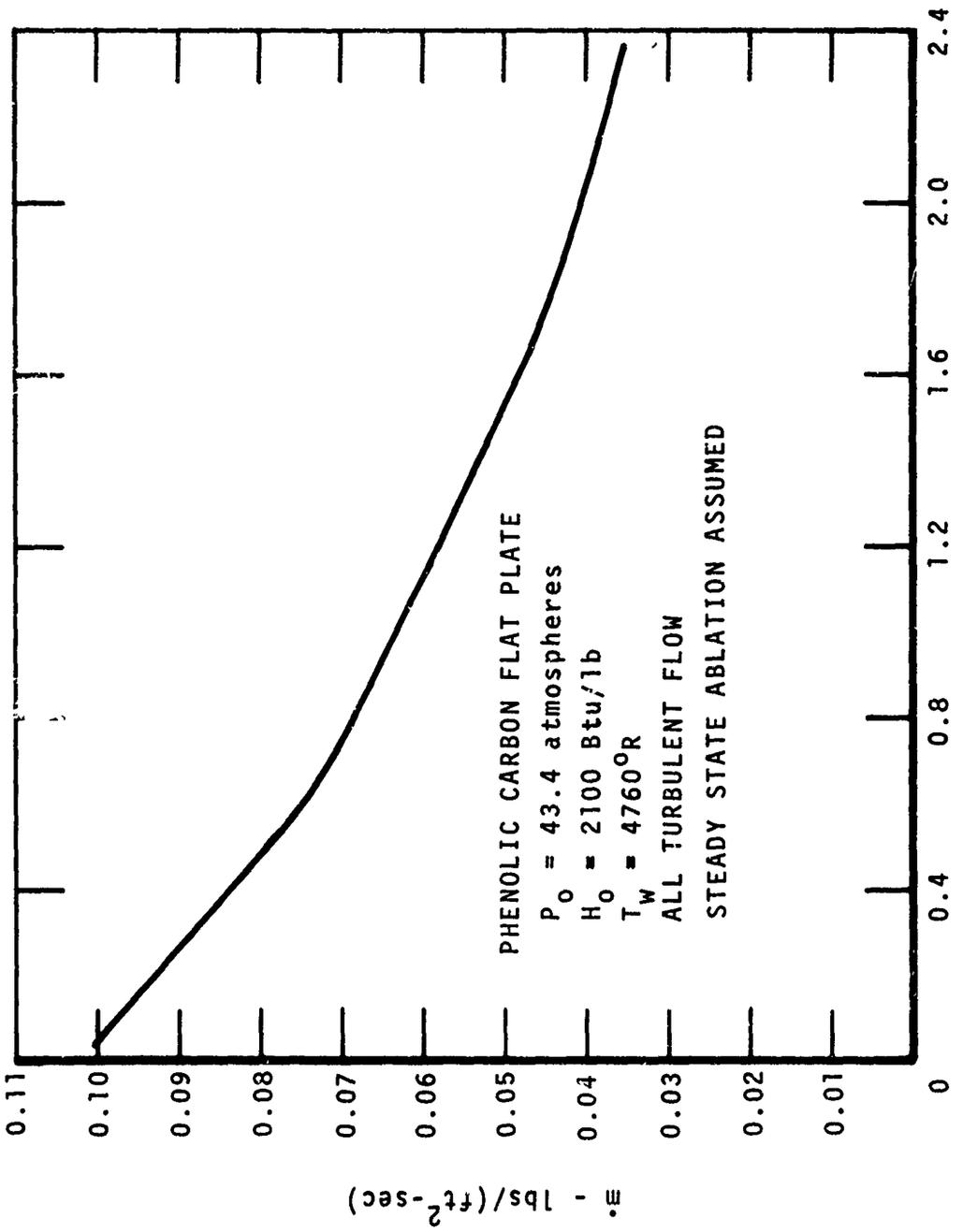

Figure 3. Streamwise Variation of Ablation Rate

over the entire length of the 2.40 foot ablating plate. Additional solutions were found at S = 0.3646, 0.6979, 1.1562, 1.6979 and 2.3646 feet. The variations of calculated local drag coefficient, Reynolds number on momentum thickness, and shape factor may be seen in Figures 4, 5, and 6. The flow is actually transitional in nature, being weakly turbulent at the beginning of the plate and strongly turbulent at the end. This fact combined with the free stream acceleration and decreasing rate of blowing along the plate produces the unusual Re_θ and shape factor variations.

Velocity profiles at three representative stations may be seen in Figure 7. These curves clearly show the transitional nature of the flow, with a nearly laminar velocity profile shape near the beginning of the plate and a more characteristic turbulent profile near the end of the plate. Figure 8 presents the velocity profile at S = 0.03125 feet again, this time in semi-logarithmic coordinates. The laminar sublayer, transitional wall region, and the wake region are clearly visible in these coordinates, with the data points shown actually representing solution points or nodes in the computer solution. This smooth variation of the velocity ratio from the wall to the wake region with this solution technique is of particular interest in this figure. Eddy viscosity normalized by the edge value of kinematic viscosity is shown in Figure 9. The eddy viscosity is seen to decrease to values far below the molecular viscosity as the wall is approached. Chemical species mole fraction profiles at three stations are shown in Figures 10, 11, and 12. Only the major species distributions are shown in these figures, although a total of 42 species were considered. Table I below lists the species that were considered and their maximum concentration in mole fraction at the S = 0.6979 foot station.

Total central processor run time for this problem with 13 nodes, 6 body stations, and 42 chemical species including 4 elements was 419 seconds on a CDC 6600.

2. SPHERE-CONE CONFIGURATION WITH LAMINAR AND TURBULENT FLOW

A second sample problem was selected which demonstrates some of the flexibility of the BLIMP program. The configuration chosen was a 0.500 inch nose radius, 7.5 degree half angle sphere-cone consisting of three surface materials: graphite, pyrolytic boron nitride, and phenolic carbon. Stagnation conditions were representative of a single time in a severe reentry trajectory with P_o = 242 atmospheres, H_o = 5520 Btu/lb. Figure 13 is a schematic of the sphere-cone configuration. A total surface running length of 5.0164 feet was analyzed in this problem, which required 29 body stations and thirteen nodes through the boundary layer. Figure 14 shows a portion of the pressure distribution which was assumed, the remainder of the running length being deleted from the

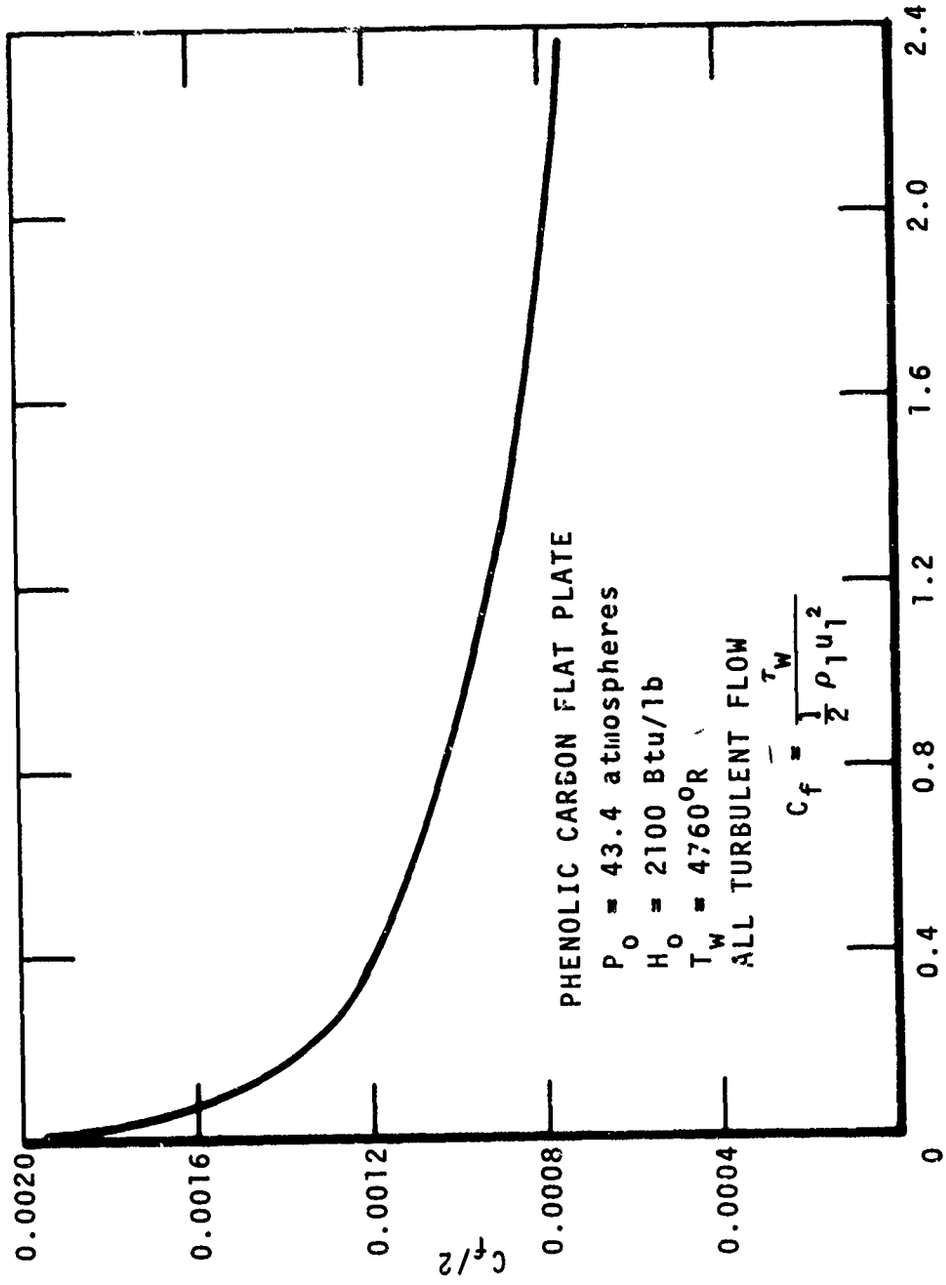

Figure 4. Calculated Drag Coefficient Variation

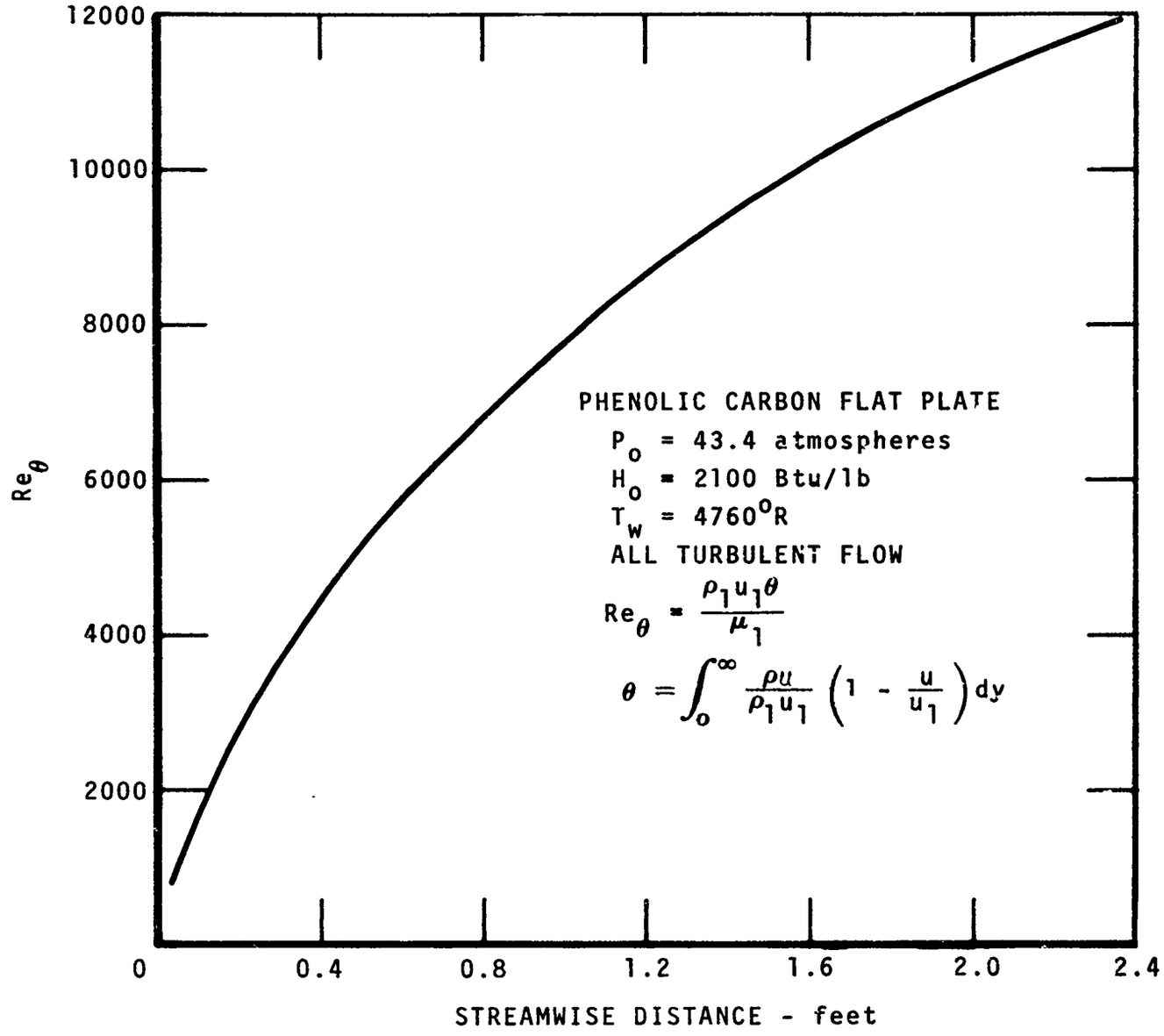

Figure 5. Calculated Momentum Thickness Reynolds Number Variation

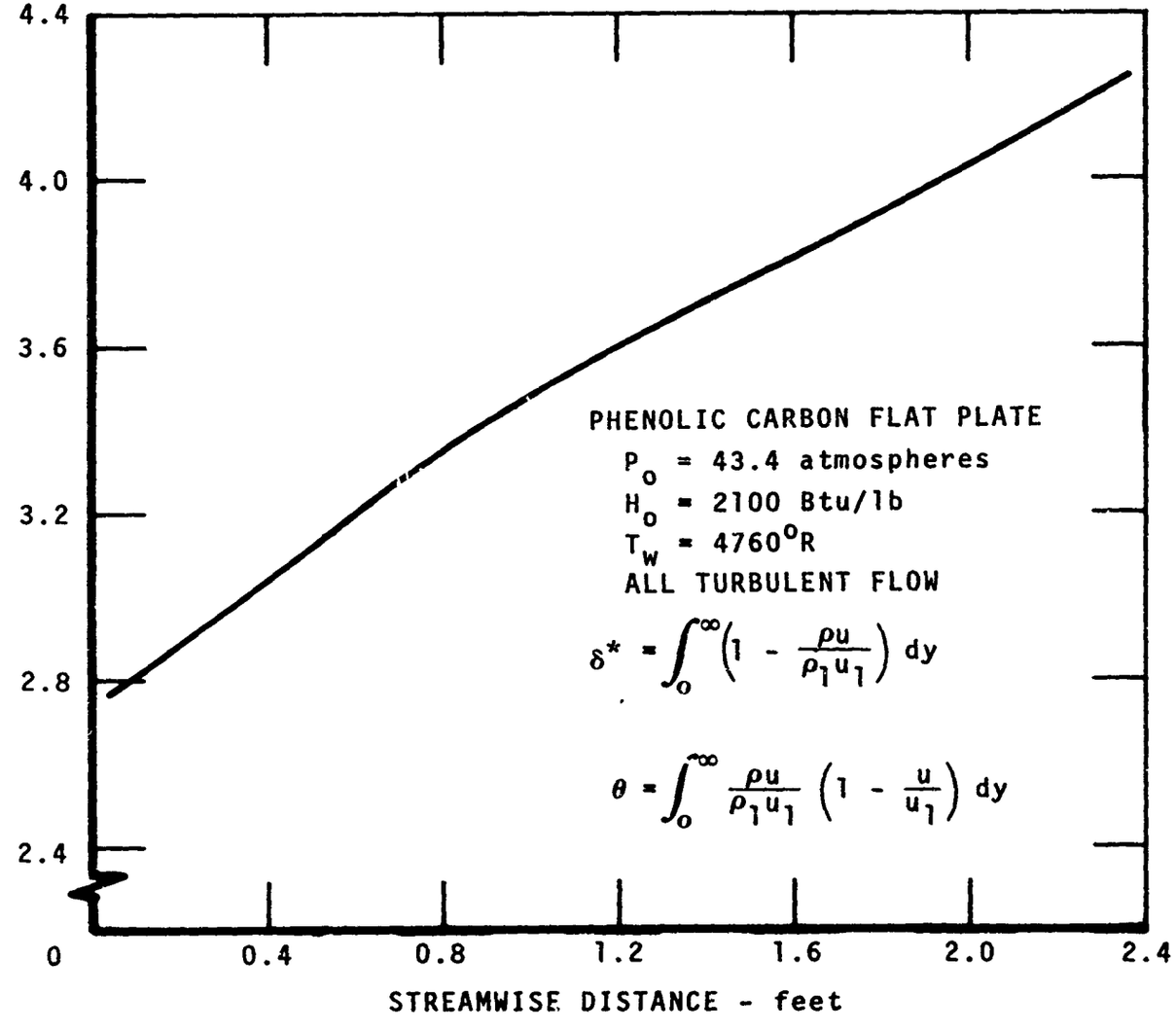

Figure 6. Calculated Shape Factor Variation

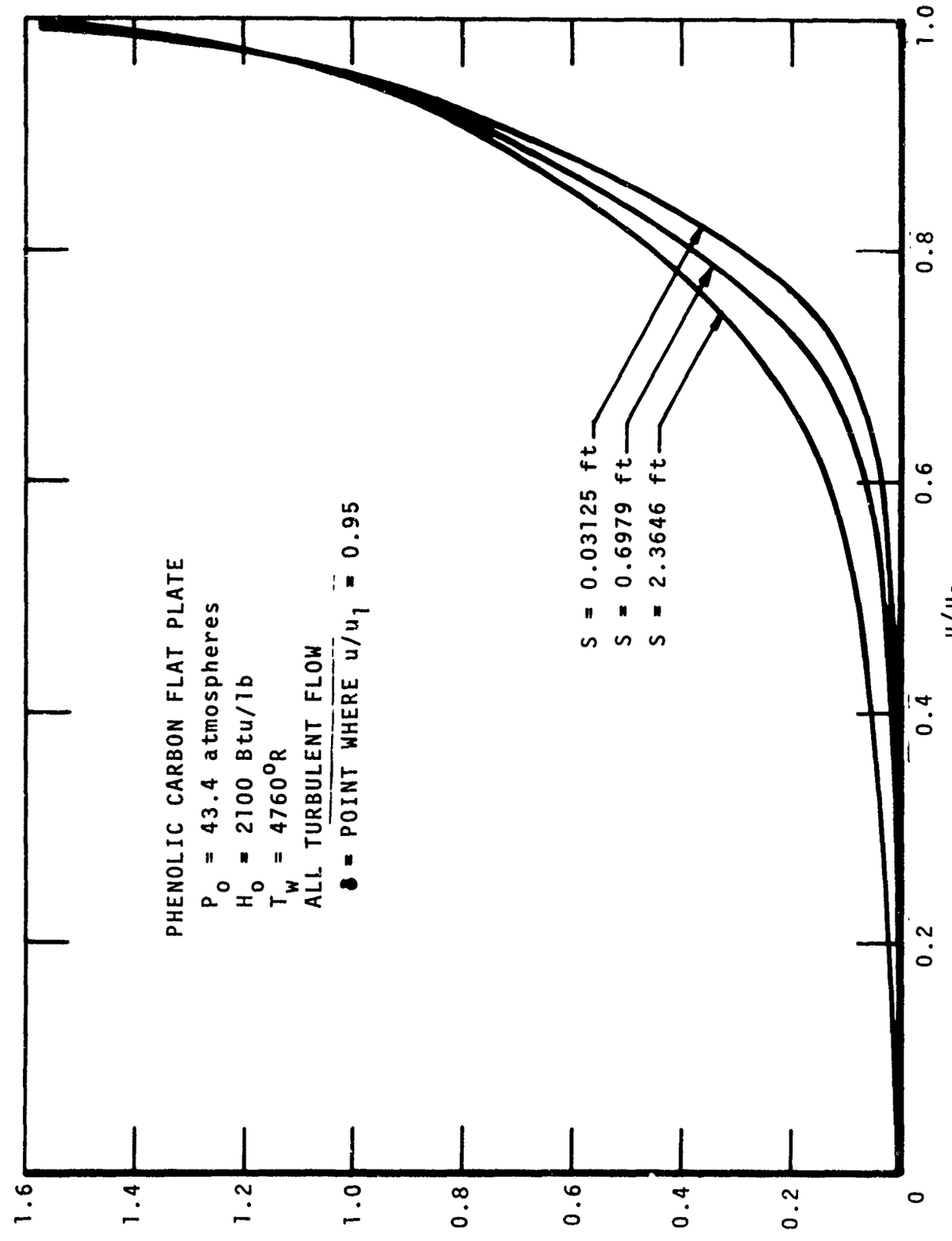

Figure 7. Velocity Profiles for Flow Over an Ablating Flat Plate

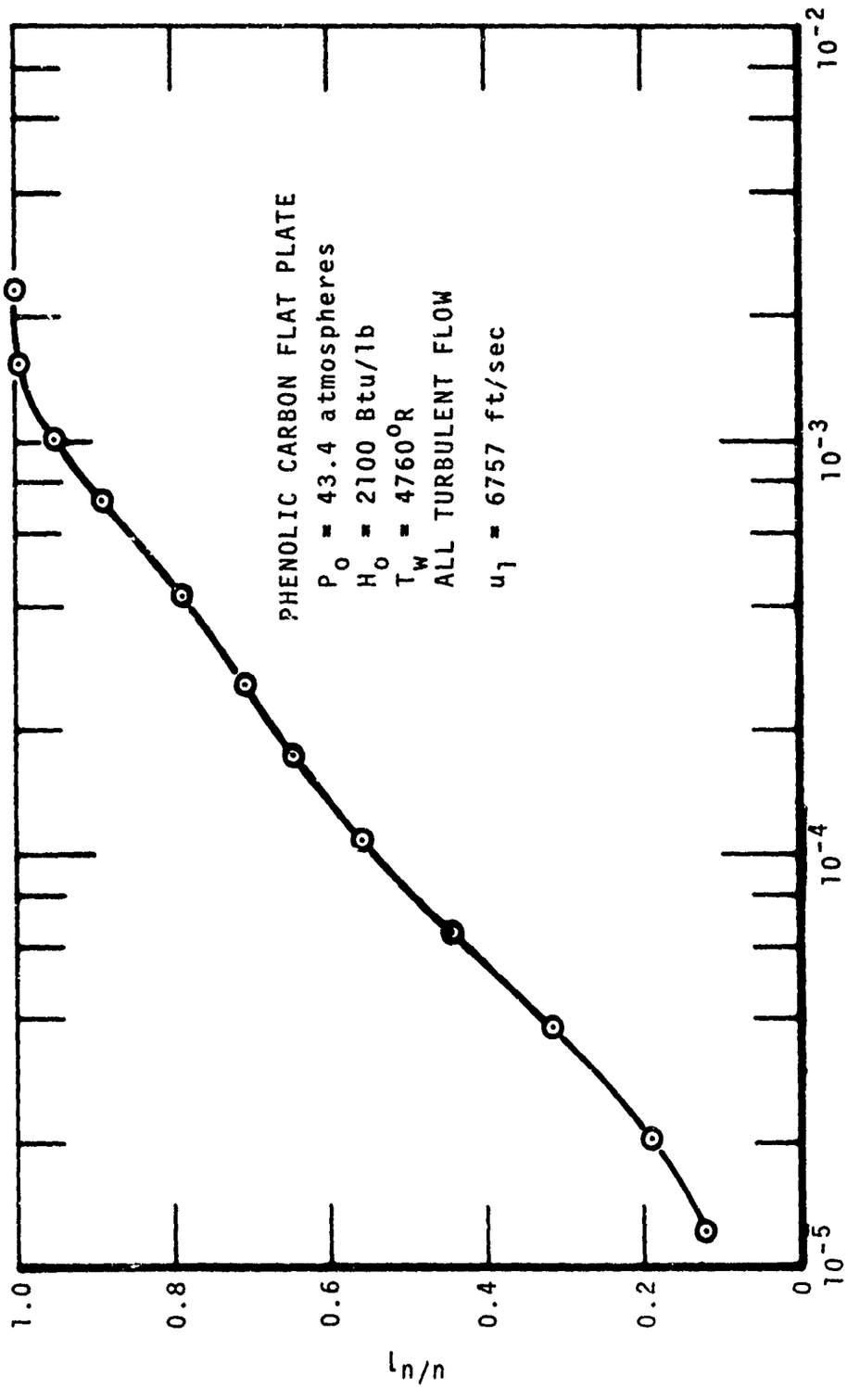

Figure 8. Logarithmic Plot of Velocity Profile at S = 0.03125 feet

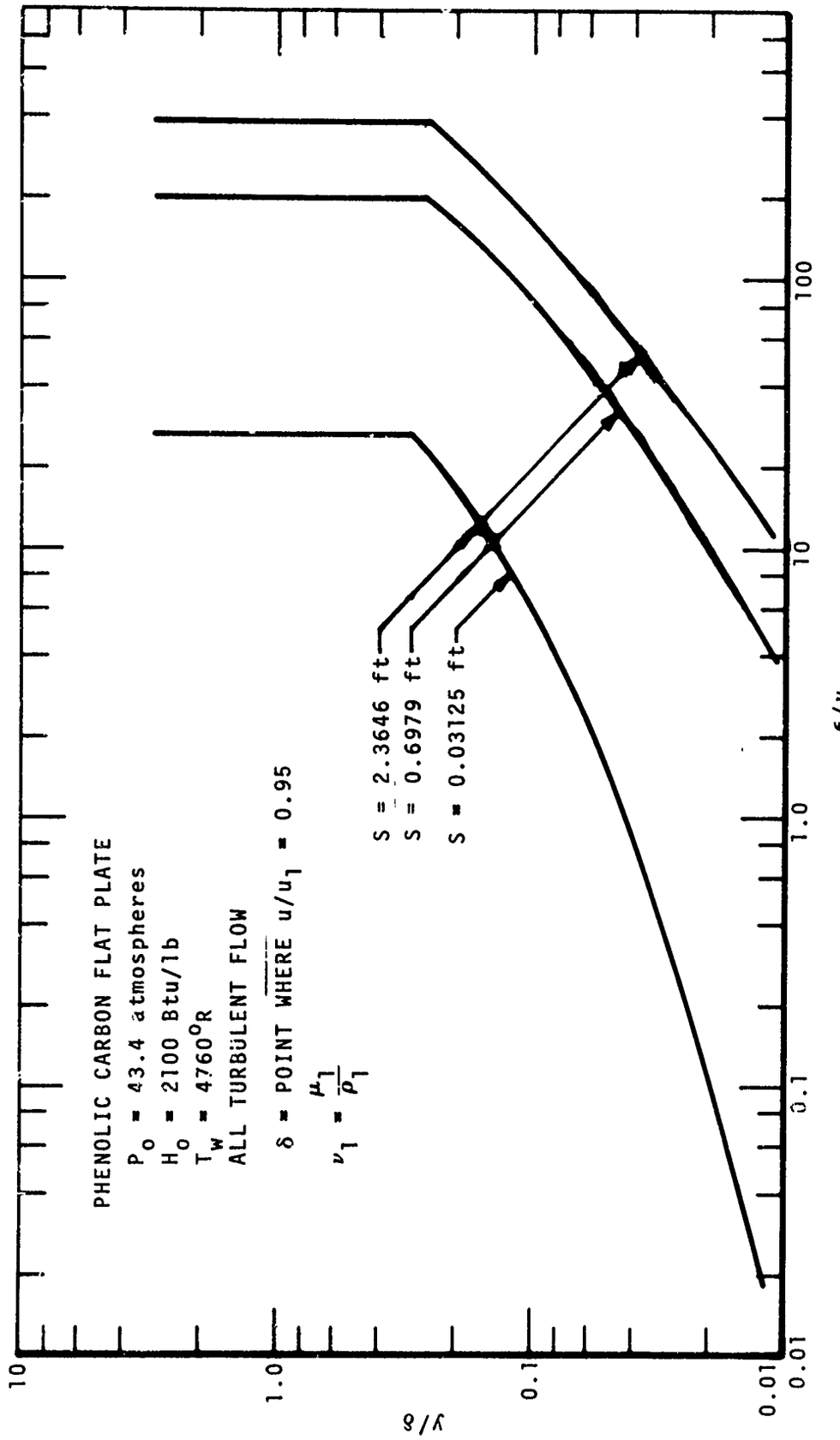

Figure 9. Eddy Viscosity Profiles for Flow Over an Ablating Flat Plate

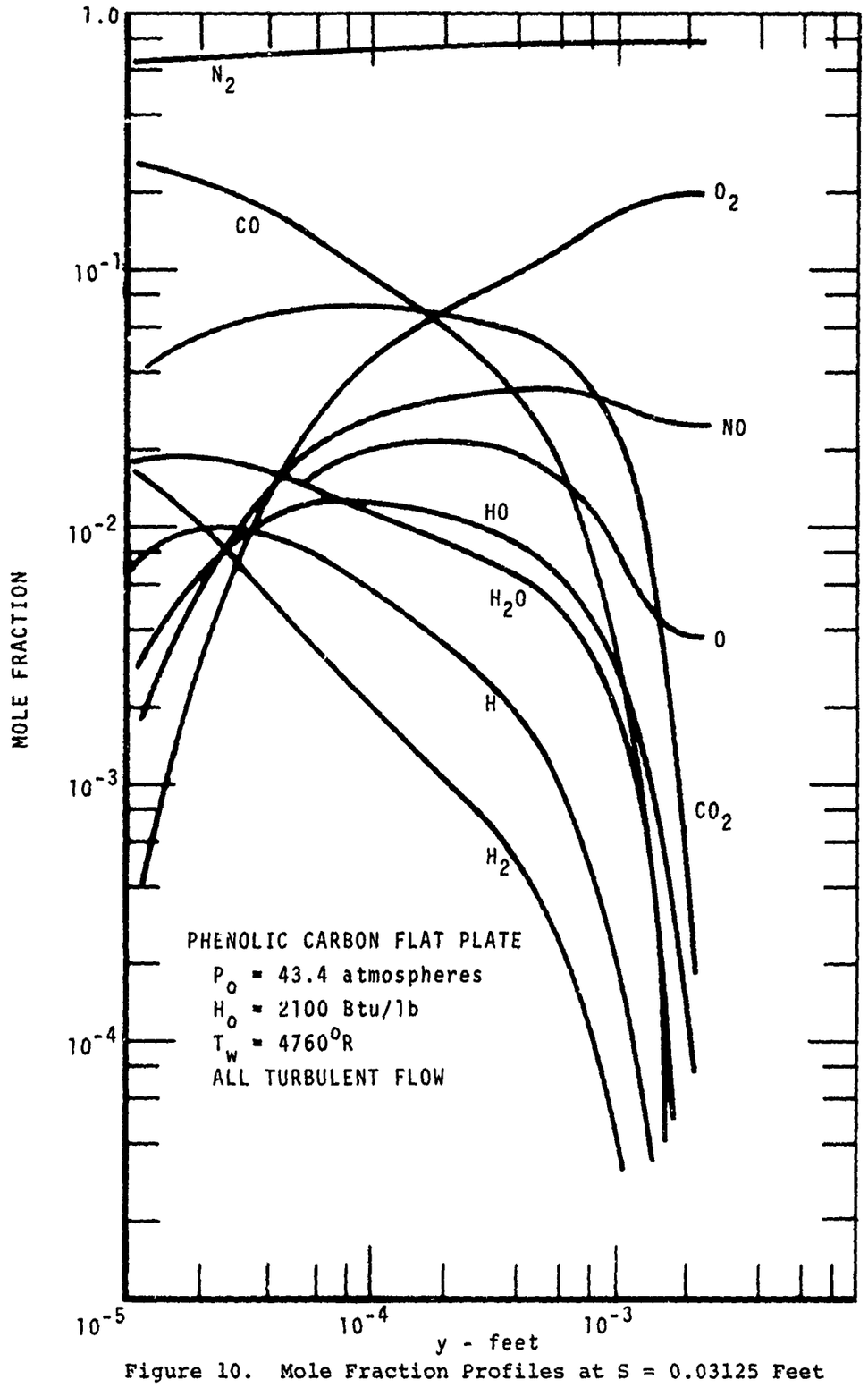

Figure 10. Mole Fraction Profiles at S = 0.03125 Feet

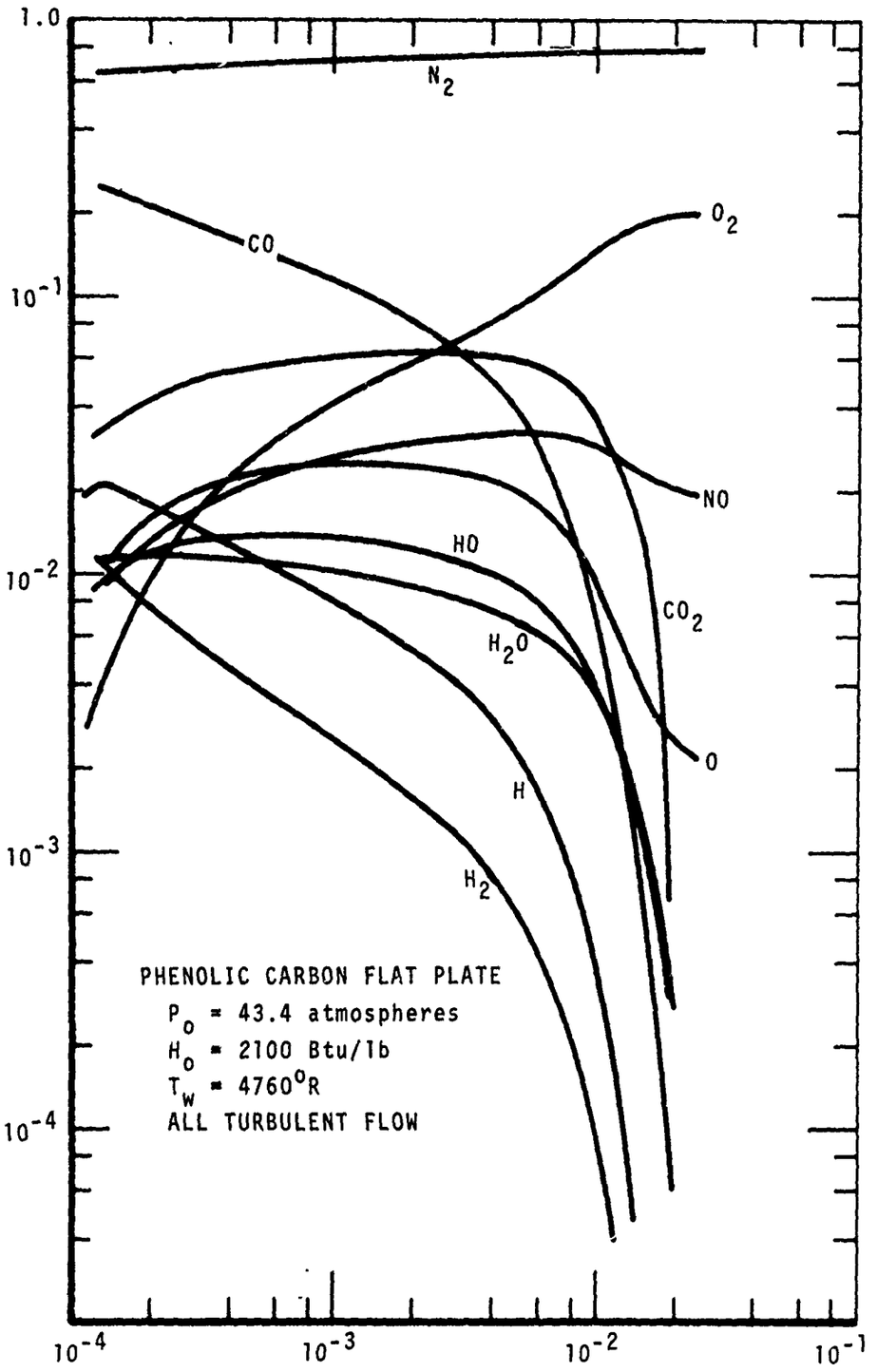

Figure 11. Mole Fraction Profiles at S = 0.6979 Feet

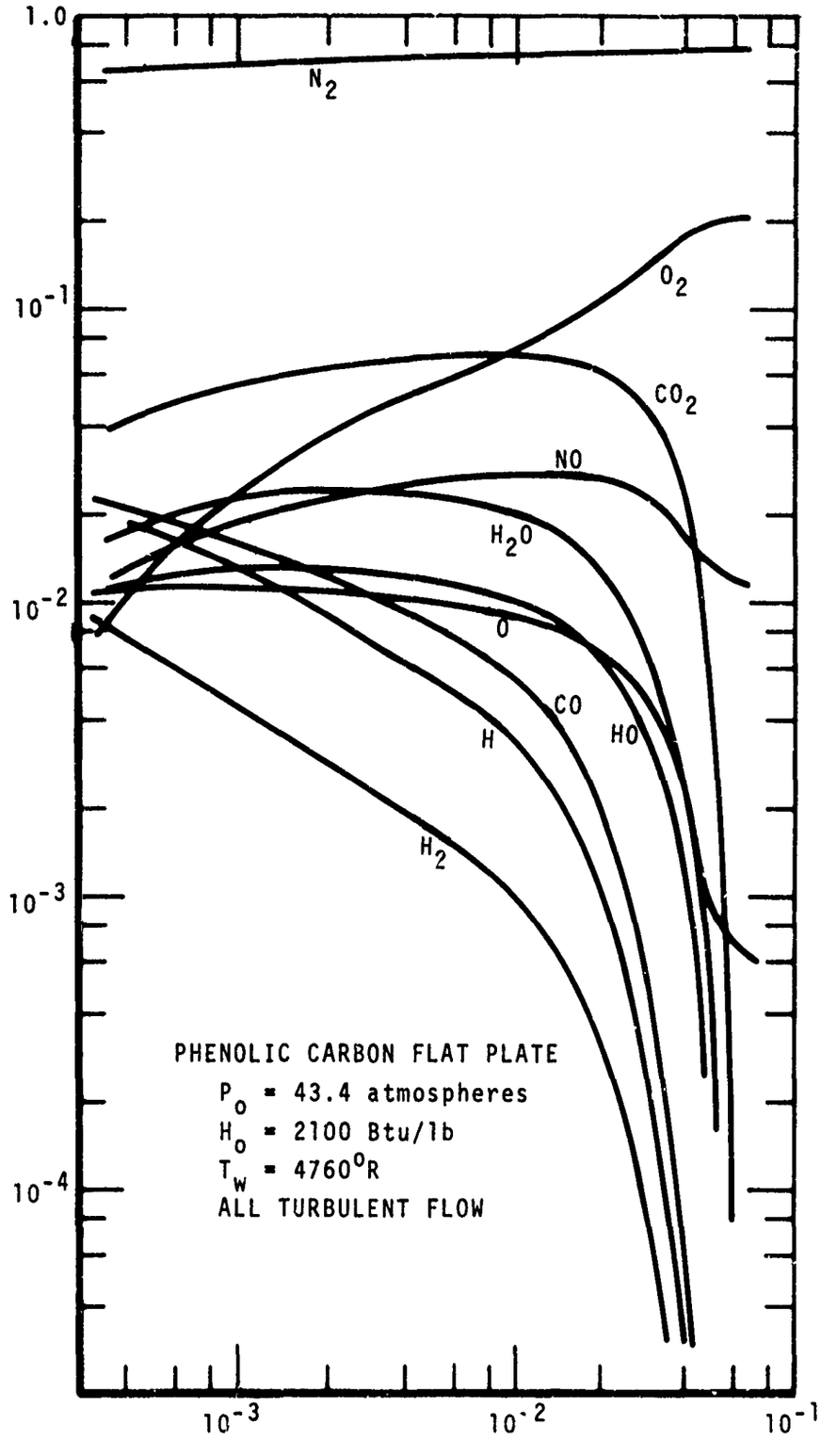

Figure 12. Mole Fraction Profiles at S = 2.3646 Feet

Table I

SPECIES CONSIDERED IN GRAPHITE PHENOLIC FLAT PLATE PROBLEM

Species	Maximum Mole Fraction at S = 0.6979 ft.
C_3	4.700×10^{-5}*
CO	3.405×10^{-1}*
H	2.037×10^{-2}
N_2	7.774×10^{-1}
e-	5.084×10^{-8}
C(s)	0.
O_2	2.009×10^{-1}
C	1.487×10^{-6}*
CH	3.217×10^{-7}*
CHN	5.546×10^{-2}*
CHO	6.167×10^{-6}
CH_2	9.211×10^{-8}*
CH_3	3.088×10^{-6}*
CH_4	4.455×10^{-7}*
CN	2.667×10^{-4}*
CO_2	6.358×10^{-2}
C_2	1.898×10^{-6}*
C_2H	1.698×10^{-3}*
C_2H_2	6.622×10^{-3}*
C_2N_2	1.392×10^{-3}*
C_3H	3.903×10^{-3}*
C_3H_2	4.818×10^{-5}*
C_3H_3	2.928×10^{-6}*
HN	5.014×10^{-6}
HO	1.355×10^{-2}
H_2	1.868×10^{-2}*
H_2N	2.447×10^{-7}
H_2O	1.184×10^{-2}

Table I (concluded)

Species	Maximum Mole Fraction at S = 0.6979 ft.
N	3.511×10^{-5}
NO	3.211×10^{-2}
O	2.509×10^{-2}
C_4	2.404×10^{-7}*
C_5	1.427×10^{-6}*
C^+	5.872×10^{-14}*
N^+	1.362×10^{-17}
N_2^+	6.549×10^{-15}
O_2^-	6.540×10^{-10}
CO^+	5.506×10^{-13}
NO^+	5.211×10^{-8}
O^+	2.881×10^{-14}
O_2^+	8.032×10^{-12}
O^-	1.133×10^{-9}

*At the surface

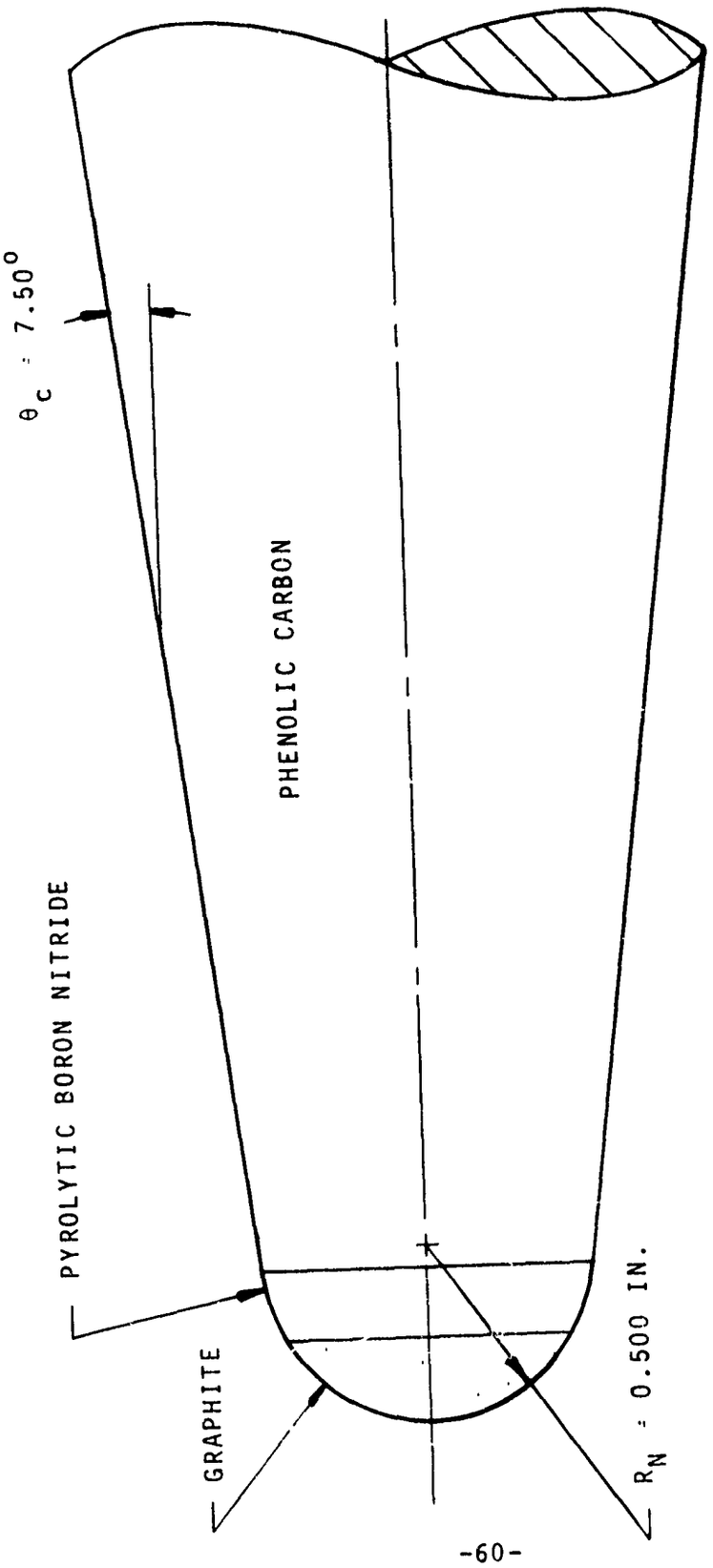

Figure 13. Schematic of Standard Sphere-Cone Configuration

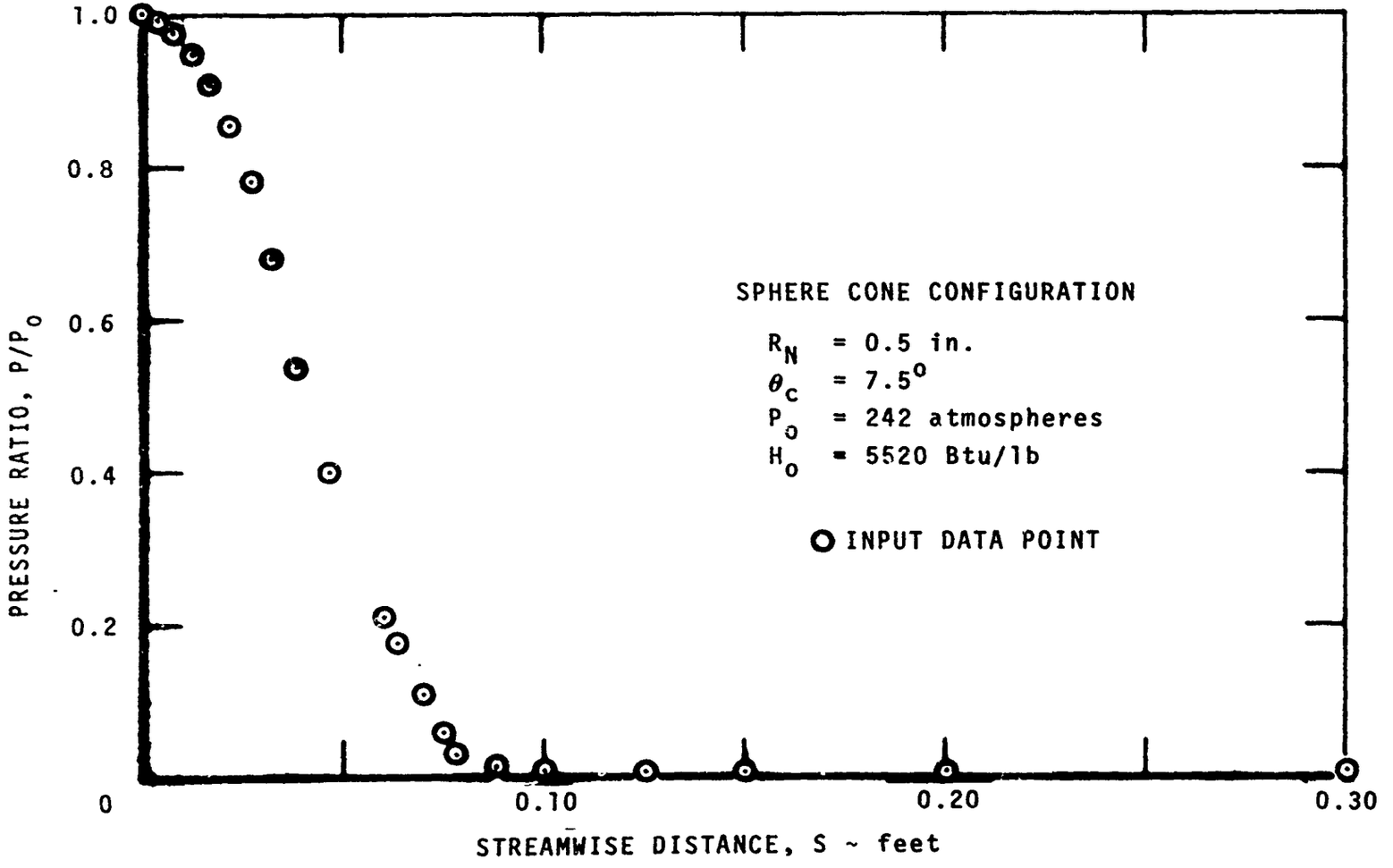

Figure 14. Prespecified Pressure Distribution

presentation here in order to expand the region of most interest. The resulting β distribution may be seen in Figure 15. It is apparent that a great deal of care must be exercised in choosing the pressure distribution data points, since β is calculated from the pressure gradient implicit in that data.

Table II summarizes the vehicle configuration in more detail. For this sample problem the option of a quasi-steady energy balance at the wall was used, in addition to demanding surface equilibrium, for all three surface materials. The program then calculates its own ablation rate, wall species concentrations, and temperature levels based on the energy balance and chemical equilibrium requirements. The quasi-steady ablation mode was selected to allow specification of a minimum of boundary condition information and to demonstrate the use of this option as opposed to arriving at an accurate ablation prediction. Indeed, the emphasis in the current program development has been the incorporation of a turbulent model into an existing laminar boundary layer code. The selection of an ablation model and the corresponding boundary conditions for a given surface material is a difficult problem in itself, requiring careful examination of the possible condensed phase products of reaction at the surface, kinetically controlled surface reactions, mechanical failure, interaction with pyrolysis gases, etc. (reference 29). For these sample problems, the intent was to de-emphasize this procedure in order to concentrate on the actual boundary layer behavior. The calculation was started at the stagnation point and allowed to transist at $Re_\theta = 250$. Figure 16 illustrates the distribution of $C_f/2$ over the first 0.30 feet of surface running length. As can be seen in the $C_f/2$ distribution, transition, occurred between S = 0.0268 and S = 0.0323 feet. Reynolds number on momentum thickness and shape factor streamwise distributions may be seen in Figures 17 and 18. Figure 19 illustrates the wall temperature distribution that results from the steady state energy balance and surface equilibrium assumption. Figure 20 illustrates the calculated quasi-steady surface recession rate.

Profile information for this problem is particularly interesting since both boundary layer transition and surface material changes occur over the forward portion of the body. Velocity profiles are presented in Figure 21. The body stations selected include the stagnation point (0.0 ft.), flow just ahead of transition (0.02681 ft.), flow just after transition which happens to be over the boron nitride just past the C-BN discontinuity (0.03231 ft.), and flow over the phenolic carbon just past the BN-phenolic carbon discontinuity (0.06273 ft.). The first two profiles are clearly laminar in nature, whereas the third is more transitional. The last profile appears to have the shape of a fully turbulent flow. This gradual evolution of a turbulent shape occurs because both laminar and turbulent transport terms are retained in the equations of motion (once the Re_θ criterion has been satisfied) and because the nonsimilar analysis retains the upstream "history" of the flow. Species concentration profiles for the same

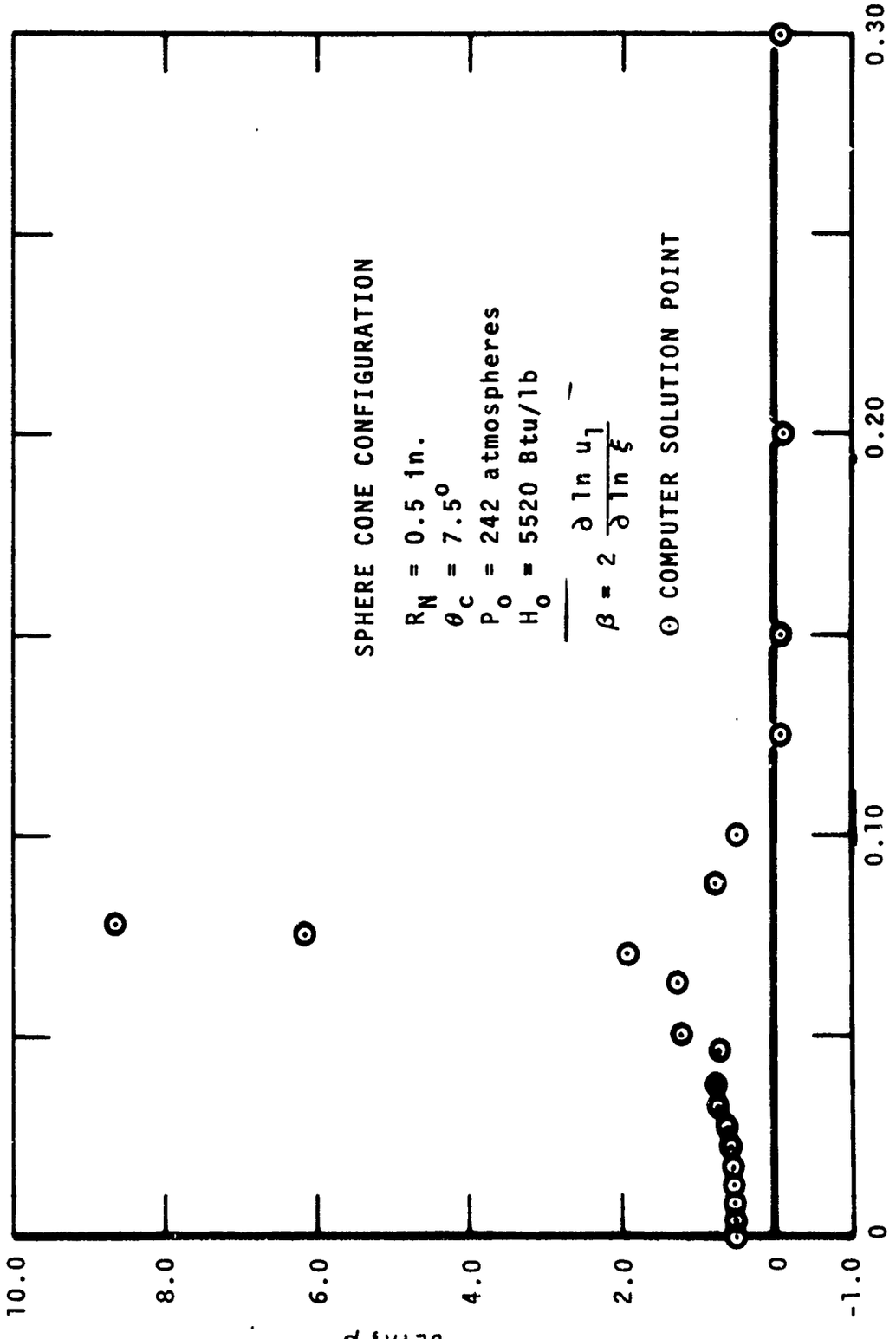

Figure 15. Calculated Beta Distribution

Table II

SPHERE-CONE CONFIGURATION SURFACE MATERIALS DETAILS

Surface Running Length (feet)	Surface Material
0.	graphite
0.004174	graphite
0.008390	graphite
0.012695	graphite
0.017146	graphite
0.021817	graphite
0.026813	graphite
0.032308	pyrolytic boron nitride
0.038637	↓
0.046657	↓
0.059975	pyrolytic boron nitride
0.062727	phenolic carbon
0.070000	↓
0.075000	↓
0.077500	↓
0.087500	↓
0.100000	↓
0.125000	↓
0.150000	↓
0.200000	↓
0.300000	↓
0.500000	↓
0.700000	↓
1.000000	↓
1.500000	↓
2.000000	↓
3.000000	↓
4.000000	↓
5.016400	phenolic carbon

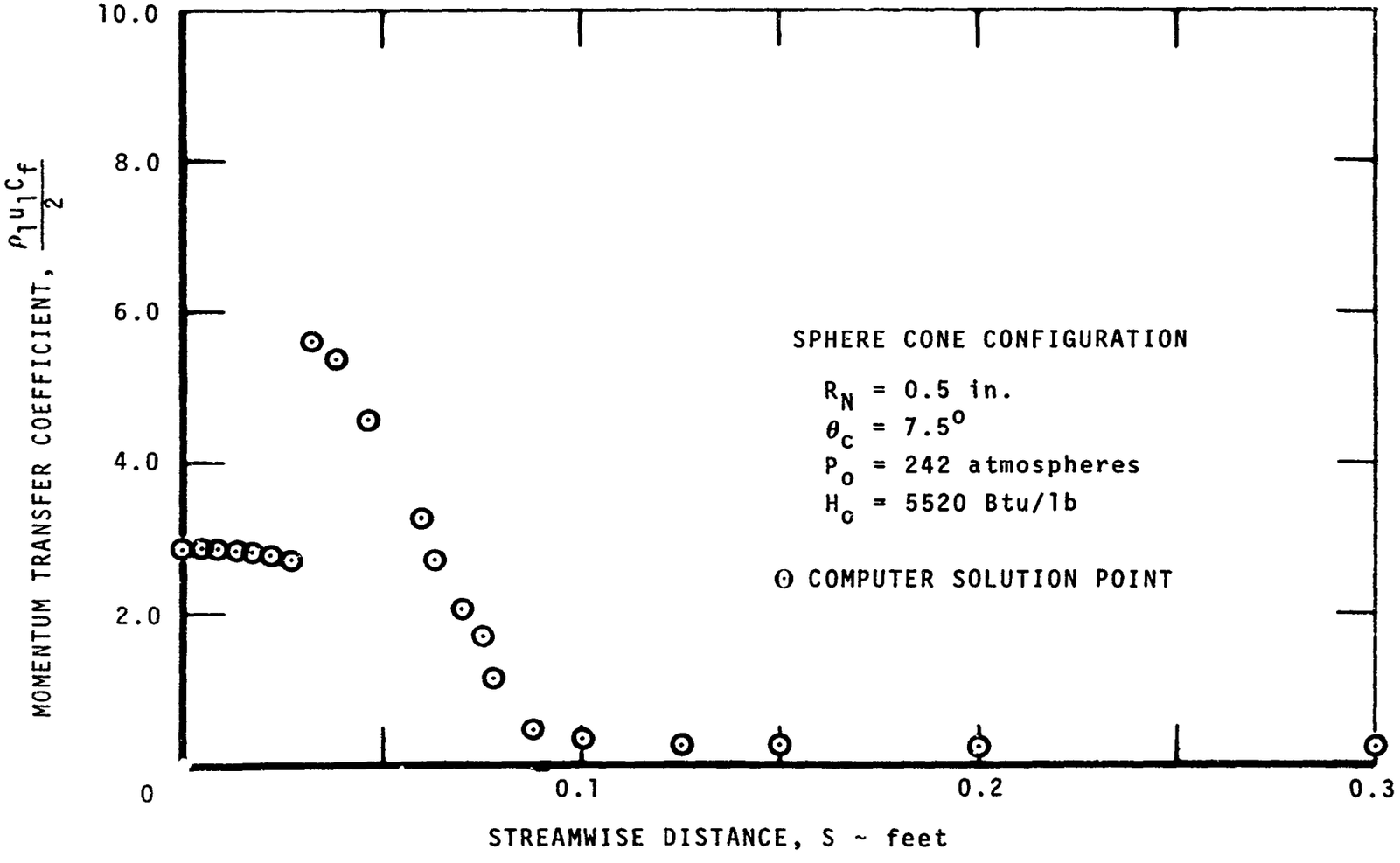

Figure 16. Momentum Transfer Coefficient Distribution

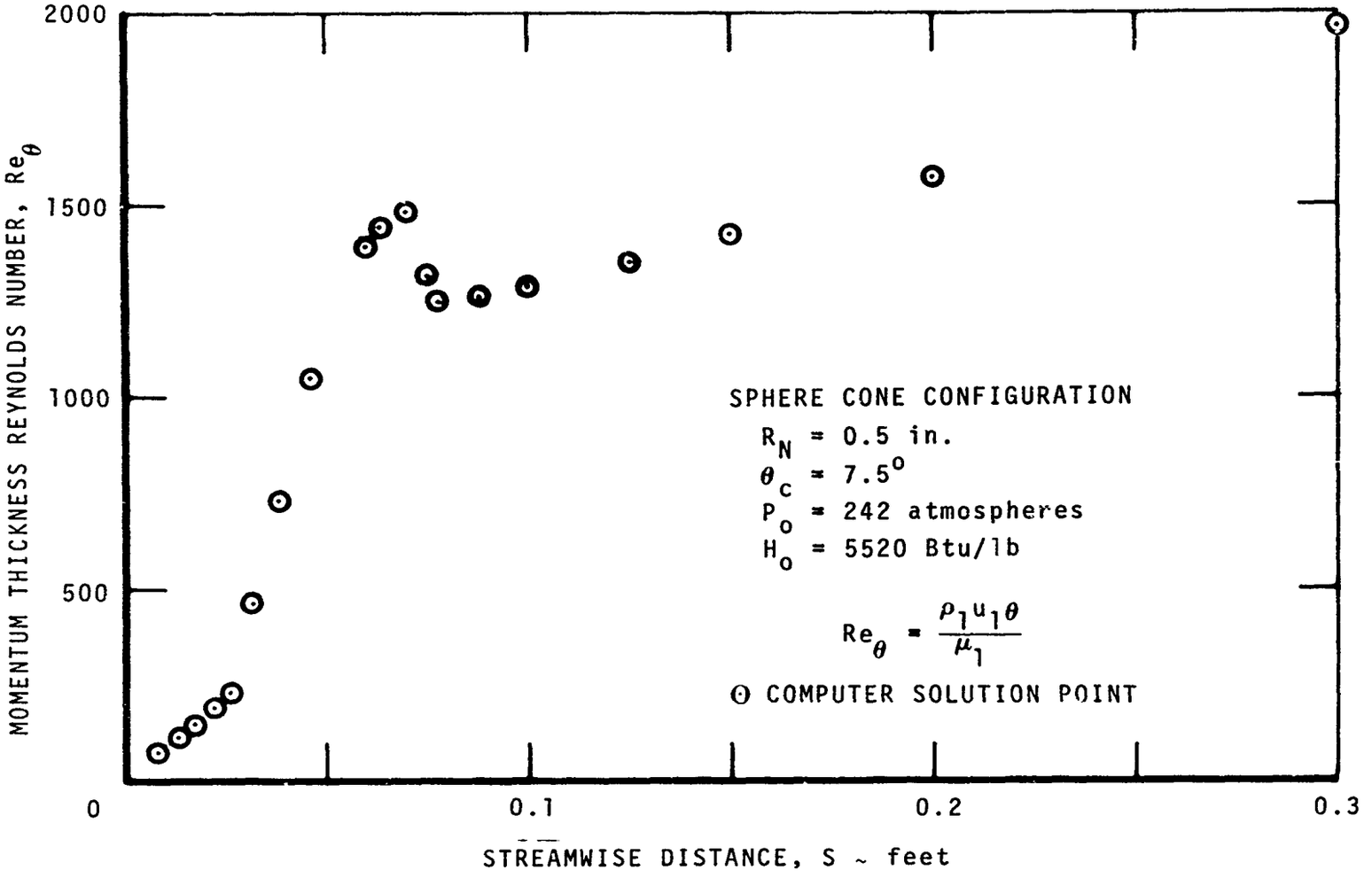

Figure 17. Momentum Thickness Reynolds Number Distribution

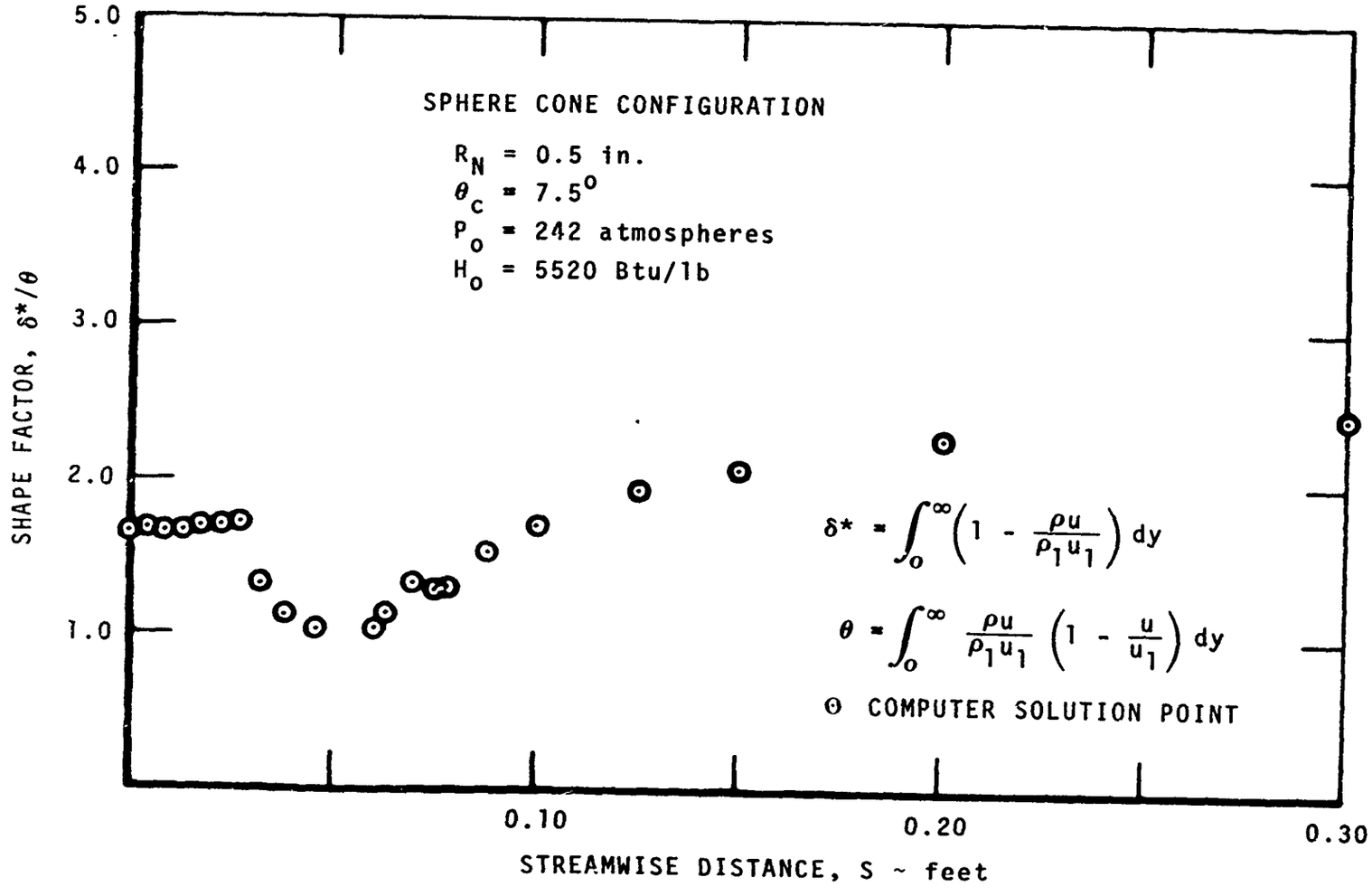

Figure 18. Shape Factor Distribution

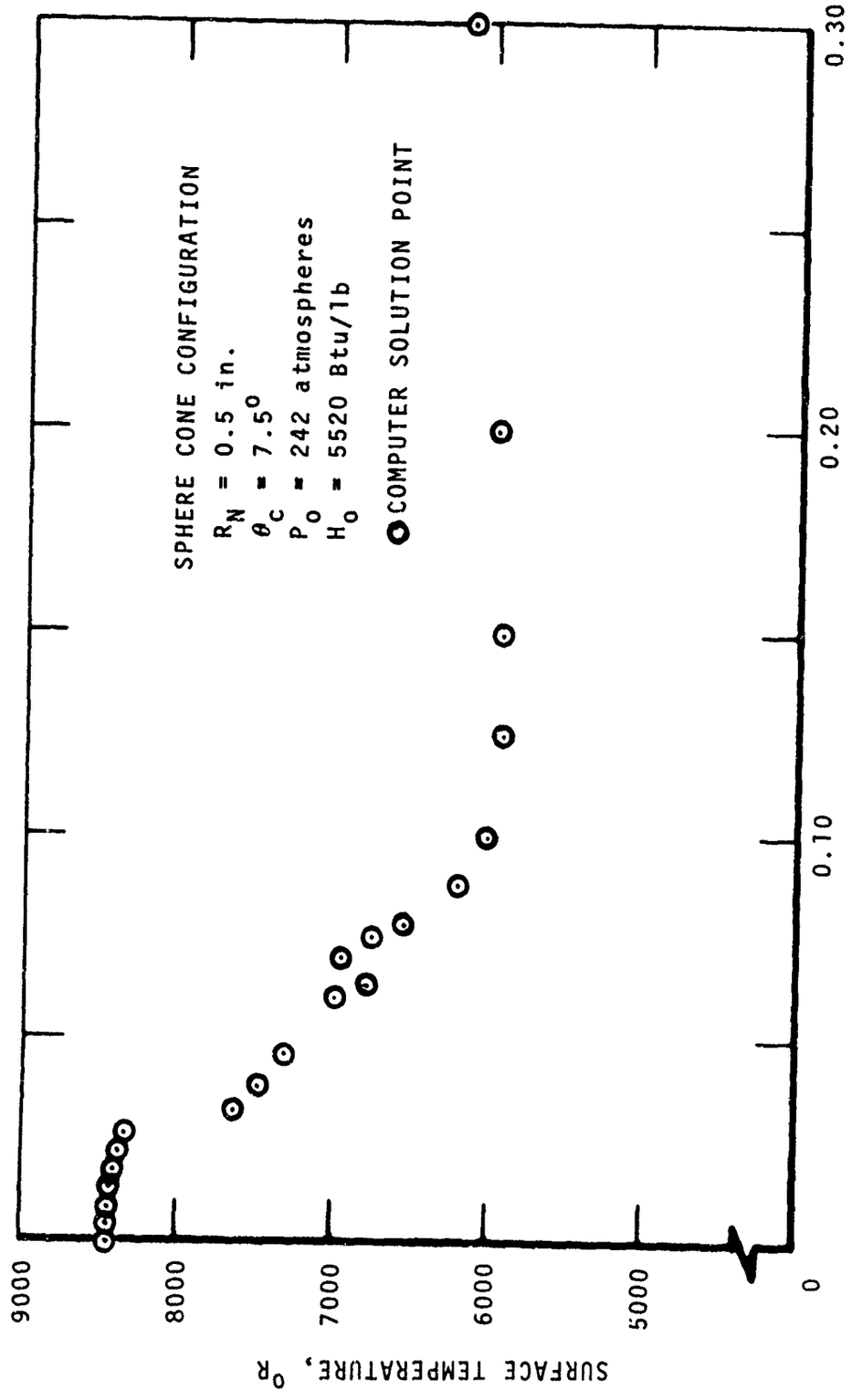

Figure 19. Calculated Surface Temperature Distribution

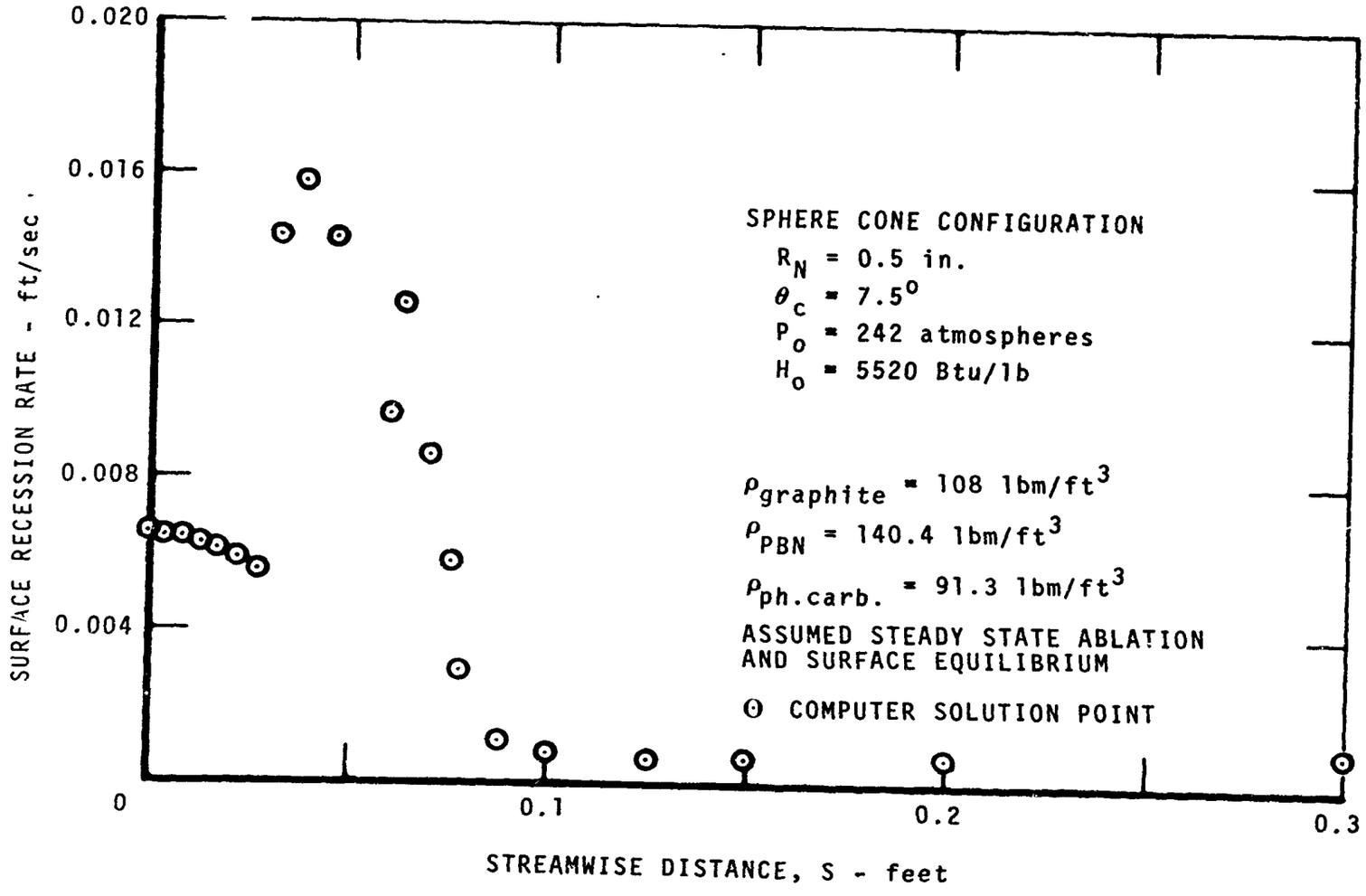

Figure 20. Calculated Surface Recession Rate

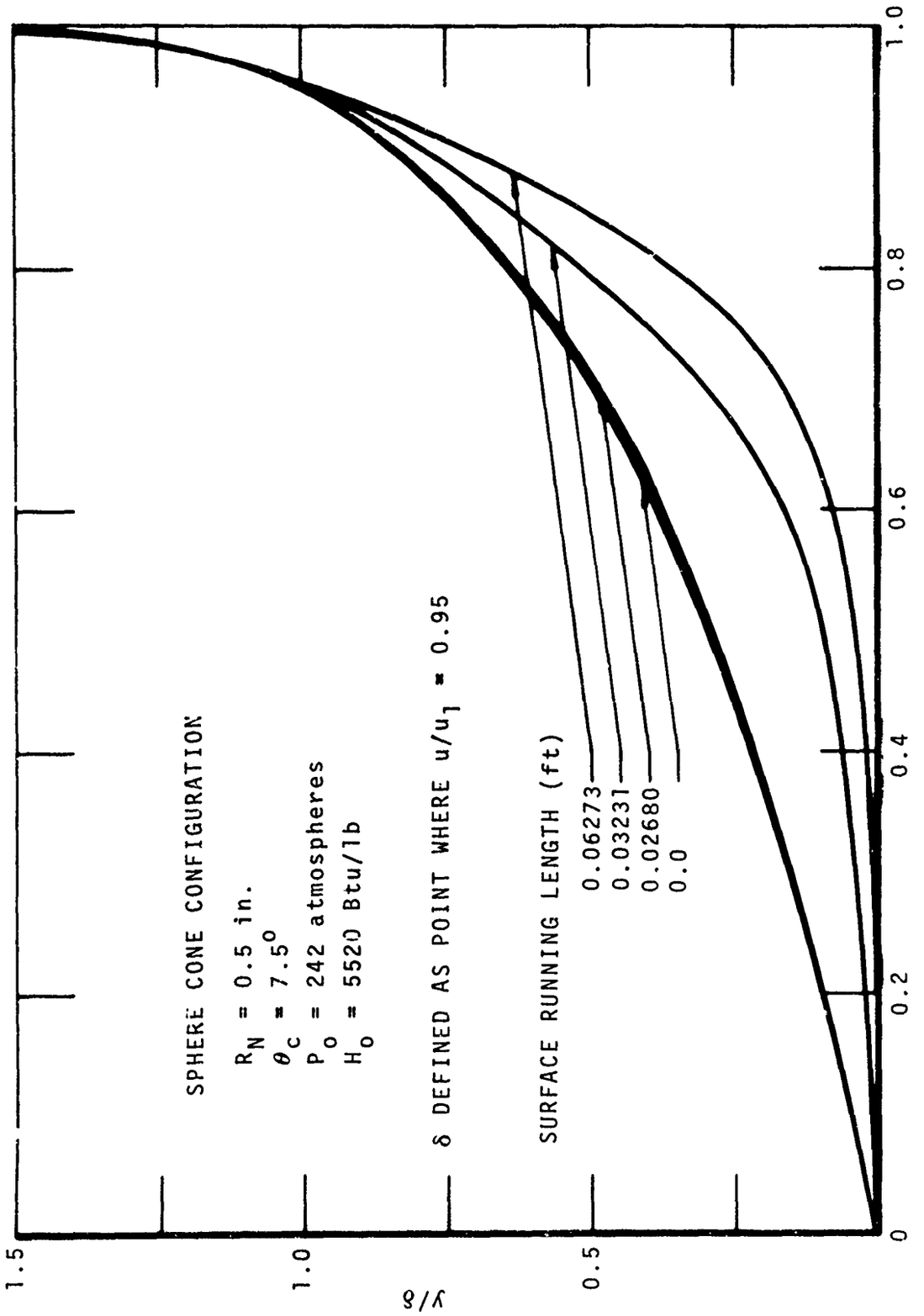

Figure 21. Velocity Profiles at Several Stations

four stations are presented in Figures 22 through 25. It is interesting to observe that the region of greatest chemical interaction appears to shrink further and further away from the outer edge of the boundary layer as the flow progresses downstream. This is consistent with the knowledge that the laminar sublayer grows at a slower rate than the turbulent core flow. Another interesting feature of these species profiles is in Figure 25, where it can be seen that a significant mole fraction of boron compounds persists in the boundary layer although the flow is adjacent to a phenolic carbon surface at that station. A total of 60 species were considered in this problem, but only those exhibiting a mole fraction greater than 0.001 somewhere in the boundary layer are shown graphically. Finally, Figure 26 presents the electron concentration profile at S = 0.03231 feet over the BN surface. The y-scale is left unlogged in this graph in order to present a better picture of the actual dimensions of the regions of importance.

3. TRANSVERSE CURVATURE EFFECTS

The transverse curvature option of the BLIMP program is operational for either laminar or turbulent reacting flows. The simplest of these, all laminar flow, was chosen for a sample problem. Air was assumed to be flowing over a sharp cone at the following conditions:

P_o = 11.27 atmospheres

H_o = 1650 Btu/lb

M_{edge} = 6.38

cone half angle = 9^o

Seven nodes were chosen through the boundary layer, and the problem was run both with and without consideration of transverse curvature (TVC). Some of the results are presented in Figures 27 through 29. Figure 27 shows the TVC effect on drag coefficient. Inclusion of transverse curvature on this 9^o cone increased C_f by as much as 25 percent. A comparison of Reynolds number on momentum thickness is presented in Figure 28. Since r/r_o is everywhere greater than one, one might expect from the definition of θ that momentum thickness will be larger when TVC effects are considered. The steeper slope of the momentum thickness curve ($d\theta/ds$) for this zero pressure gradient problem is also apparent. This increase in slope is expected for the TVC case since the drag coefficient is larger. Figure 29 shows the velocity profile comparison at S = 0.025 feet. Transverse curvature effects are seen to decrease the boundary layer thickness, thereby increasing wall shear.

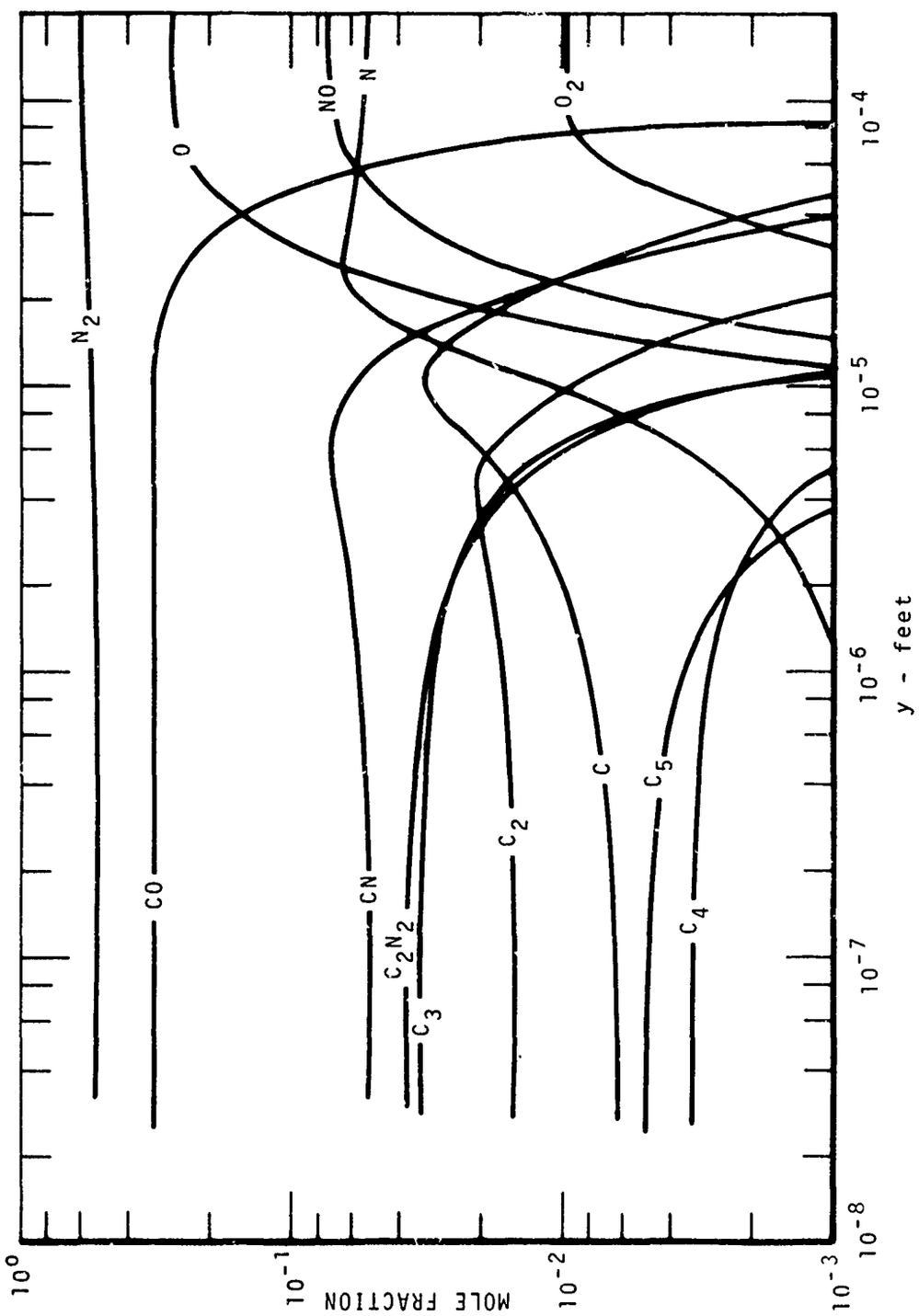

Figure 22. Species Concentration Profiles at S = 0.0 Feet for Sphere Cone Sample Case

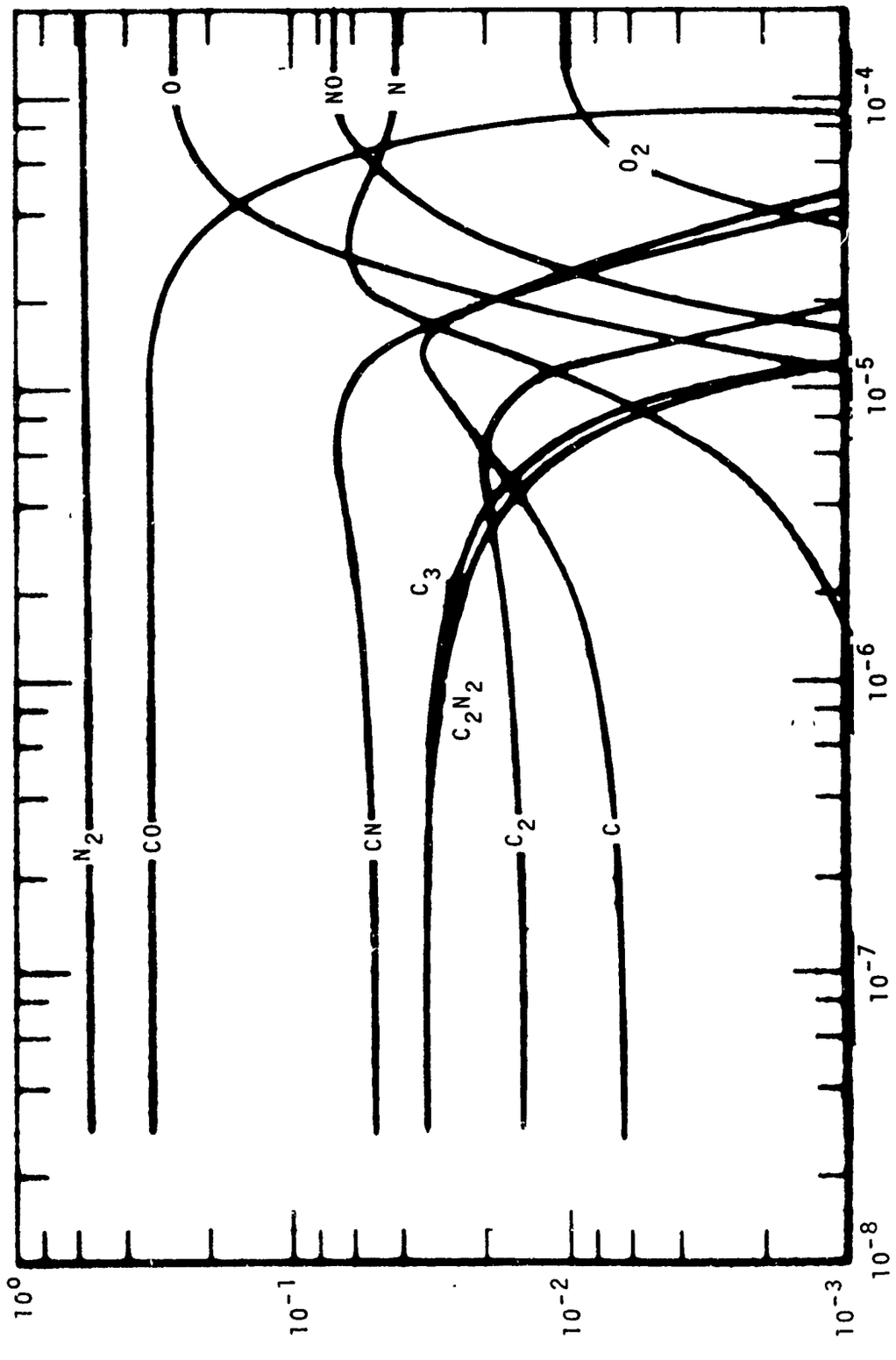

Figure 23. Species Concentration Profiles at S = 0.0268 Feet for Sphere Cone Sample Case

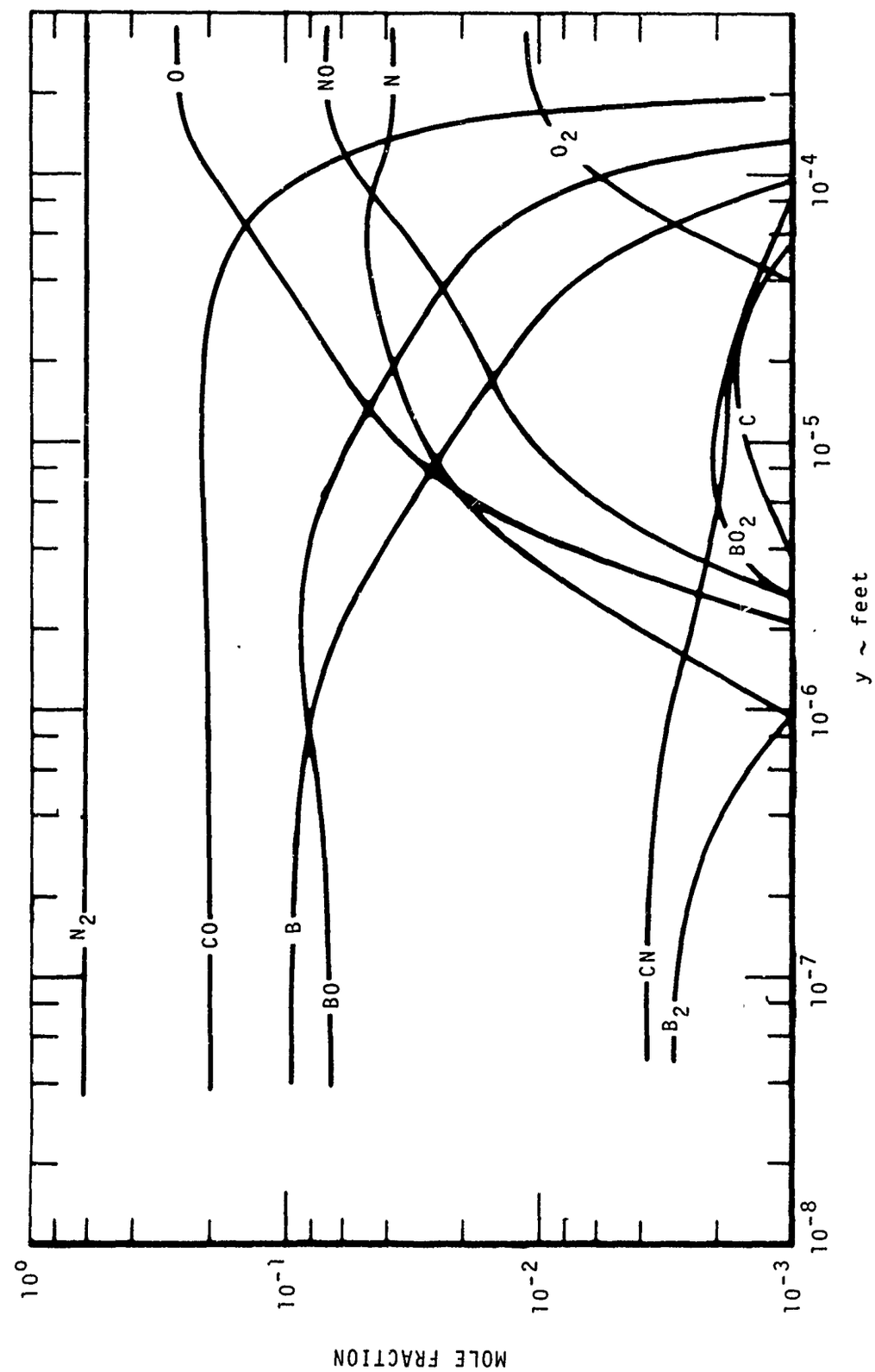

Figure 24. Species Concentration Profiles at S = 0.0321 Feet for Sphere Cone Sample Case

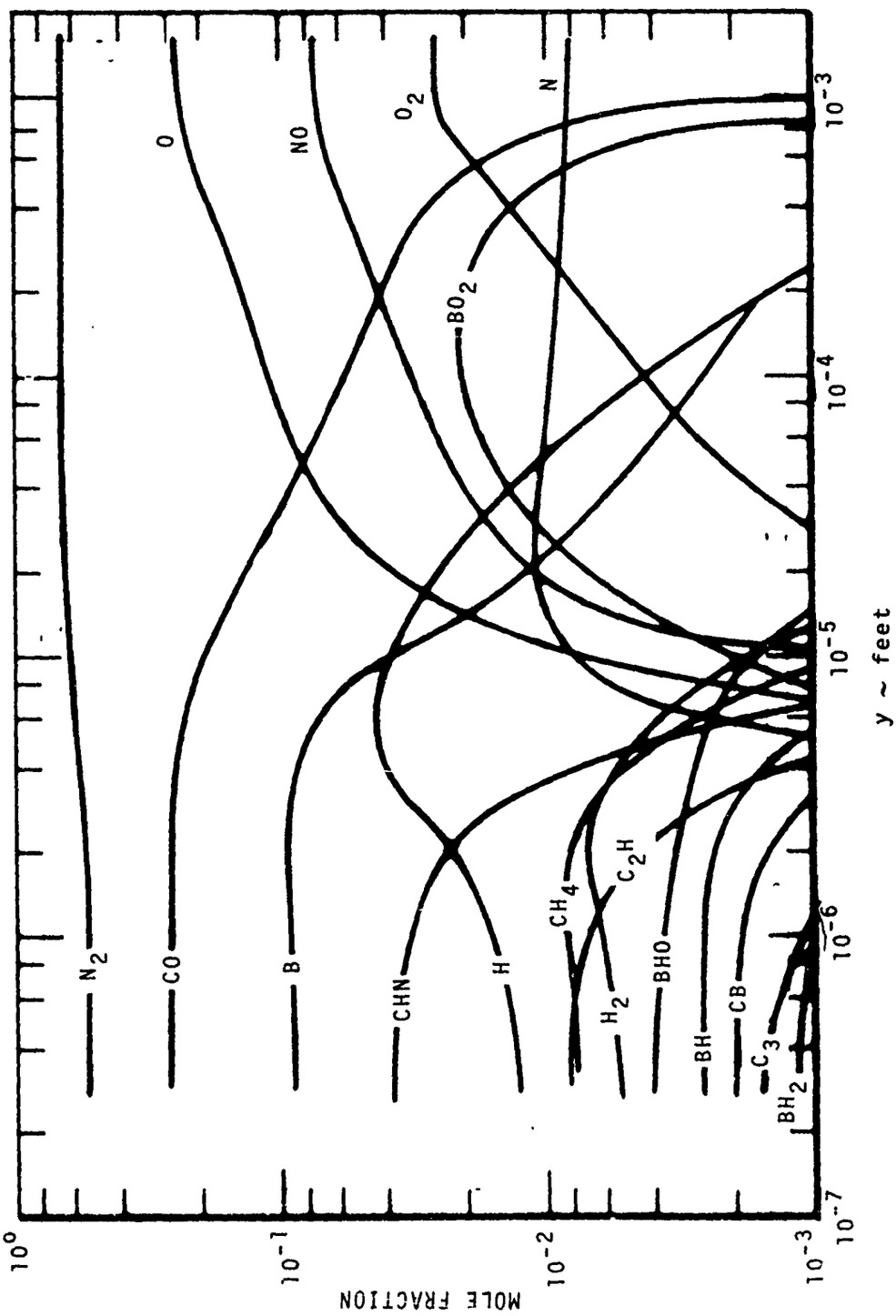

Figure 25. Species Concentration Profiles at S = 0.06273 Feet for Sphere Cone Sample Case

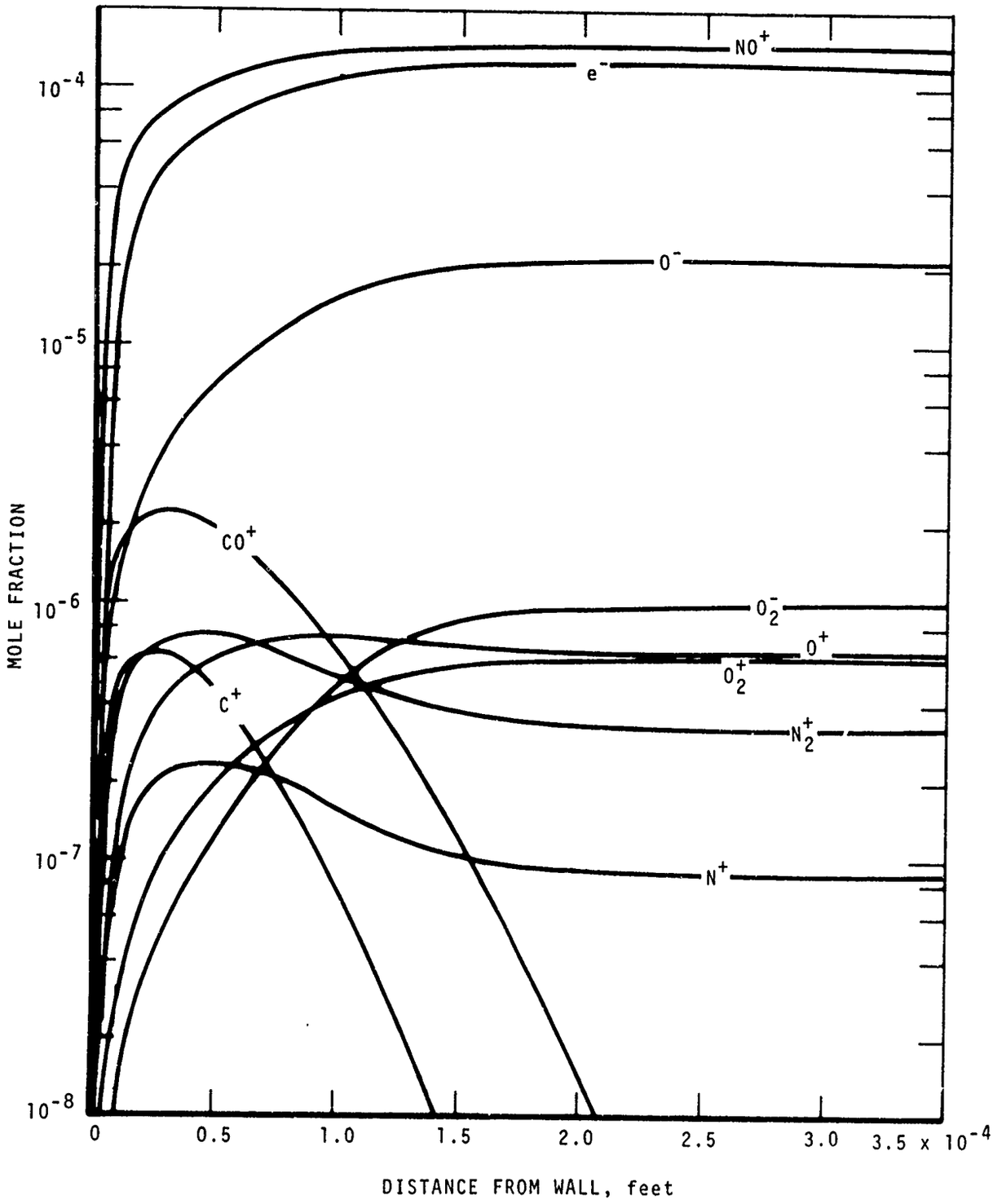

Figure 26. Charged Species Concentration Profiles at S = 0.03231 Feet

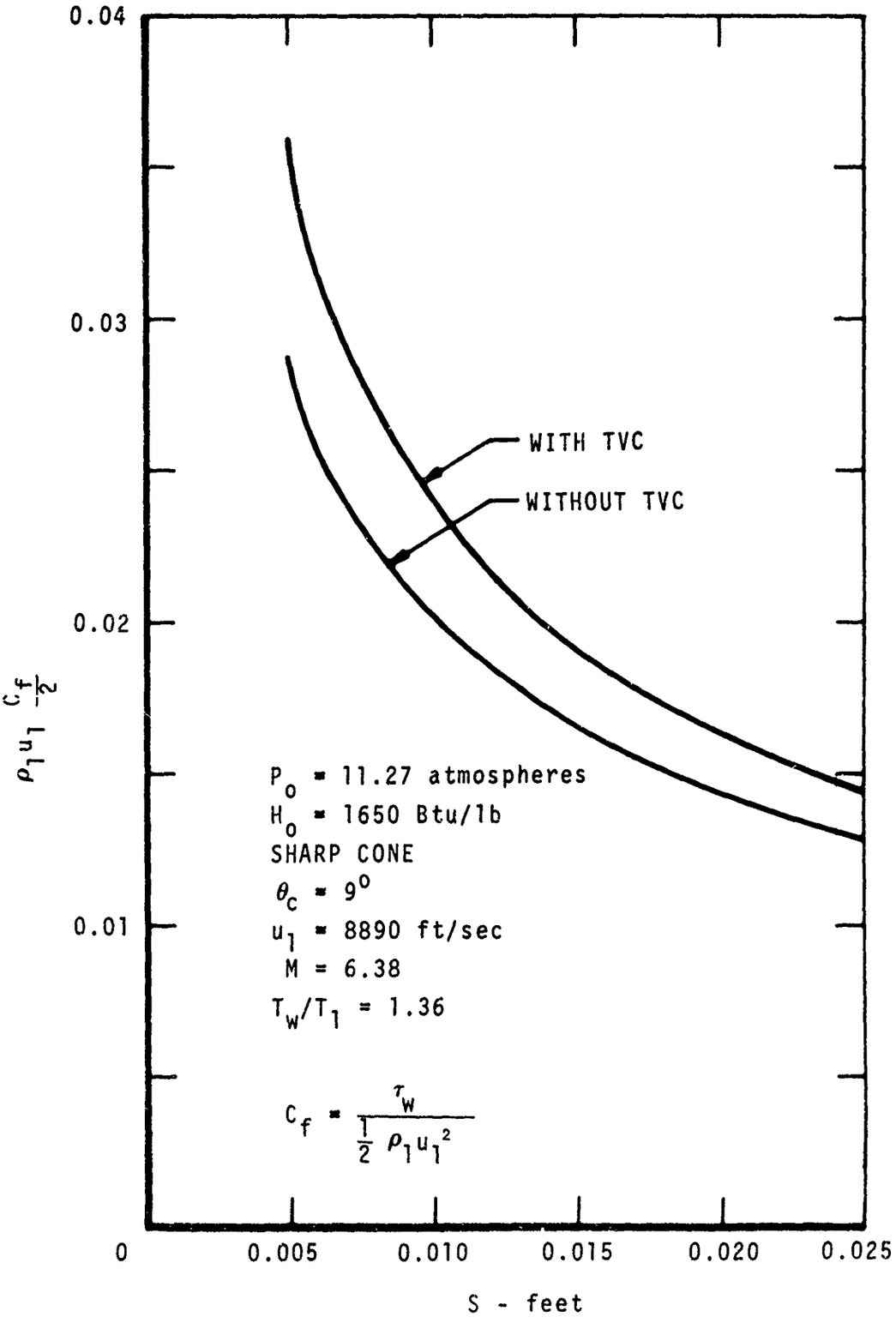

Figure 27. Variation of Drag Coefficient

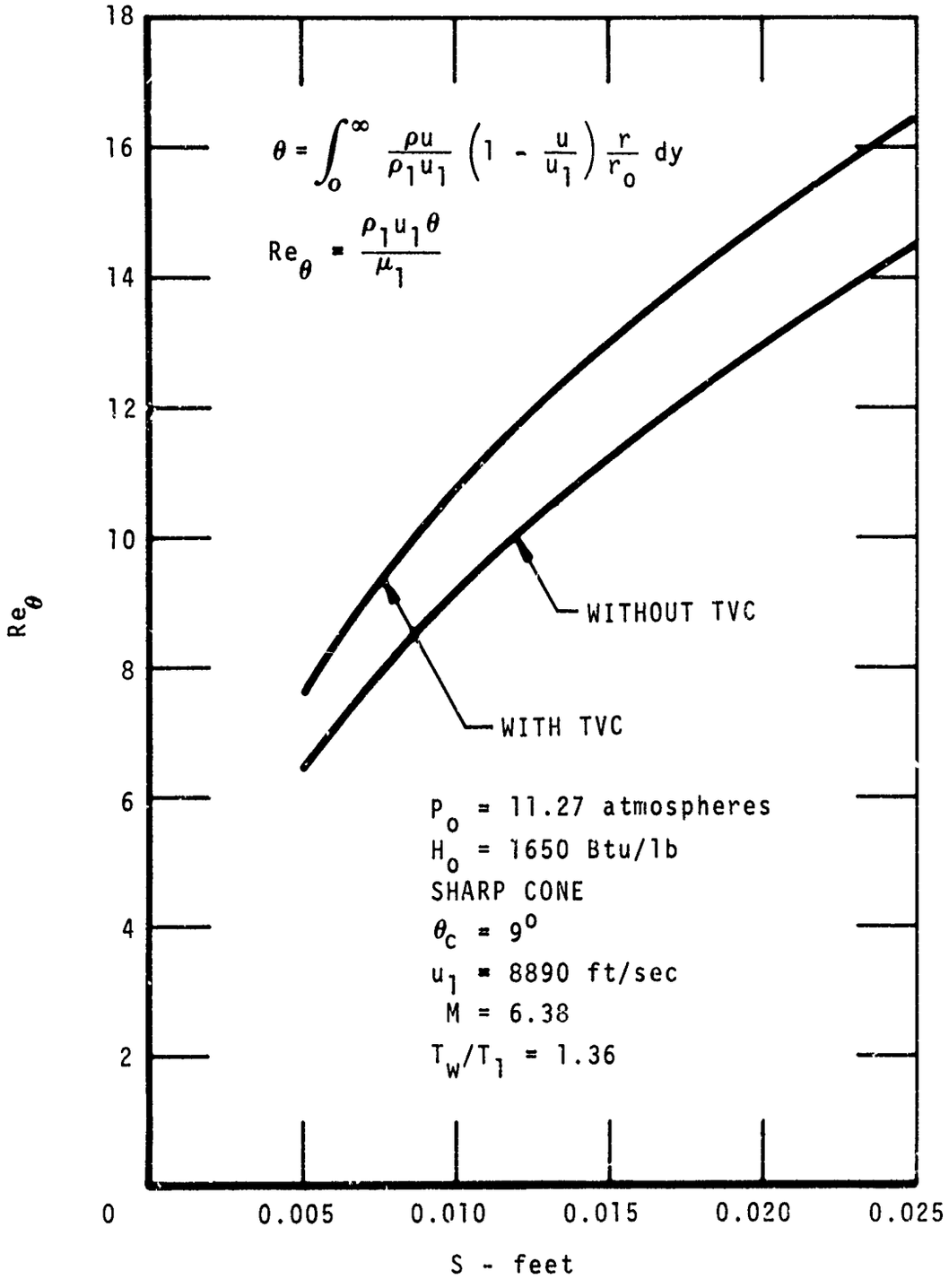

Figure 28. Variation of Momentum Thickness Reynolds Number

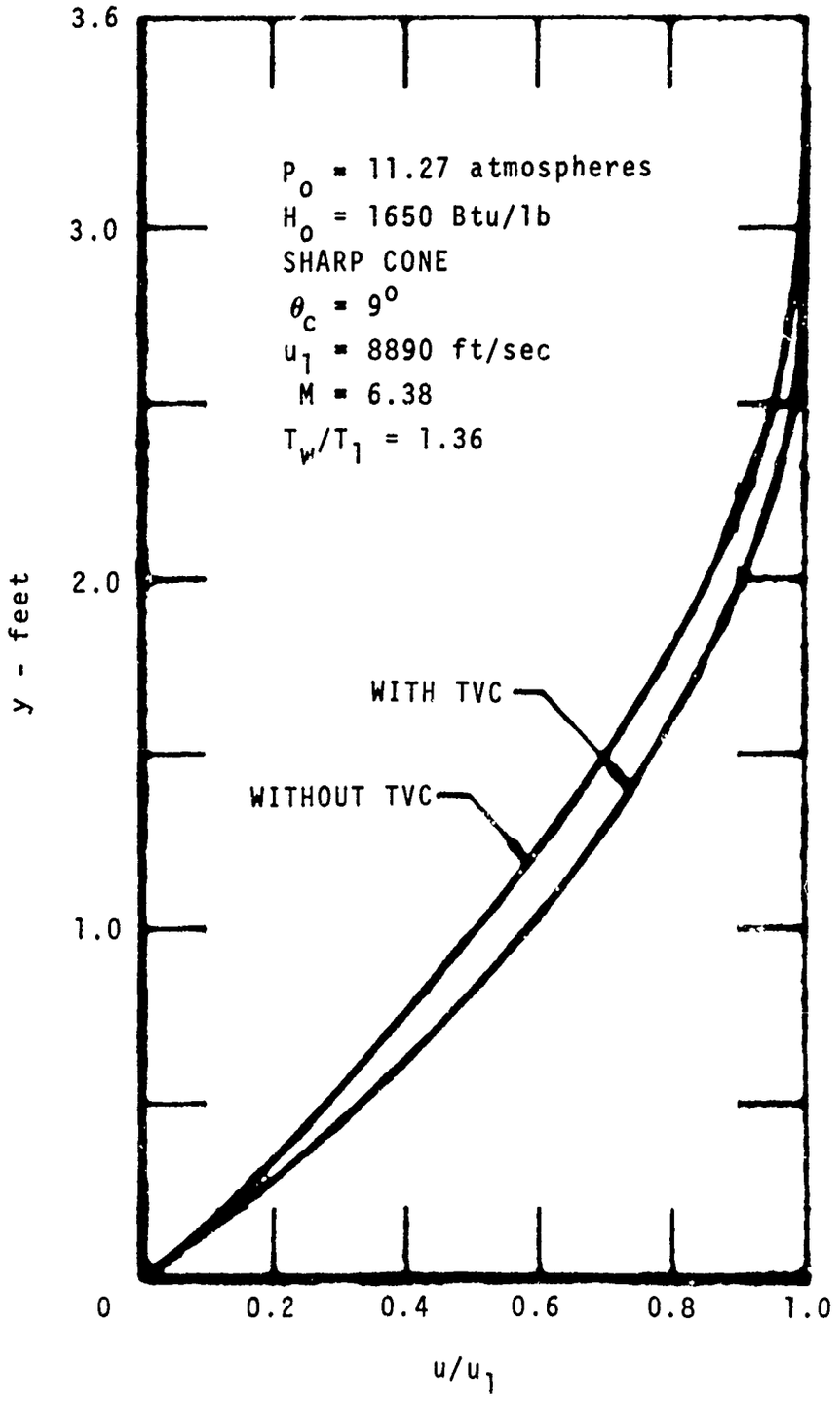

Figure 29. Velocity Profiles at S = 0.025 Feet

SECTION V

COUPLED ABLATOR BOUNDARY LAYER ENVIRONMENT PROGRAM

The usual ablating heat shield or nozzle material performance analysis requires separate determinations of the inviscid flow field over the body, the boundary layer flow near the surface, and the surface and in-depth response of the ablating material. The thought has no doubt crossed the mind of most thermodynamics-fluid dynamics engineers working in this field that some or all of these analyses should be combined to represent the coupled physical processes more correctly and to eliminate some of the wasted effort in carrying out separate analyses. Indeed, a coupled approach is desirable since the material response affects the structure of the boundary layer, and the boundary layer determines the energy and mass fluxes at the material surface which in turn control the heat shield response. Of course, any change in body shape will affect the inviscid flow field. The totally coupled analysis is, unfortunately, an enormous problem if accurate boundary layer and material response calculations are required, hence the present separate analysis state of the art. Still, it is possible to investigate coupled charring material, multicomponent boundary layer flow problems within the context of certain limiting assumptions. The CABLE program incorporates subroutine versions of the BLIMP program, described earlier in this report, and the Charring Material Ablation (CMA) program, described in reference 30, to accomplish this coupling. An earlier version of the CABLE program has been described elsewhere (reference 31) therefore its operation will only be summarized in Section V.1. Section V.2 describes recent results obtained with the program.

1. COUPLING THE CMA AND BLIMP PROGRAMS

The CMA program is an implicit finite difference one-dimensional charring ablation material analysis program which accounts for area change due to material curvature in a general fashion, with planar, cylindrical, and spherical geometries as special cases. Temperature dependent thermal properties are allowed, and the user may specify kinetically controlled pyrolysis reactions. Due to its one-dimensional nature however, the CMA program may not be particularly accurate in regions where lateral conduction is significant, such as sharp nose tips. Also, since local static pressure is input into the BLIMP program, no account is taken of the body shape change on the pressure distribution for the coupled analysis. Within these limitations, the CABLE program gives a very detailed, accurate picture of the ablation-boundary layer interaction.

There are a number of ways in which the boundary layer and charring ablation programs can be coupled. In the procedure which has been adopted, the CMA program is effectively the controlling program, calling BLIMP whenever necessary. Since the time (θ) steps in a charring ablation analysis are typically quite small (0.001-1.0 seconds), yet the times of significant change in a boundary layer flow are fairly far apart (0.5-10.0 seconds), it would be uneconomical to require a boundary layer solution at every CMA time step. Therefore the CABLE technique is to input mandatory solution times at which complete boundary layer solutions are carried out. Between these mandatory times boundary layer parameters are found by interpolation, and these boundary layer parameters are provided to the CMA program as boundary conditions. Another computer time saving device is the use of discrete values of normalized pyrolysis gas mass flow rates ($\dot{m}_g^*$) and normalized char mass flow rates ($\dot{m}_c^*$). As the charring ablation program proceeds in time, a new combination of $\dot{m}_g^*$ and $\dot{m}_c^*$ evolves from the CMA solution at each time step. It would not be possible to anticipate and calculate the boundary layer flows for each of these $\dot{m}_g^*$-$\dot{m}_c^*$ combinations at every mandatory solution time, therefore a grid of $\dot{m}_g^*$-$\dot{m}_c^*$ values is preselected at which BLIMP calculations may be run. The BLIMP program is automatically run at several of the preselected grid points in the assigned injection, surface equilibrium (or kinetically controlled reaction) mode, and the required boundary layer parameters are found from a three way interpolation of the boundary layer solutions in the $\dot{m}_g^*$, $\dot{m}_c^*$, θ coordinate array. It is significant that not all BLIMP solutions in the $\dot{m}_g^*$, $\dot{m}_c^*$, θ array need be run, but rather only those which are needed to provide interpolation values for the current CMA solution. Initially, eight BLIMP solutions are required, which consist of two values of $\dot{m}_g^*$ with two values of $\dot{m}_c^*$, all at the first two mandatory times. The CMA solution then proceeds until the solution "path" exceeds the limits of the "cube" defined by the first eight ($\dot{m}_g^*$, $\dot{m}_c^*$, θ) coordinate points. Additional BLIMP solutions are then called for at the new required grid points ($\dot{m}_g^*$, $\dot{m}_c^*$, θ) such that ordinary interpolation can take place, whereupon the CMA program again proceeds. Thus, although a fairly extensive array of $\dot{m}_g^*$, $\dot{m}_c^*$, θ values may be defined, only the required BLIMP solutions will be run. This procedure will be explained more thoroughly by an example below.

In the procedure which has been adopted, the transient charring ablation solution is effectively the controlling program. The charring ablation solution at a given station proceeds noniteratively, calling the boundary-layer procedure as needed to fill in the surface boundary condition matrix. The complete time history at each body station is performed prior to advancing to the next body station. As an example of the procedure, consider a single body point being analyzed by the coupled program between two mandatory solution times θ_1 and θ_2. The diagrams below indicate the projections in the planes $\theta = \theta_1$ and $\theta = \theta_2$ of a hypothetical history of $\dot{m}_g^*$ and $\dot{m}_c^*$ as generated by the CMA program between the two mandatory times.

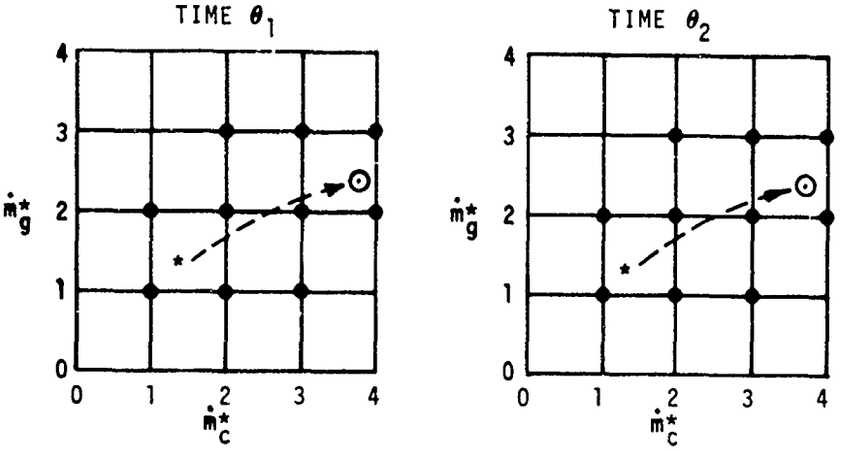

The solution at time θ_1 is indicated by asterisks, whereas the solution at time θ_2 is indicated by circles. The grid values for $\dot{m}_g^* = 0, 1, 2, \ldots$ and $\dot{m}_c^* = 0, 1, 2, \ldots$ are the preselected values for these parameters at which parametric boundary layer solutions are conducted if and when needed. Based on the point (*) at time θ_1, boundary-layer solutions are generated for the ($\dot{m}_g^*$, $\dot{m}_c^*$) points (1,1), (1,2), (2,1), and (2,2) at times θ_1 and θ_2. Charring ablation solutions can be obtained for times $\theta_1 < \theta < \theta_2$ by linear interpolation as long as $\dot{m}_g^*$ and $\dot{m}_c^*$ stay within these values. Suppose that the course of the calculation between times θ_1 and θ_2 is as indicated in the sketch. Then, additional solutions at $\dot{m}_g^*$, $\dot{m}_c^*$ of (1,3) and (2,3), then (3,2) and (3,3) and finally (2,4) and (3,4) would be required, each at both times. When time θ_2 (point ⊙) is approached, the BLIMP program is called upon for a solution at time θ_2 for the exact values of $\dot{m}_g^*$ and $\dot{m}_c^*$ required by CMA. This boundary-layer solution is printed out and that information needed for future reference (at downstream stations) is saved on tape. Solutions are then performed for time θ_3 for the current bracketing values of $\dot{m}_g^*$, $\dot{m}_c^*$ (in the present example, values of ($\dot{m}_g^*$, $\dot{m}_c^*$) of (2,3), (3,3), (2,4), and (3,4)). These boundary layer solutions at time θ_3 are placed over those for θ_1 by a tape flip-flop since the latter are no longer needed. The charring ablation solution next proceeds from time θ_2 to time θ_3, calling the BLIMP program only in the event that this range of ($\dot{m}_g^*$, $\dot{m}_c^*$) is exceeded.

The above described procedure is over-simplified to some extent since for many materials of interest in certain ablation regions the use of $\dot{m}_c^*$ as an independent variable is a poor choice. Consider the peculiarities of carbon ablating with air, for example, as illustrated in Figure 30, which shows the dependence on temperature of carbon ablation rates in air. Over a wide range of temperature $\dot{m}_c^*$ is for all practical purposes independent of temperature; in this

range the only useful independent variable in the surface thermochemical solution process is temperature, since it would be nearly impossible to select a sequence of $\dot{m}_c^*$ values distributed along the plateau. At high temperatures, however, $\dot{m}_c^*$ becomes strongly dependent on T, so that $\dot{m}_c^*$ is the preferred independent variable. The CABLE program logic has been altered recently to accept either $\dot{m}_c^*$ or T_w as an independent variable. In the typical problem situation, the user begins his sequence of independent variables with temperature entries starting at the lowest temperature of interest and extending up to (as a minimum objective) the point where $\dot{m}_c^*$ begins to rise above the plateau value for the lowest pressure to be encountered. It would be conservative and preferable to add temperatures even beyond the "rise point" at the highest pressure in case these points should be needed during the solution. After these temperature values, $\dot{m}_c^*$'s are added to

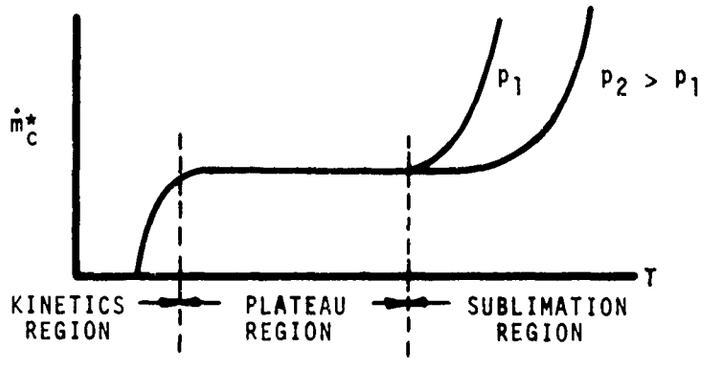

Figure 30. Ablation Rate $\dot{m}_c^*$ Versus Temperature for Carbon in Air

span the expected range of $\dot{m}_c^*$. The user is careful to pick a minimum $\dot{m}_c^*$ slightly above the plateau value. An $\dot{m}_c^*$ value near the start of the plateau or off the plateau in the low temperature region is extremely undesirable for two reasons:

1. The lowest assigned m_c^* determines the break between assigned temperature solutions and assigned $\dot{m}_c^*$ solutions; a low $\dot{m}_c^*$ will in effect "disqualify" all of the assigned temperature points across the plateau and leave a large "hole" in the array of surface thermochemical solutions.
2. For equilibrium calculations, assigned $\dot{m}_c^*$ solutions at $\dot{m}_c^*$ values below the plateau have a high probability of nonconvergence.

The coupling procedure which has been summarized above is very straightforward in practice, although difficult to describe in words. The sample problem presented in Section V.2 should clarify some of the more difficult points.

The storage requirements for this coupling procedure are surprisingly small. In the first place, the charring ablation solutions are noniterative and the complete solution for all times at any one station is accomplished and the results printed out before advancing to the next station. Thus no historic information relative to the charring ablation solution has to be stored. With regard to the boundary layer, only two mandatory times with four ($\dot{m}_g^*$, $\dot{m}_c^*$) combinations at each of these times need to be considered at the same time. The only quantities in the boundary layer which need to be dimensioned for the full time array are three input quantities of time, total pressure, and total enthalpy. Edge conditions are computed around the body at the time of the stagnation-point calculation since the necessary integrations are performed by curve fitting. This necessitates that streamwise dimension, static pressure, edge velocity, edge density, edge viscosity, edge temperature, body curvature (r_o), transformed streamwise dimension (ξ), pressure gradient parameter (β), and the flux normalizing parameter (α^*) be dimensioned for the number of streamwise positions (but not for time). About 300 numbers must be stored during the flip-flop operation associated with the two times which are being considered simultaneously, whereas about 500 numbers must be stored on tape to reenter the boundary layer at the same time but at the next downstream station (used for first guesses and for calculation of nonsimilar terms). Thus, both permanent machine storage requirements and tape storage requirements are not excessive as a consequence of coupling.

This coupling approach has the important feature that the CMA program operates very nearly as it does when used in conjunction with the ACE program (see reference 32). In the CMA/ACE approach, complete surface tables are computed a priori and independently with the ACE program and these are available to the CMA solution. In the coupled approach, these surface tables are initialized with the word VOID. When the CMA program encounters this word, the BLIMP program is called to supply the requisite information for that θ, $\dot{m}_g^*$ and $\dot{m}_c^*$ (or T_w). It is thus significant that the CMA/ACE approaches have been used extensively and very successfully for a wide variety of materials and environments. Likewise, the boundary-layer calculations are performed with assigned $\dot{m}_g^*$ and $\dot{m}_c^*$ or assigned $\dot{m}_g^*$ and T_w, together with the requirement of surface equilibrium (with possible specified rate-controlled surface reactions), options of the BLIMP program which also have been exercised extensively with success. Furthermore, this replacement of the wall mass and energy balances by these simple assignment statements adds stability to the boundary-layer solution.

2. A SAMPLE PROBLEM AND RESULTS

As a demonstration of the CABLE program, a coupled transient solution was run for a sphere-cone reentry body with a nose radius of 0.5 inches and a cone half-angle of eight degrees. A single body point at a surface running length of

10 inches (based on the original body shape) was analyzed although there is no reason other than computer time limitations why more body stations could not have been specified. Laminar flow was assumed for the boundary layer to hold the required number of nodes to a minimum. The heat shield material was one-inch thick phenolic carbon with properties as described in reference 28 and was insulated at the back face. The vehicle trajectory is shown in Figure 31. Total flight time from 300,000 feet is 27 seconds with an impact velocity of 17,000 ft/sec. Pressure ratio P/P_o at the body station of interest was assumed to be 0.0262 for the entire 27 seconds. Mandatory BLIMP solution times were 0.0, 7.0, 14.0, 18.0, 21.0, 23.0, 25.0, and 27.0 seconds. A total of 144 BLIMP solutions in the assigned injection, surface equilibrium mode exclusive of these mandatory solutions were run to provide the CMA program with boundary conditions.

Typical CABLE results are shown in Figures 32-40. Surface temperature history is shown in Figure 32, where it is seen that a maximum temperature of 4480°R was reached at the end of the flight. Figure 33 illustrates the pyrolysis gas flow rate history at the surface. Little or no pyrolysis occurs during the first ten seconds of flight, with a peak outgassing rate of approximately 0.028 lbs/ft^2sec reached near the end of the flight. Figure 34 describes the progression of the pyrolysis and char fronts into the heat shield material. The pyrolysis front is arbitrarily defined as the point where the local material density is equal to the char density plus 98 percent of the difference between the virgin and char densities. The char front is similarly defined as that point where the local material density is equal to the char density plus 2 percent of the difference between the virgin and char densities. The pyrolysis front penetrates 0.208 inches of the heat shield during this trajectory, whereas the fully charred material reaches a depth of only 0.067 inches by the end of the flight. No surface recession occurs at this body station.

Figures 35-37 show profiles for some of the thermodynamic variables of interest for this particular body station at t = 21 seconds. The subsurface density profile of Figure 35 indicates the extent of the pyrolysis region. Figure 36 contains the velocity profile for the boundary layer flow, while Figure 37 presents temperature profile information. The coupling of the boundary layer to the subsurface material is particularly apparent in the surface temperature continuity illustrated in Figure 37. Figures 38-40 contain the species mole fraction profiles through the boundary layer at three times of interest. At t = 0.0 seconds, the cold wall forces a recombination of N atoms to N_2, O atoms to O_2, etc., giving the unusual profiles of Figure 38. At t = 21 seconds (Figure 39) significant pyrolysis has occurred with the resulting gases being injected into the boundary layer flow. Hydrogen, carbon, and species containing these atoms are evident in the boundary layer gas. At t = 27 seconds (Figure 40) the boundary layer species are much the same, however the lower edge temperature caused by the slowing down of the vehicle has allowed many more trace species to be formed.

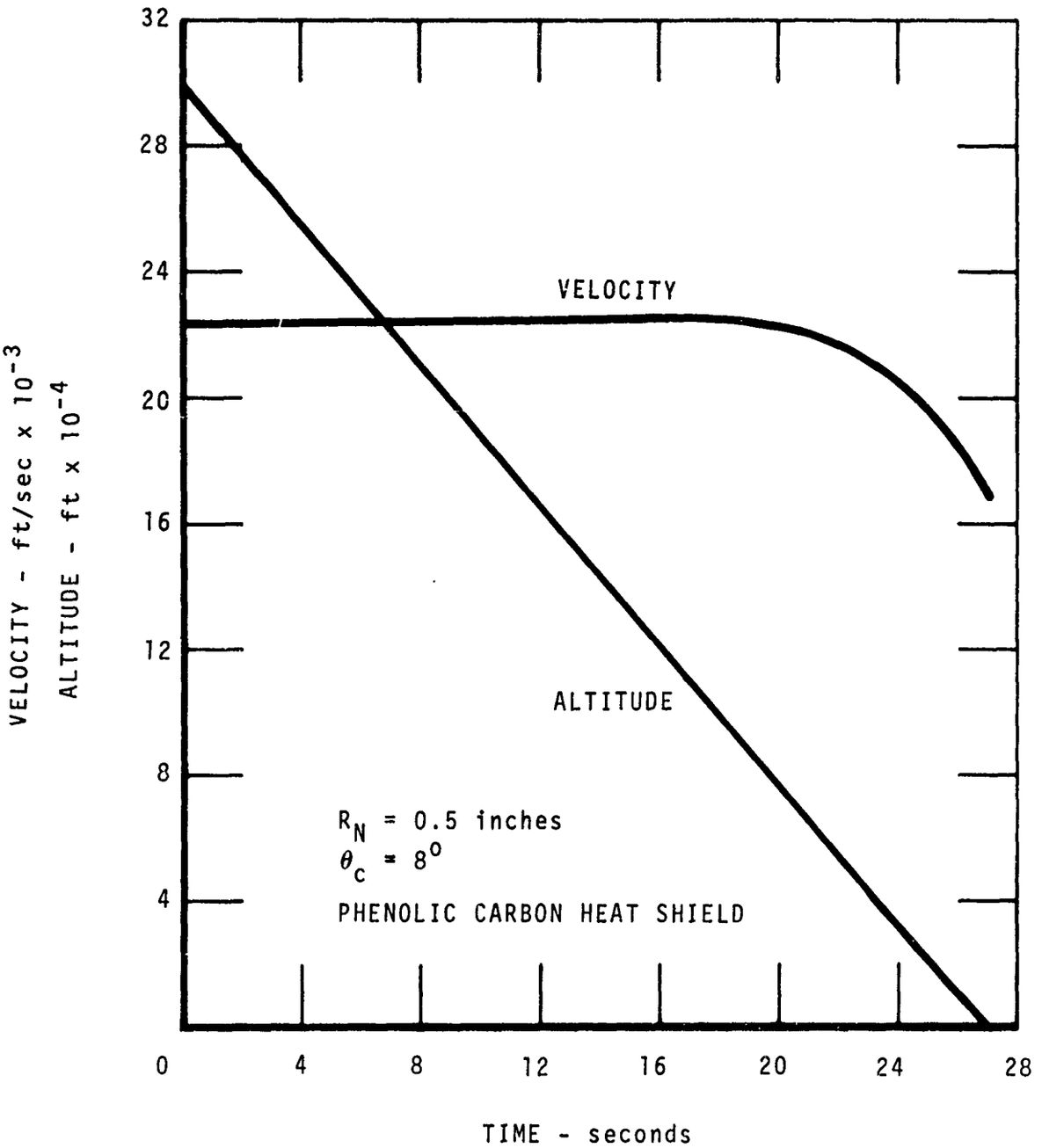

Figure 31. Trajectory for CABLE Sample Problem

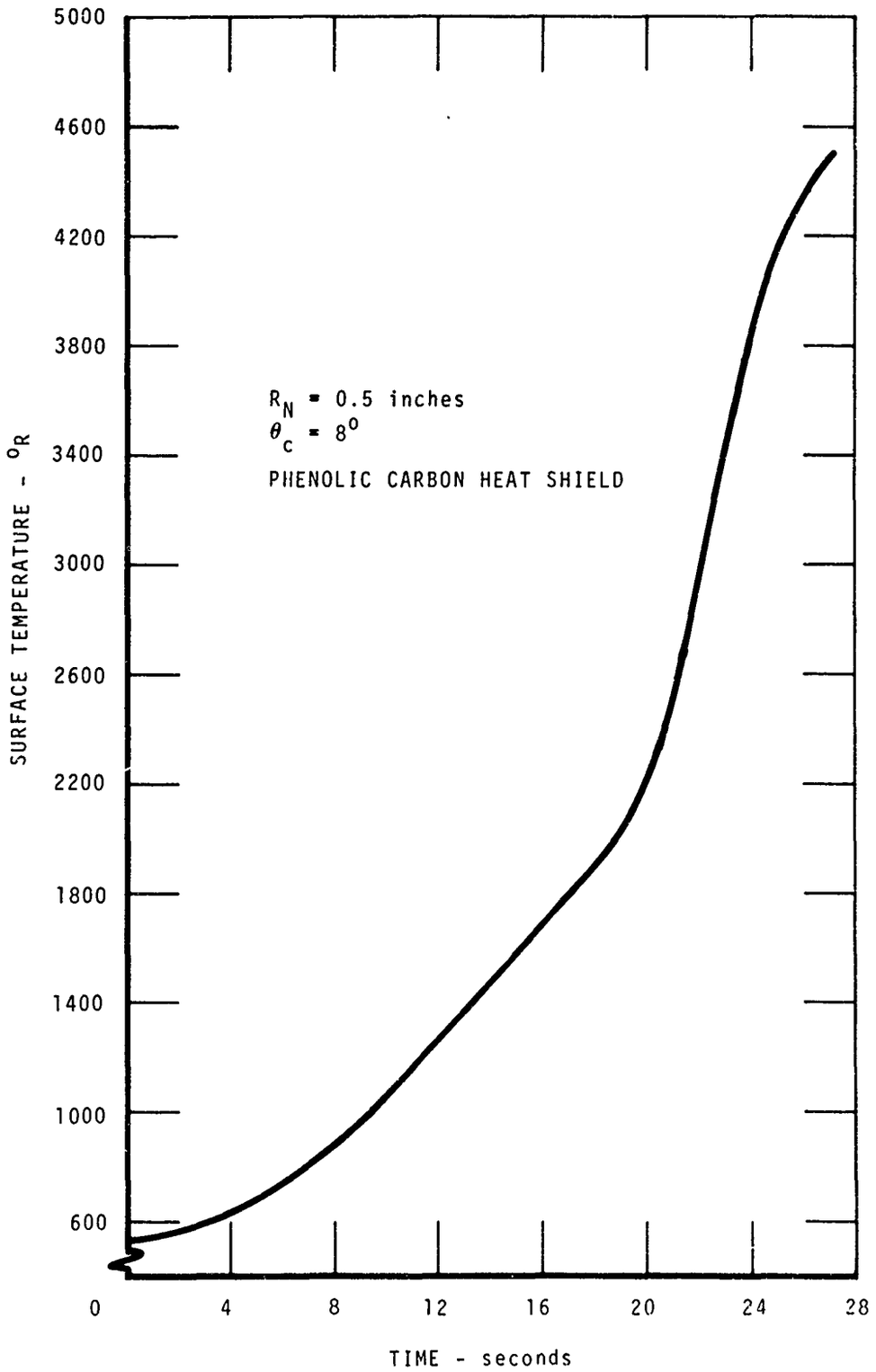

Figure 32. Surface Temperature History at S = 10.0 Inches

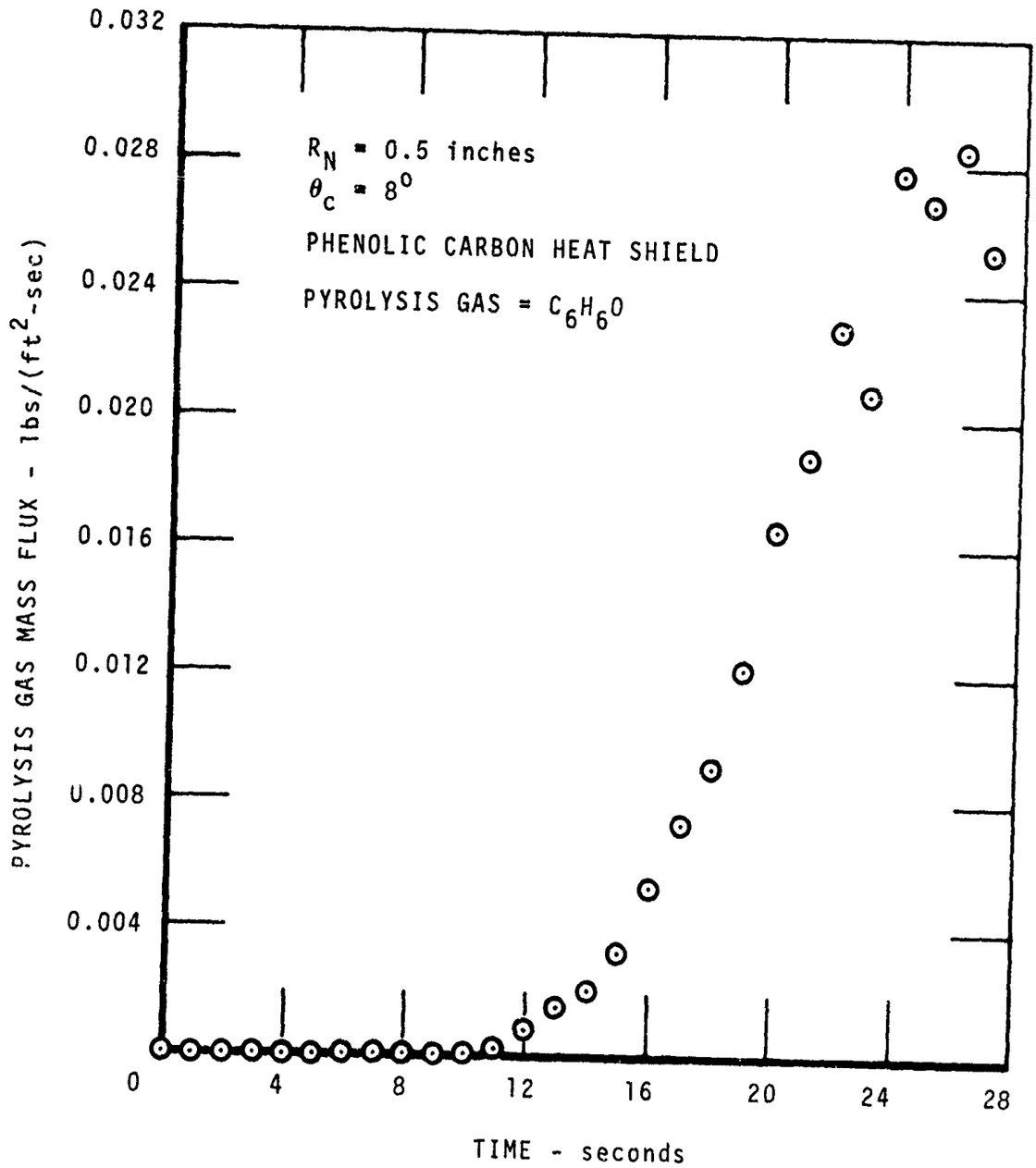

Figure 33. Pyrolysis Gas Flow Rate History at S = 10.0 Inches

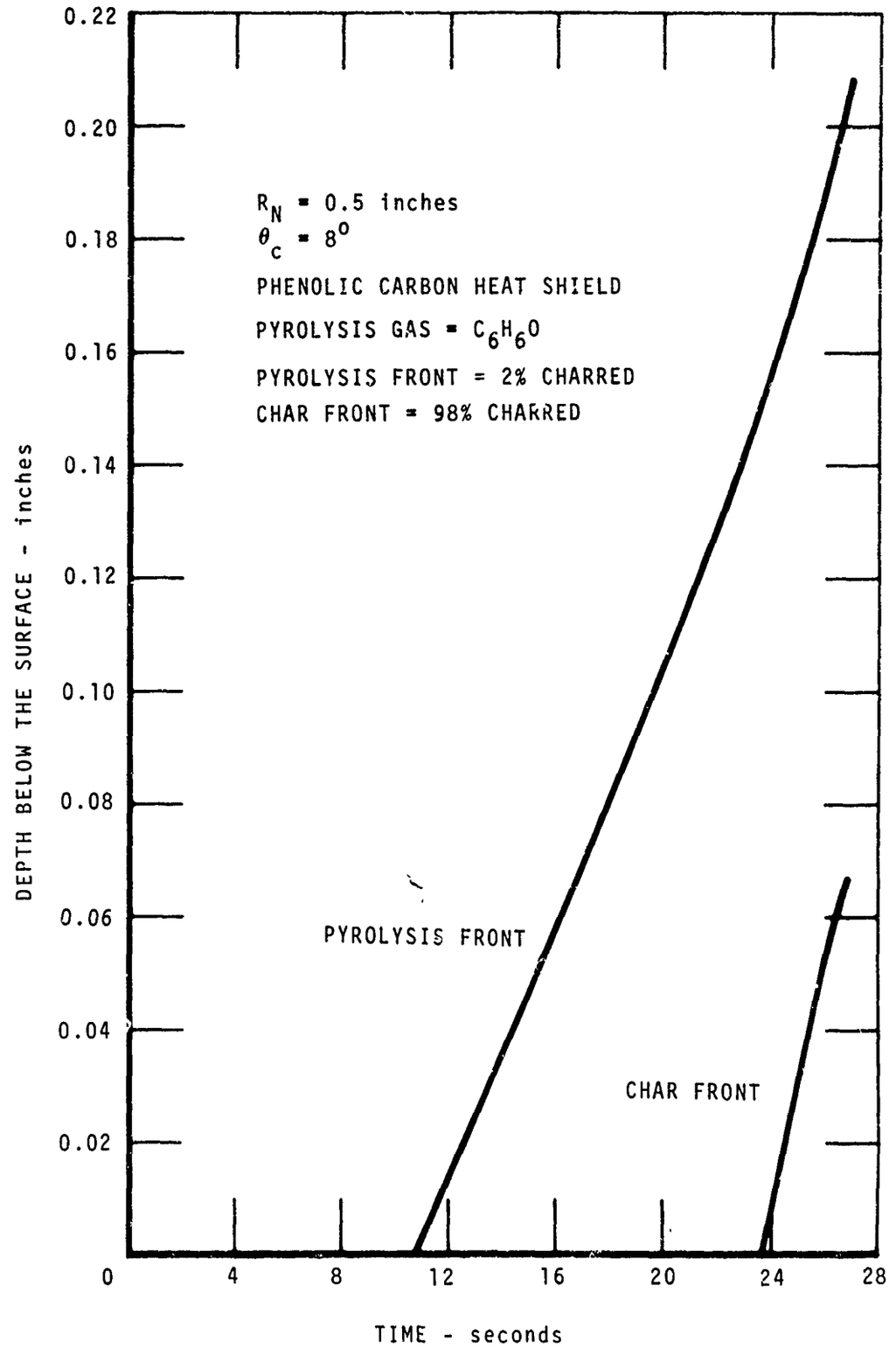

Figure 34. Pyrolysis and Char Front Histories at S = 10.0 Inches

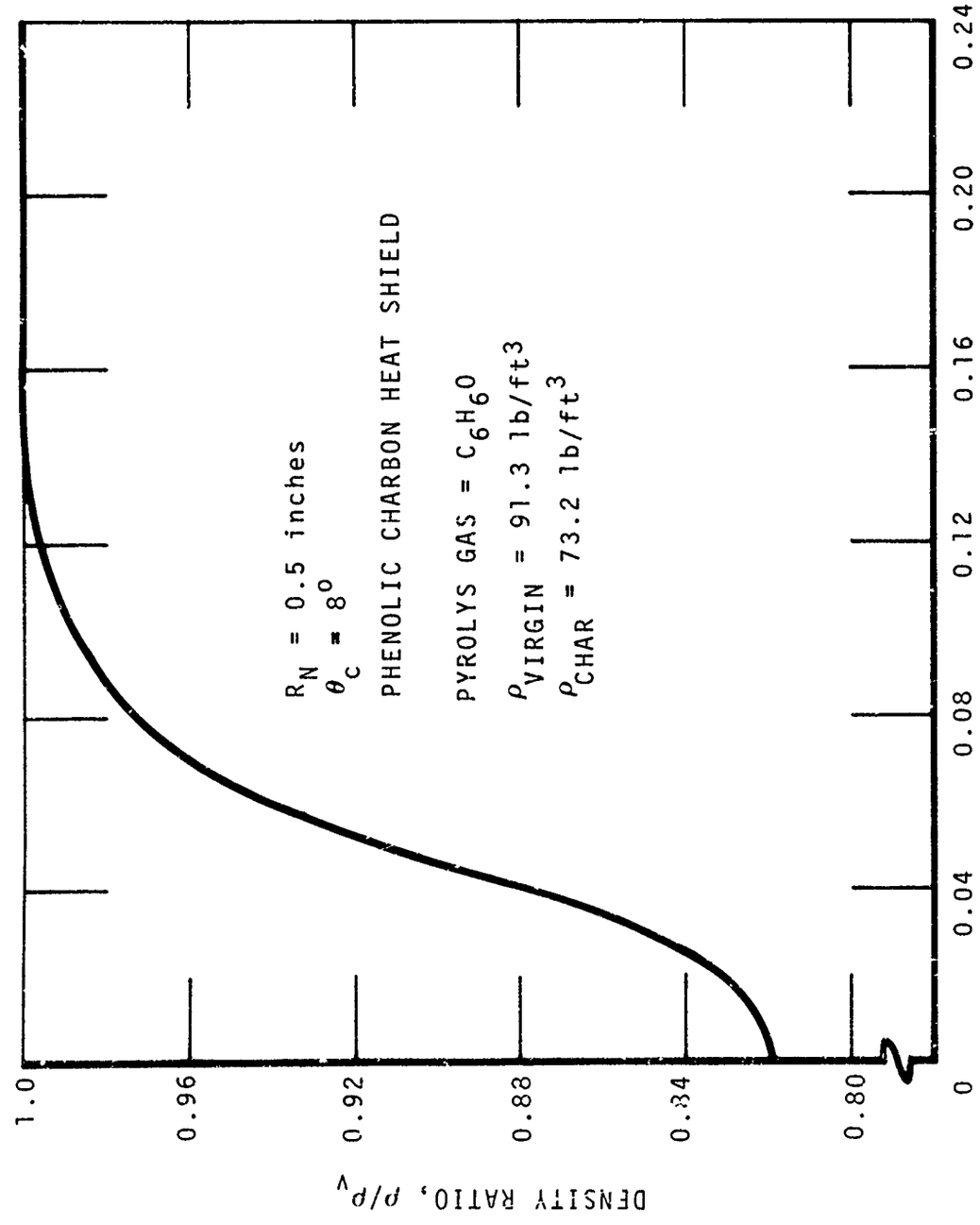

Figure 35. Density Profile at S = 10.0 Inches, t = 21.0 Seconds

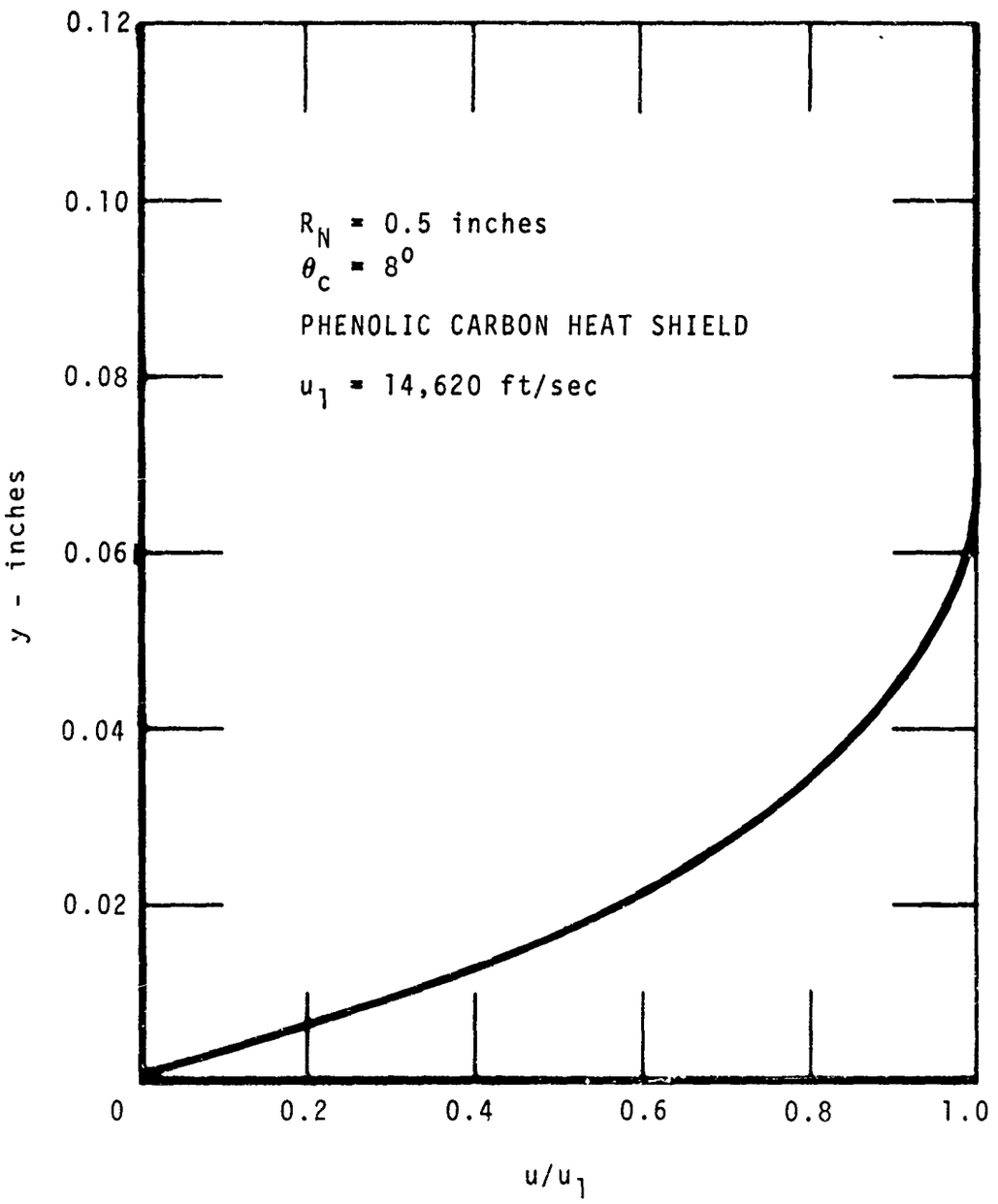

Figure 36. Boundary Layer Velocity Profile at S = 10.0 Inches, t = 21.0 Seconds

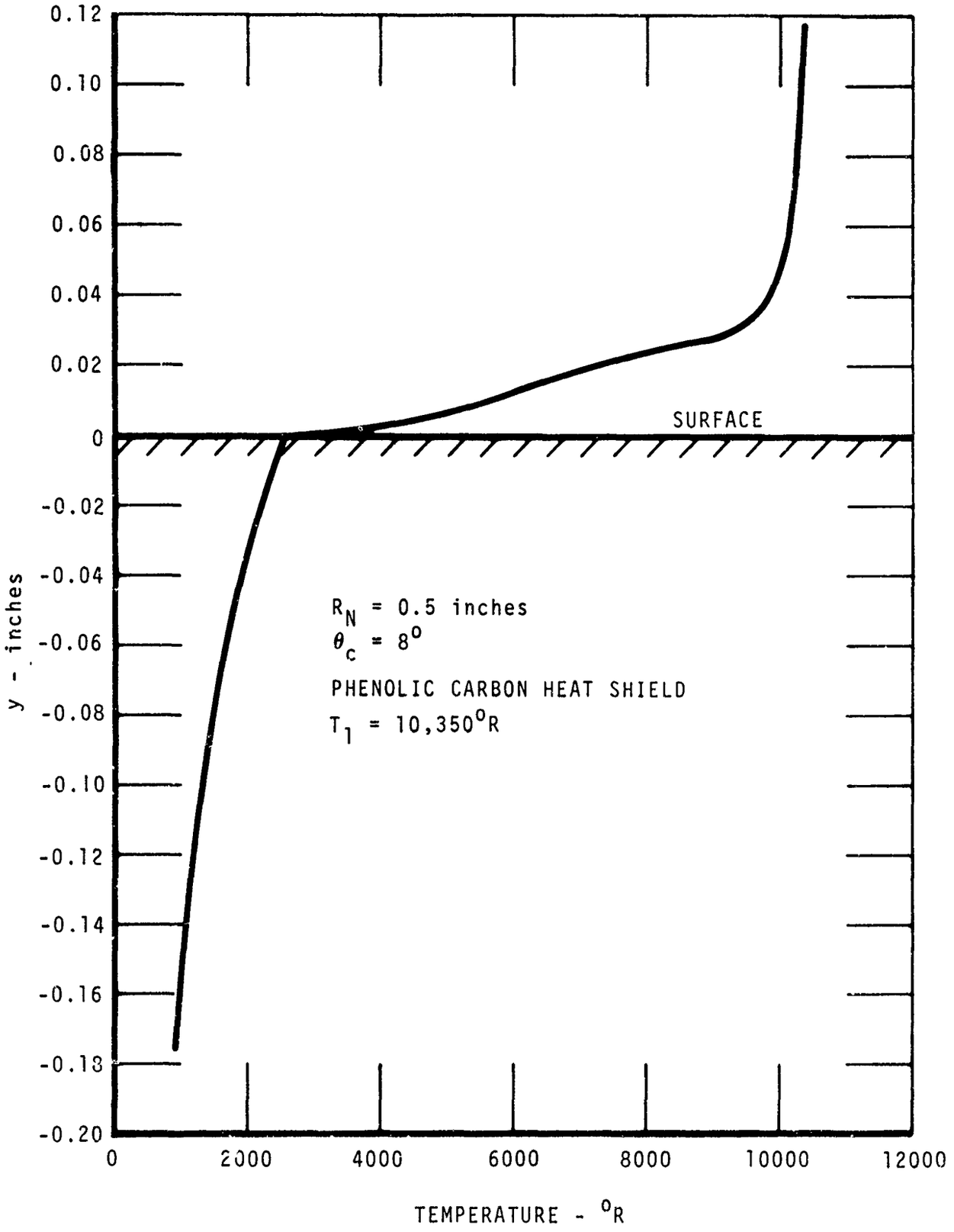

Figure 37. Boundary Layer and Subsurface Temperature Profile for S = 10.0 Inches, t = 21.0 Seconds

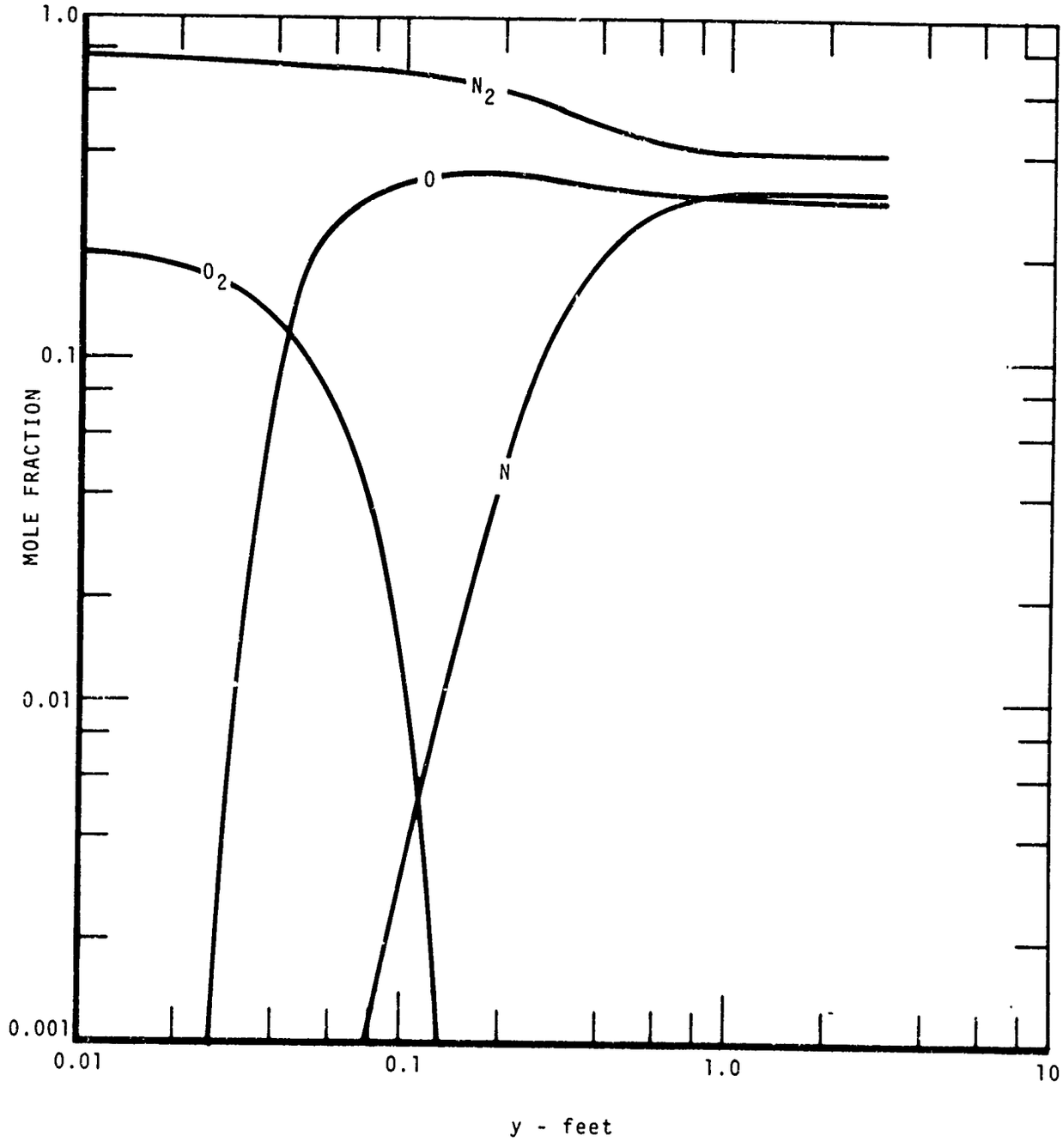

Figure 38. Mole Fraction Profiles at S = 10.0 Inches, t = 0.0 Seconds

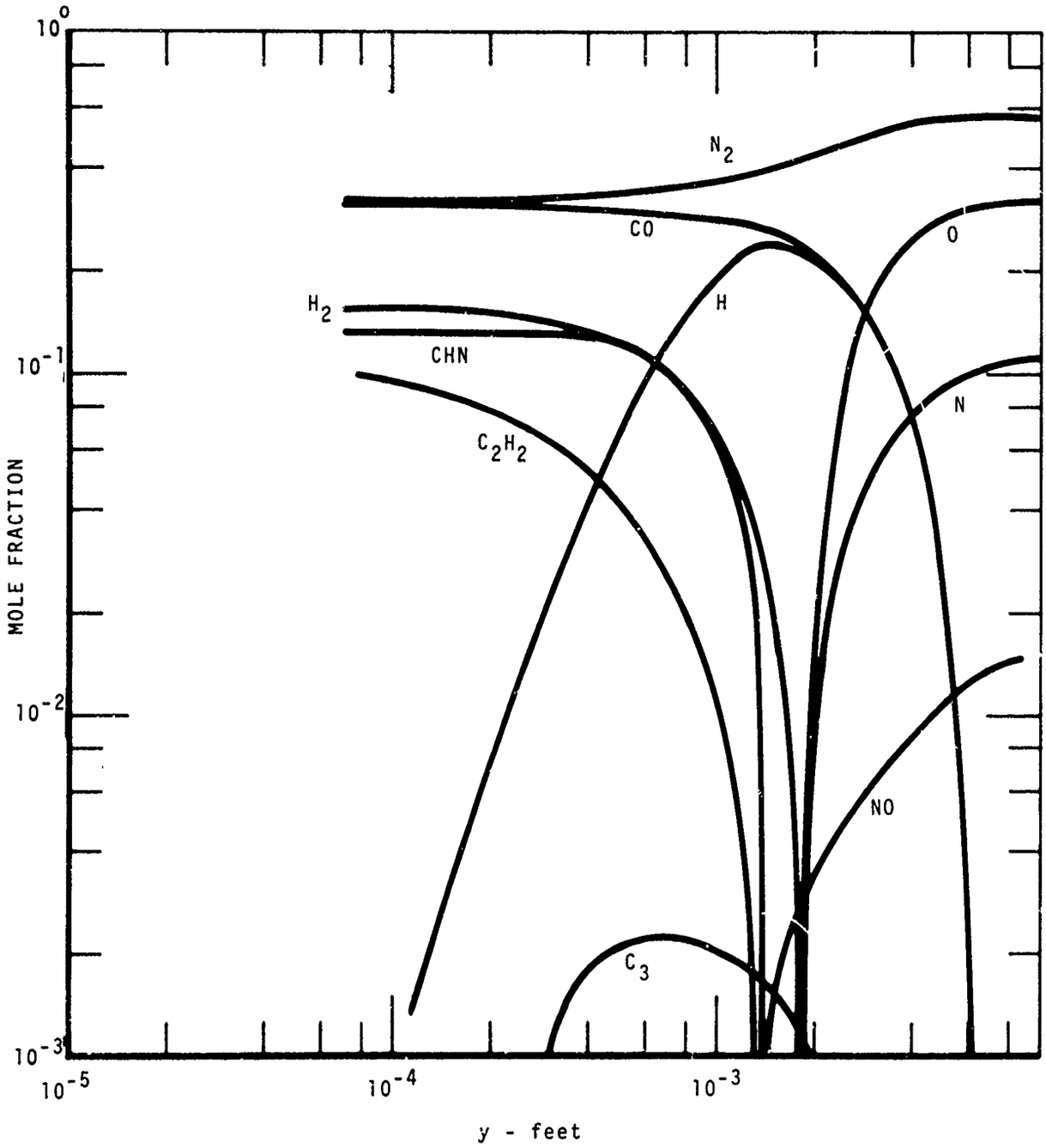

Figure 39. Mole Fraction Profiles at S = 10.0 Inches, t = 21.0 Seconds

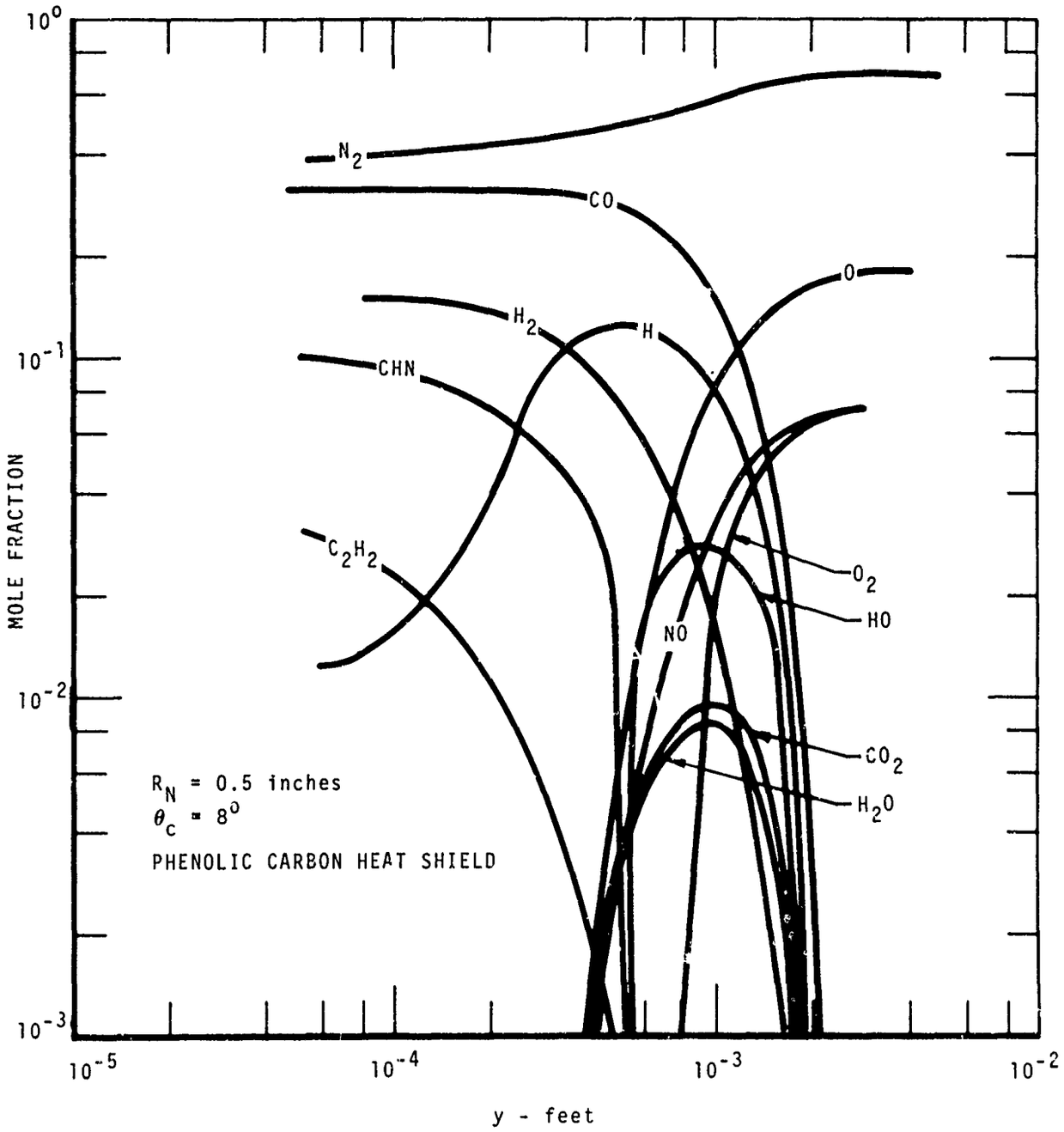

Figure 40. Mole Fraction Profiles at S = 10.0 Inches, t = 27.0 Seconds

The above-described CABLE run, comprised of a total of 152 BLIMP solutions plus the in-depth charring material solution, required approximately 30 minutes on a UNIVAC 1108 computer. Solutions at succeeding body stations should proceed somewhat faster due to the better initial guesses provided by the upstream solution, however if turbulent flow situations are expected, about twice as many boundary layer nodes would be needed. Thus, it is estimated that a complete reentry vehicle body solution with the CABLE program, including 29 body stations in a 27 second trajectory, would require from 10 to 20 hours of UNIVAC 1108 computer time.

SECTION VI

CONCLUSIONS AND RECOMMENDATIONS FOR FURTHER WORK

The BLIMP boundary layer code has been successfully extended to include turbulent flows and flows with transverse curvature. The basic analytical technique offers the advantages of completely general multicomponent chemistry, preservation of nonsimilar terms in the equations of motion, and intimate coupling to the surface material behavior. The coupling occurs through requirements of surface equilibrium and/or a surface energy balance, or a complete coupling with an in-depth conduction and charring ablation code.

There are several areas where the code and the analytical model which it includes can be improved or extended. One of these is in the general area of modeling turbulence in the equations of motion. The purpose of the work presented in this report was to incorporate a turbulent model into the BLIMP program. The model that was used is perhaps the best available for general hypersonic flows with arbitrary species injection, however an extensive investigation into the generality of the model in all flow situations is called for. Experimental data comparisons at high Mach numbers and possible model changes to match these data would be most valuable.

Two smaller changes in the program would make it more accurate and convenient to use on some problems. The first of these involves the α_H or coordinate stretching parameter. On very long bodies, the boundary layer thickness varies over two or three orders of magnitude. The α_H parameter forces the boundary layer thickness to remain constant in the solution plane, thereby eliminating the need for a large number of nodes which are unused near the stagnation point or leading edge. For turbulent flows, the laminar sublayer grows at a much slower rate than the total boundary layer. As the normal coordinate is stretched in the solution plane, the nodes nearest the wall eventually can be pulled outside the sublayer altogether, resulting in poor convergence of the numerical technique and inaccurate solutions. A different stretching technique scaled to the sublayer as well as the boundary layer edge must be invented to avoid this problem. The second change involves nonisentropic expansions. It is currently possible to specify entropy and pressure in order to fix the edge state of the boundary layer gas for "entropy layer" flows. This technique introduces some inaccuracy however since an entropy gradient in the streamwise direction also requires a velocity gradient in the normal direction (nonzero vorticity). The analysis should be modified to include this edge velocity gradient for nonisentropic expansions.

The final recommendation is in the general category of electron collision models. At present, a very simple clean air collision frequency model is included in the program, and electron distributions are calculated assuming equilibrium chemistry. More accurate clean air collision frequency models are available and could be incorporated into the program. However, based on the level of sophistication of the rest of the boundary layer analysis, it seems appropriate to attempt to take into account the effect of the ablation products on the electron collision frequencies. Also, charge separation effects may alter the equilibrium electron distribution significantly. It is recommended that a study be undertaken to establish the importance of charge separation and ablation products on the basic parameters of interest in communications and that these effects be included in the BLIMP code if necessary.

APPENDIX I

COORDINATE TRANSFORMATIONS

A convenient coordinate transformation for use in boundary layer problems with transverse curvature, and the one used in the present analysis, can be arrived at by nondimensionalizing and simplifying the continuity and momentum equations in a relatively straightforward manner. The momentum equation for a turbulent flow with transverse curvature is

$$\rho u r^K \frac{\partial u}{\partial s} + \rho v r^K \frac{\partial u}{\partial y} = \frac{\partial}{\partial y}\left[\rho r^K (\nu + \varepsilon_M) \frac{\partial u}{\partial y}\right] - r^K \frac{\partial P}{\partial s} \tag{146}$$

while the requirement of continuity yields

$$\frac{\partial \rho u r^K}{\partial s} + \frac{\partial \rho v r^K}{\partial y} = 0 \tag{147}$$

The two equations can be conveniently combined by the definition of a stream function f, with an arbitrary wall value, f_w:

$$f - f_w = \int_o^y \frac{\rho u r^K}{\rho_r u_r r_o^K} \frac{dy}{\delta} \tag{148}$$

The stream function is made dimensionless by the introduction of reference conditions ρ_r and u_r and by the y-dimension scaling parameter $\delta(x)$. The reference condition $(\ )_r$ will be taken as the isentropic boundary layer edge condition, while the scaling length δ remains to be defined. Solving the continuity equation for $\rho v r^K$, it is easily shown that

$$\rho v r^K = \rho_w v_w r_o^K - \frac{\partial}{\partial s}\left[r_o^K \rho_r u_r \delta (f - f_w)\right] \tag{149}$$

Using this result in the momentum equation yields

$$\rho u r^K \frac{\partial u}{\partial s} + \left\{\rho_w v_w r_o^K - \frac{\partial}{\partial s}\left[r_o^K \rho_r u_r \delta (f - f_w)\right]\right\} \frac{\partial u}{\partial y}$$

$$= \frac{\partial}{\partial y}\left[\rho r^K (\nu + \varepsilon_M) \frac{\partial u}{\partial y}\right] - r^K \frac{\partial P}{\partial s} \tag{150}$$

Introducing

$$\tilde{u} = \frac{u}{u_r}$$
$$\tilde{y} = \frac{y}{\delta} \tag{151}$$

The momentum equation becomes

$$\rho\tilde{u}r^{K}u_r\left[\tilde{u}\frac{du_r}{ds} + u_r\frac{\partial\tilde{u}}{\partial s} - u_r\frac{\tilde{y}}{\delta}\frac{d\delta}{ds}\frac{\partial\tilde{u}}{\partial\tilde{y}}\right] + \left\{\rho_w v_w r_o^{K} - \right.$$
$$\left. - \frac{\partial}{\partial s}\left[r_o^{K}\rho_r u_r\delta(f - f_w)\right] + \frac{\tilde{y}}{\delta}\frac{d\delta}{ds}\frac{\partial}{\partial\tilde{y}}\left[r_o^{K}\rho_r u_r\delta(f - f_w)\right]\right\}\left[\frac{u_r}{\delta}\frac{\partial\tilde{u}}{\partial\tilde{y}}\right]$$
$$= \frac{1}{\delta}\frac{\partial}{\partial\tilde{y}}\left[\rho r^{K}\frac{u_r}{\delta}(\nu + \varepsilon_M)\frac{\partial\tilde{u}}{\partial\tilde{y}}\right] - r^{K}\frac{dP}{ds} \tag{152}$$

A new normal coordinate is now defined which allows a simple relationship between the dimensionless stream function f and dimensionless velocity ũ. Noting that

$$\frac{\partial f}{\partial\tilde{y}} = \frac{\rho u r^{K}}{\rho_r u_r r_o^{K}} \tag{153}$$

then if we define

$$d\eta = \frac{1}{\alpha_H}\frac{\rho r^{K}}{\rho_r r_o^{K}}d\tilde{y} \tag{154}$$

the relation between f and ũ becomes

$$\frac{\partial f}{\partial\eta} = f' = \alpha_H\tilde{u} \tag{155}$$

The α_H is a stretching parameter on the normal coordinate η such that the boundary layer is contained within a constant η range, 0 to η_{edge} (see Section II.3). Using the new η coordinate and expressing ũ in terms of f', the momentum equation takes the form

$$f'^2 \frac{d \ln u_r}{ds} + f' \frac{\partial f'}{\partial s} - \frac{1}{\alpha_H} \frac{d\alpha_H}{ds} f'^2 + \left\{ \left[\frac{\rho_w v_w r_o^K}{\rho_r u_r r_o^K} + \frac{1}{\rho_r u_r r_o^K} \frac{\partial}{\partial s} (r_o^K \rho_r u_r \delta f_w) \right] - \delta f \frac{d \ln r_o^K \rho_r u_r \delta}{ds} \right\} - \delta \frac{\partial f}{\partial s} \left\{ \frac{f''}{\delta} = \frac{1}{\delta^2 \alpha_H \rho^2 u_r r_o^{2K}} \left(\rho^2 r^{2K} (\nu + \epsilon_M) f'' \right)' - \frac{\alpha_H^2}{\rho u_r^2} \frac{dP}{ds} \right. \tag{156}$$

Since f_w is as yet undefined, the equation can be simplified by defining f_w such that the square bracket term [ ] goes to zero. This yields

$$f_w = \frac{-1}{\rho_r u_r \delta r_o^K} \int_o^s \rho_w v_w r_o^K ds \tag{157}$$

It is convenient to define some new dependent variables at this point:

$$C \equiv \frac{\rho \mu}{\rho_r \mu_r} \tag{158}$$

$$\tilde{\epsilon}_M = \frac{\rho^2 \epsilon_M}{\rho_r \mu_r} \tag{159}$$

$$t \equiv \left(\frac{r}{r_o} \right)^{2K} \tag{160}$$

Also, the static pressure gradient is related to the reference velocity gradient

$$\frac{dP}{ds} = - \rho_r u_r \frac{du_r}{ds} \tag{161}$$

Inserting these new definitions

$$\left(f'^2 - \frac{\alpha_H^2 \rho_r}{\rho} \right) \frac{d \ln u_r}{ds} + f' \frac{\partial f'}{\partial s} - \frac{f'^2}{\alpha_H} \frac{d\alpha_H}{ds} - f'' \left[\frac{\partial f}{\partial s} + f \frac{d\left(\ln r_o^K \rho_r u_r \delta \right)}{ds} \right] = \frac{\mu_r}{\delta^2 \rho_r u_r} \left[\frac{t(C + \tilde{\epsilon}_M) f''}{\alpha_H} \right]' \tag{162}$$

An additional coordinate transformation will bring the equation to a more compact form. Defining

$$d\xi = Q ds \tag{163}$$

where Q(s) is as yet undefined, the streamwise derivatives become

$$\frac{d(\ )}{ds} = \frac{Q}{\xi} \frac{d(\ )}{d \ln \xi} \tag{164}$$

$$\frac{d \ln u_r}{ds} = \frac{Q}{\xi} \frac{d \ln u_r}{d \ln \xi} = \frac{Qf}{2\xi} \tag{165}$$

which leads to

$$\beta\left(f'^2 - \alpha_H \frac{\rho_r}{\rho}\right) + 2f' \frac{\partial f'}{\partial \ln \xi} - 2f'^2 \frac{d \ln \alpha_H}{d \ln \xi} - f'' \left[2 \frac{\partial f}{\partial \ln \xi} + 2f \frac{d \ln (r_o^K \rho_r u_r \delta)}{d \ln \xi}\right] = \frac{2\mu_r \xi}{Q\delta^2 \rho_r u_r} \left[\frac{t(C + \tilde{\varepsilon}_M) f''}{\alpha_H}\right]' \tag{166}$$

Defining Q and δ properly will yield unity for two groups of terms in the current version of the equation. Choosing the group in the left hand side first

$$2 \frac{d \ln (r_o^K \rho_r u_r \delta)}{d \ln \xi} = 1 \tag{167}$$

which requires

$$\delta = \frac{\sqrt{2\xi}}{r_o^K \rho_r u_r} \tag{168}$$

The second group of terms is

$$\frac{2\mu_r \xi}{Q\delta^2 \rho_r u_r} = 1 \tag{169}$$

which requires

$$Q = \rho_r u_r \mu_r r_o^{2K} \tag{170}$$

With these changes, the momentum equation becomes

$$ff'' - \beta\left(f'^2 - \alpha_H^2 \frac{\rho_r}{\rho}\right) + \left[\frac{t(C + \tilde{\epsilon}_M)f''}{\alpha_H}\right]'$$

$$= 2\left[f' \frac{\partial f'}{\partial \ln \xi} - f'' \frac{\partial f}{\partial \ln \xi} - f'^2 \frac{d \ln \alpha_H}{d \ln \xi}\right] \tag{171}$$

The final coordinate transformation is

$$\xi = \int_o^s \rho_r u_r \mu_r r_o^{2K} \, ds \tag{172}$$

$$\eta = \frac{\rho_r u_r r_o^K}{\alpha_H \sqrt{2\xi}} \int_o^y \frac{\rho r^K}{\rho_r r_o^K} \, dy \tag{173}$$

while the other definitions take the form

$$f - f_w = \frac{1}{\sqrt{2\xi}} \int_o^y \rho u r^K dy \tag{174}$$

$$f_w = - \frac{1}{\sqrt{2\xi}} \int_o^s \rho_w v_w r_o^K ds \tag{175}$$

APPENDIX II

DEVELOPMENT OF A RECURSION FORMULA FOR MIXING LENGTH

The mixing length differential equation has been shown to be of the form

$$\frac{d\tilde{\ell}}{d\eta} = (K\alpha_H\eta - \tilde{\ell})P \tag{176}$$

where

$$P(\eta) \equiv \frac{\alpha_H \rho_1 \delta\sqrt{\tau/\rho}}{y_a^+ \mu} \tag{177}$$

The general solution is

$$\tilde{\ell} = K\alpha_H(\eta - L) \tag{178}$$

where

$$L(\eta) \equiv \frac{\int_o^\eta e^{\int_o^{\eta'} P d\eta''} d\eta'}{e^{\int_o^\eta P d\eta'}} \tag{179}$$

In the definition of L at the i'th node, the integrals from 0 to η_i can be broken into two parts, 0 to η_{i-1} and η_{i-1} to η_i to give

$$L_i = \frac{L_{i-1}}{e^{\int_{\eta_{i-1}}^{\eta_i} P d\eta}} + \frac{\int_{\eta_{i-1}}^{\eta_i} e^{\int_{\eta_{i-1}}^{\eta_i} P d\eta'} d\eta}{e^{\int_{\eta_{i-1}}^{\eta_i} P d\eta}} \tag{180}$$

Assuming a linear variation of $P(\eta)$ over the interval η_{i-1} to η_i, the first term of the L_i expression becomes

$$\frac{L_{i-1}}{e^{\int_{\eta_{i-1}}^{\eta_i} P d\eta}} = BL_{i-1} \tag{181}$$

where

$$B \equiv e^{-\Delta\eta_i\left[\frac{P_i+P_{i-1}}{2}\right]} \tag{182}$$

$$\Delta\eta_i \equiv \eta_i - \eta_{i-1} \tag{183}$$

The second term is more difficult; however, the linear assumption for $P(\eta)$ plus sufficient algebraic manipulation yields

$$\frac{\int_{\eta_{i-1}}^{\eta_i} e^{\int_{\eta_{i-1}}^{\eta_i} P d\eta'} d\eta}{e^{\int_{\eta_{i-1}}^{\eta_i} P d\eta}} = \int_0^{\Delta\eta_i} e^{\left[\int_0^{\eta-\eta_i} P d(\eta-\eta_{i-1}) - \int_0^{\Delta\eta_i} P d(\eta-\eta_i)\right]} d(\eta-\eta_{i-1})$$

$$= \int_0^{\Delta\eta_i} e^{\left(\left[\frac{(\eta-\eta_{i-1})}{A} + c\right]^2 - \left[\frac{\Delta\eta}{A}+c\right]^2\right)} d(\eta-\eta_{i-1})$$

$$= e^{-d^2}\int_c^d Ae^{\tilde{\eta}^2} d\tilde{\eta} \tag{184}$$

where

$$A \equiv \left[\frac{2\Delta\eta_i}{P_i - P_{i-1}}\right]^{\frac{1}{2}} \tag{185}$$

$$c \equiv \frac{AP_{i-1}}{2} \tag{186}$$

$$d \equiv \frac{\Delta\eta_i}{A} + c \tag{187}$$

This last integral term can be broken into two pieces to give

$$\frac{\int_{\eta_{i-1}}^{\eta_i} e^{\int_{\eta_{i-1}}^{\eta_i} P d\eta'} d\eta}{\int_{e^{\eta_{i-1}}}^{\eta_i} P d\eta} = e^{-d^2}\left[\int_0^d A e^{\tilde{\eta}^2} d\tilde{\eta} - \int_0^c A e^{\tilde{\eta}^2} d\tilde{\eta}\right]$$

$$= A\left[D_w(d) - BD_w(c)\right] \tag{188}$$

The Dawson Integral, $D_w(\ )$*, can be evaluated from tables (Ref. 23) or, in the case of the present analysis, by a series method. The quantity L_i is given by

$$L_i = BL_{i-1} + A\left\{D_w\left(\frac{AP_i}{2}\right) - BD_w\left(\frac{AP_{i-1}}{2}\right)\right\} \tag{189}$$

which is a recursion formula for L_i in terms of the value for L at the previous node and the local values of $P(\eta)$.

*$D_w(x) = e^{-x^2}\int_0^x e^{+y^2} dy$

REFERENCES

1. Anderson, L. W., Bartlett, E. P., and Kendall, R. M.; User's Manual, Boundary Layer Integral Matrix Procedure, AFWL-TR-69-114, Vol. I, Air Force Weapons Laboratory, Kirtland AFB, NM, October 1969.

2. Bartlett, E. P., and Kendall, R. M.; Nonsimilar Solutions of the Multicomponent Laminar Boundary Layer by an Integral Matrix Method, Aerotherm Corporation Final Report No. 66-7, Part III, March 14, 1967; also, AIAA Journal, 6, pp. 1089-1097, 1968.

3. Anderson, L. W. and Kendall, R. M.; Nonsimilar Solution of an Incompressible Turbulent Boundary Layer by an Integral Matrix Method, Aerotherm Corporation Final Report No. 68-38, Part IV, October 15, 1968.

4. Walsh, J. L., Ahlberg, J. H., and Nilson, E. N.; "Best Approximation Properties of the Spline Fit," J. Math. and Mech., 11, pp. 225-234, 1962.

5. Pallone, A. J.; "Nonsimilar Solutions of the Compressible-Laminar-Boundary-Layer Equations with Applications to the Upstream-Transpiration Cooling Problem" J. Aerospace Sci., 28, pp. 449-456, 492, 1961.

6. Leigh, D. C. F.; "The Laminar Boundary Layer Equation: A Method of Solution by Means of an Automatic Computer," Cambridge Phil. Soc. Proc., 51, pp. 320-332, 1955.

7. Kendall, R. M.; A General Approach to the Thermochemical Solution of Mixed Equilibrium-Nonequilibrium, Homogeneous or Heterogeneous Systems, Aerotherm Corporation, Final Report No. 66-7, Part V, March 14, 1967; also, NASA CR 1064, June, 1968.

8. Bartlett, E. P., Kendall, R. M., and Rindal, R. A.; A Unified Approximation for Multicomponent Boundary Layer Applications, Aerotherm Corporation, Final Report No. 66-7, Part IV, March 14, 1967; also, NASA CR 1053, June, 1968.

9. Reynolds, W. C.; "A Morphology of the Prediction Methods," Proceedings of the 1968 AFOSR-IFP-Stanford Conference on Computation of Turbulent Boundary Layers, S. J. Kline, et. al., editors, Stanford University, August, 1968.

10. Kendall, R. M., and Anderson, L. W., "Nonsimilar Solution of the Incompressible Turbulent Boundary Layer," Proceedings of the 1968 AFOSR-IFP-Stanford Conference on Computation of Turbulent Boundary Layers, S. J. Kline, et. al, editors, Stanford University, August, 1968.

11. Clauser, F. H.; "The Turbulent Boundary Layer," Advances in Applied Mechanics, IV, pp. 1-51, 1956.

12. Kendall, R.M., Rubesin, M. W., Dahm, T. J., and Mendenhall, M.R.; Mass, Momentum, and Heat Transfer Within a Turbulent Boundary Layer with Foreign Gas Mass Transfer at the Surface, Part I - Constant Fluid Properties, Vidya Division, Itek Corporation, Final Report No. 111, 1964.

13. Reichardt, H.; "Complete Representation of the Turbulent Velocity Distribution in Smooth Pipe," Z. Angew. Math. u. Mech., 31, No. 7, July 1951.

14. Rannie, W. D.; "Heat Transfer in Turbulent Shear Flow," Jour. Aero. Sci., 23, No. 5, May 1956.

15. Deissler, R.G.; Analysis of Turbulent Heat Transfer, Mass Transfer, and Friction in Smooth Tubes at High Prandtl and Schmidt Numbers, NACA TN 3145, May 1954.

16. Rotta, J.; "Velocity Law of Turbulent Flow Valid in the Neighborhood of a Wall," Ingr. Arch., 18, p. 277, 1950.

17. von Karman, T.; "The Analogy between Fluid Friction and Heat Transfer," Trans. ASME, 61, pp. 705-710, 1939.

18. van Driest, E. R.; "On Turbulent Flow Near a Wall," Jour. Aero. Sci., 23, No. 11, November 1956.

19. Mickley, H. S., Curl, R., Gessner, A., and Ginwala, K.; Heat and Momentum Transfer for Flow Over a Flat Plate with Blowing and Main Stream Acceleration. MIT, Chemical Engineering Department, Report on Work Performed under NACA Contract Naw 6228, February, 1955.

20. Kendall, R. M.; Interaction of Mass and Momentum Transfer in the Turbulent Boundary Layer, Ph. D. Dissertation, M.I.T., 1959.

21. Jaffe, N. A., Lind, R. C., and Smith, A.M.O.; "Solution to the Binary Diffusion Laminar Boundary Layer Equations with Second Order Transverse Curvature," AIAA Journal, 5, pp. 1563-1569, September, 1967.

22. Denison, M. R.; "Estimating Transient Temperature Distributions During Ablation," ARS Journal, 30, pp. 562-563, June, 1960.

23. Dorodnitsyn, A. A.; "General Method of Integral Relations and Its Application to Boundary Layer Theory," Advances in Aeronautical Sciences, 3, Macmillan, New York, 1960.

24. Abramowitz, M., and Stegun, I., editors; Handbook of Mathematical Functions with Formulas, Graphs, and Mathematical Tables, National Bureau of Standards, Applied Mathematics Series, 55. U.S. Govt. Printing Office, Washington, 1964.

25. Bartlett, E. P. and Grose, R. D.; The Multicomponent Laminar Boundary Layer over Graphite Sphere-Cones: Solutions for Quasi-Steady Ablation and Application to Transient Reentry Trajectories, Aerotherm Corporation, Final Report No. 68-35, May 29, 1968.

26. Bartlett, E. P., Nicolet, W. E., Anderson, L. W., and Kendall, R. M.; Further Studies of the Coupled Chemically Reacting Boundary Layer and Charring Ablator, Aerotherm Corporation, Final Report 68-38, Part I, October 15, 1968.

27. Dahm, T. J.; Subsurface, Surface, and Boundary Layer Interaction of Various Transpirants with Carbon, Aerotherm Corporation, Final Report No. 69-62, June 30, 1969.

28. Rindal, R. A., et. al.; Experimental and Theoretical Analysis of Ablative Material Response in a Liquid Propellant Rocket Engine, NASA CR-72301, Aerotherm Corporation Report No. 67-15, September 1, 1967.

29. Bartlett, E. P. and Anderson, L. W.; An Evaluation of Ablation Mechanisms for the Apollo Heat Shield Material, Aerotherm Corporation, Final Report No. 68-38, Part II, October, 1968.

30. Moyer, C. B., and Rindal, R. A.; Finite Difference Solution for the In-Depth Response of Charring Materials Considering Surface Chemical and Energy Balances, Aerotherm Corporation, Final Report No. 66-7, Part II, March 14, 1967; also, NASA CR-1061, June, 1968.

31. Kendall, R. M., Bartlett, E. P., Rindal, R. A., and Moyer, C. B.; An Analysis of the Coupled Chemically Reacting Boundary Layer and Charring Ablator, Aerotherm Corporation, Final Report 66-7, Part I, March 14, 1967; also, NASA CR-1060, June, 1968.

32. Powars, C. A., and Kendall, R. M.; User's Manual, Aerotherm Chemical Equilibrium (ACE) Computer Program, Aerotherm Corporation Final Report No. 69-7, May, 1969.

This page intentionally left blank.

UNCLASSIFIED

Security Classification

DOCUMENT CONTROL DATA - R & D

(Security classification of title, body of abstract and indexing annotation must be entered when the overall report is classified)

1 ORIGINATING ACTIVITY (Corporate author)	2a. REPORT SECURITY CLASSIFICATION
Aerotherm Corporation Mountain View, California 94040	UNCLASSIFIED
	2b. GROUP

3 REPORT TITLE

A NONSIMILAR SOLUTION FOR MULTICOMPONENT REACTING LAMINAR AND TURBULENT BOUNDARY LAYER FLOWS INCLUDING TRANSVERSE CURVATURE

4 DESCRIPTIVE NOTES (Type of report and inclusive dates)

March 1968-October 1969

5 AUTHOR(S) (First name, middle initial, last name)

Larry W. Anderson; Robert M. Kendall

6 REPORT DATE	7a. TOTAL NO OF PAGES	7b. NO OF REFS
March 1970	124	32

8a CONTRACT OR GRANT NO	F29601-68-C-0062	9a. ORIGINATOR'S REPORT NUMBER(S)	
b. PROJECT NO	5791		AFWL-TR-69-106
c. Task No.	27	9b. OTHER REPORT NO(S) (Any other numbers that may be assigned this report)	
d.			

10 DISTRIBUTION STATEMENT This document is subject to special export controls and each transmittal to foreign governments or foreign nationals may be made only with prior approval of AFWL (WLEE), Kirtland AFB, NM, 87117. Distribution is limited because of the technology discussed in the report.

11 SUPPLEMENTARY NOTES	12. SPONSORING MILITARY ACTIVITY
	AFWL (WLEE) Kirtland AFB, NM 87117

13 ABSTRACT

(Distribution Limitation Statement No. 2)

A mathematical model of a multicomponent reacting nonsimilar laminar or turbulent boundary layer flow including transverse curvature effects is presented, and a method of solution is given. The formulation is an extension of an earlier work in which thermal and molecular diffusion were treated in terms of a bifurcation approximation for binary diffusion coefficients. In the present analysis, a turbulent model is added which employs a mixing length model for eddy viscosity in the wall region with consideration of injection or suction effects. The wake region eddy viscosity is taken to be proportional to the free stream velocity and local velocity defect thickness. Transverse curvature effects are also incorporated into the present analysis. A modification of the Levy-Lees transformation is used to transform the equations of motion to the (ξ,η) coordinate plane, where the conservation equations are integrated across boundary layer strips. Derivatives in the normal direction are related to one another by Taylor series truncated to reflect a quadratic or cubic approximation, and streamwise derivatives are expressed in finite difference form. The resultant set of equations is solved by general Newton-Raphson iteration.

DD FORM 1 NOV 68 1473

UNCLASSIFIED

Security Classification

14 KEY WORDS	LINK A		LINK B		LINK C	
	ROLE	WT	ROLE	WT	ROLE	WT
Turbulent boundary layer						
Viscous flow						
Plasma sheath						
Missile reentry						
Computer program						
Nonsimilar boundary layer						